Digital Photogrammetry for Visualisation in Architecture and Archaeology

Submitted to the University of Cape Town in partial fulfilment of the requirements for the Degree of Master of Science in Engineering.

By

Simon Antony Hull

Department of Geomatics

February 2000.

Declaration

I hereby declare that this thesis is my original work and has not been submitted in any form to another university.

Simon Hull

Abstract

The task of recording our physical heritage is of significant importance: our past cannot be divorced from the present and it plays an integral part in the shaping of our future. This applies not only to structures that are hundreds of years old, but relatively more recent architectural structures also require adequate documentation if they are to be preserved for future generations. In recording such structures, the traditional 2D methods are proving inadequate. It will be beneficial to conservationists, archaeologists, researchers, historians and students alike if accurate and extensive digital 3D models of archaeological structures can be generated. This thesis investigates a method of creating such models, using digital photogrammetry. Three different types of model were generated:

1. the simple CAD (Computer Aided Design) model;
2. an amalgamation of 3D line drawings; and
3. an accurate surface model of the building using DSMs (Digital Surface Models) and orthophotos.

Close on 100 stereo models were taken of the inside and outside of the ancient palace, Horvat Minnim, situated on the west shore of the Sea of Galilee, Israel. Using a conventional digital photogrammetric workstation (DPW) running LH system's SOCET SET 4.0.9 software for Windows NT, 3D digital models and orthophotos were created from each stereo pair. Some of these models were brought together in a visualisation system, CosmoWorlds, using Virtual Reality Modelling Language (VRML). Visualising the structure using a Geographical Information Systems (GIS) package, ArcView, with 3D Analyst extension, was also attempted. Computer processing power, speed and storage space, using a Pentium II 333 MHz processor with 64 Mb RAM, were insufficient for the entire structure to be viewed as one 3D model. For comparative purposes, a simpler CAD model was also created, using AutoCAD software.

It was found that the image matching algorithms of SOCET SET struggled and sometimes failed to extract the digital data from the architectural object. Extensive editing of the data was often necessary. This is not a shortcoming peculiar to SOCET

SET, but applies to most current DPWs. VRML with CosmoWorlds was found to be a useful tool for visualisation of structures in their full 3D extent, including texture-mapping of orthophotos onto the surfaces. ArcView, although a useful GIS package, could only visualise structures in 2.5D.

Acknowledgements

Jesus has stood by me incredibly throughout the past two years. Thank you for your love, support, guidance and wisdom. What I've learnt while writing this thesis can be summed up by Ecclesiastes 12:12 –

> "My son, … there is no end to the writing of books, and too much study will wear you out."

To my supervisor, Prof. Dr. Heinz Rüther, thanks for your constructive criticism and guidance throughout, and especially thank you for making this opportunity for study available to me. Also thank you to all the staff at the UCT Department of Geomatics, especially Andrea, Sue, Mike and Sydney, for all your help in so many ways.

The National Research Foundation, formally the Foundation for Research Development, have assisted me financially over the past two years. Much appreciated.

To Mom and Dad, Patrick and Marissa, thanks for the biscuits, money, love and wise words while I've been away. Your encouragement and support for me in whatever I do are always appreciated.

The Miller family, my 'home away from home', thanks for all your encouragement while I've been writing, patience with me throughout, empathy and kindness.

To the gents at 2 Bare Feet, what can I say? Ryan Matthews, Nik Haus and Kerwin Shaw, we had an awesome year, one I'll never forget. Thanks for your friendship, for putting up with my weird ways and late suppers, and for being godly men whom I could look up to. I've learnt a lot during my stay with you.

To the GAPS Tea Club (Simon Taylor, Ross Rozendaal, Terry Richards and Justin Davey), as well as *Dr.* Ulrike Brüssler, we've had a good time despite the hard work and stress. All the best for the future, and thanks for all your input.

In memory of Prof. Herman van Gysen.

Contents

List of Figures

List of Tables

CHAPTER 1
Introduction

1.1. Aims

The research described in this thesis was initiated by the Getty Conservation Institute (GCI) which approached Prof. Dr. Heinz Rüther of the Department of Geomatics at the University of Cape Town. The GCI wanted a quick, precise and accurate survey of two ancient buildings, Horvat Minnim and Tel Dan, for the purposes of documentation and conservation thereof. Line drawings of the stones making up the walls of the buildings and orthophotos of the same were to be produced. Since data acquisition by means of photography is quick, capturing a vast amount of data in one fell swoop, Prof. Rüther proposed that a photogrammetric survey be carried out. The high precision attainable through photogrammetric measurements and the ease of data capture make it a meritorious candidate for data acquisition and analysis in a wide variety of applications (see section 3.1 for a more detailed account of the applicability of photogrammetry to architecture and archaeology). Since the quality of the measured data is both reliable and good, a three dimensional reconstruction of the buildings was deemed feasible. It is hoped that this may form the basis for the subsequent construction of a 3D GIS. This does not, however, form part of this thesis.

Although the generation of Digital Terrain Models (DTMs[1]) and orthophotos from aerial photography using the state of the art in digital photogrammetric workstations (DPWs) has become a routine task, the same does not always apply to close-range applications. The generation of Digital Surface Models (DSMs) and the production of orthophotos in the close-range case of photogrammetry, are a relatively new and growing field. Especially lacking is an adequate environment in which to display a structure in all three dimensions, with orthophotos laid over the DSM, essentially

[1] DTMs, DEMs and DSMs are discussed in detail in section 2.3.4.1.

reconstructing the object accurately and precisely on a personal computer. This is what was attempted in this thesis.

Besides meeting the requirements of the GCI, what is envisaged is a complete three-dimensional reconstruction of a structure in such a way that the model itself can be used for further analysis once the initial survey is complete. Researchers, be they archaeologists, architects, photogrammetrists, teachers or students, will be able to view the entire structure using a personal computer. (The data may be accessed off a CD-ROM or downloaded from the World Wide Web.) Analysis may take the form of measurements or sections, or the rate of decay of the structure may be investigated if successive surveys are conducted. Any information besides the surface information supplied through photogrammetry (the DSMs, line drawings and orthophotos) will have to come from archaeologists or architects.

Besides the scientific benefits mentioned, the 3D model will have application in education and publicity as well, by making sensitive or difficult to access archaeological sites accessible in digital form. Virtual tourism may not, however, be an ideal way in which to see the wonders of the world. Recreating the ambience or mystique surrounding an historical site is like electronically simulating a piano or violin: although computer simulations can be very good and very near to the real thing, they will never be able to fabricate it exactly. However, as with musical instruments, there are instances where a simulation, jaded though it may be, is appropriate or at least satisfactory. It may be difficult or even impossible for some people to visit areas of archaeological or historical significance. The Internet is expanding and becoming more and more accessible to a wider audience; no longer is it a tool for the workplace alone, but schools and even many homes these days have access to the World Wide Web. The information age in which we live is allowing access to a world some would not otherwise have the opportunity of seeing, and although it may be a while yet before a truly accurate, complete 3D portrayal of a building finds its way onto the Web, that time will undoubtedly come.

The fundamental purpose behind 3D model construction lies in mankind's innate desire for knowledge, particularly of the past. Evidence from the archaeological record yields clues as to how our ancestors lived. The task of recording our

archaeological inheritance is thus of significant importance, especially since our past cannot be divorced from the present and it plays an integral part in the shaping of our future. If we can gain a better understanding of the way in which our predecessors lived, we will be better equipped to face the challenges posed to us in modern living. And if we do not look after our cultural heritage while we can, it may be lost forever. Where historic buildings are concerned, these must be constantly cared for and restored regularly if they are to be kept for future generations. 3D models play an important part in this process.

To this end, three different types of 3D model will be used to represent an archaeological structure. These forms of representation are (in order of increasing complexity):

1. the simple CAD (Computer Aided Design) model;
2. an amalgamation of 3D line drawings; and
3. an accurate surface model of the building using DSMs and orthophotos.

1.2. Thesis Outline

The thesis is divided into five chapters.

CHAPTER 1 contains introductory information regarding the purpose of the thesis, background to the thesis, the thesis outline, and the scope and limitations of the research.

CHAPTER 2 deals with the theory behind digital photogrammetry under the headings System-Level Tasks, Low-Level Tasks, and Middle-Level Tasks. System-Level Tasks are associated with the display, storage and compression of digital images. Low-Level Tasks involve image processing and orientation, and the generation of digital models and production of orthophotos. Middle-Level Tasks are those tasks concerned with the visualisation of digital 3D models.

CHAPTER 3 is a review of related work, beginning with the feasibility of using photogrammetry to document archaeological and architectural structures. The

importance of 3D as opposed to 2D documentation is discussed. Previous and current work in this field is reviewed and the use and applicability of different software and hardware are addressed.

CHAPTER 4 presents the results of the work done in this thesis. A description of the survey is followed by the choice of software packages. A detailed account of the extraction of DSMs and the creation and editing of digital 3D models follows. In this regard, SOCET SET output is given in Appendix C, the parameters of which are described in Appendices A and B.

CHAPTER 5 concludes the thesis by looking at the relevance of the research and future scope.

Having dealt with the purpose of the thesis, the rest of this chapter discusses the historical background of the building under investigation, and sets out the objectives and limitations of the research to provide the reader with a framework within which to assess the project.

1.3. Historical Background

The Minnim palace was probably built by one of the first Umayyad rulers in the 8th century AD. The Umayyad were the first Arab ruling dynasty to govern over the Middle East. Their capital was Damascus (from 661 AD), and they were known to be tolerant and respectful of other religions, but they were also able to convince many to convert to Islam with incentives such as tax regulations. Their dynasty ended with a revolutionary movement initiated by the Abbasids in 747 AD, who became the new dominating dynasty and moved the capital to Baghdad. Demas and Rosen-Ayalon (1999) describe Horvat Minnim as a site of ruins that belong to one of the most interesting groups of buildings of Islamic architecture: the Umayyad Palaces. It is the only site of its kind in Israel. The palace architecture belongs essentially to a single period, with few later (post-Umayyad architecture) additions. Any evidence of a later occupation did not cause significant change to the original palace. Investigation of the palace in 1959 defined significant re-use of the building in Mameluke times (1250-

1517 AD), when it was a major stopping place on the caravan route from Egypt to Syria. The Mamelukes were soldiers who had been brought to Egypt as property of the ruler from the Central Asian steppes.

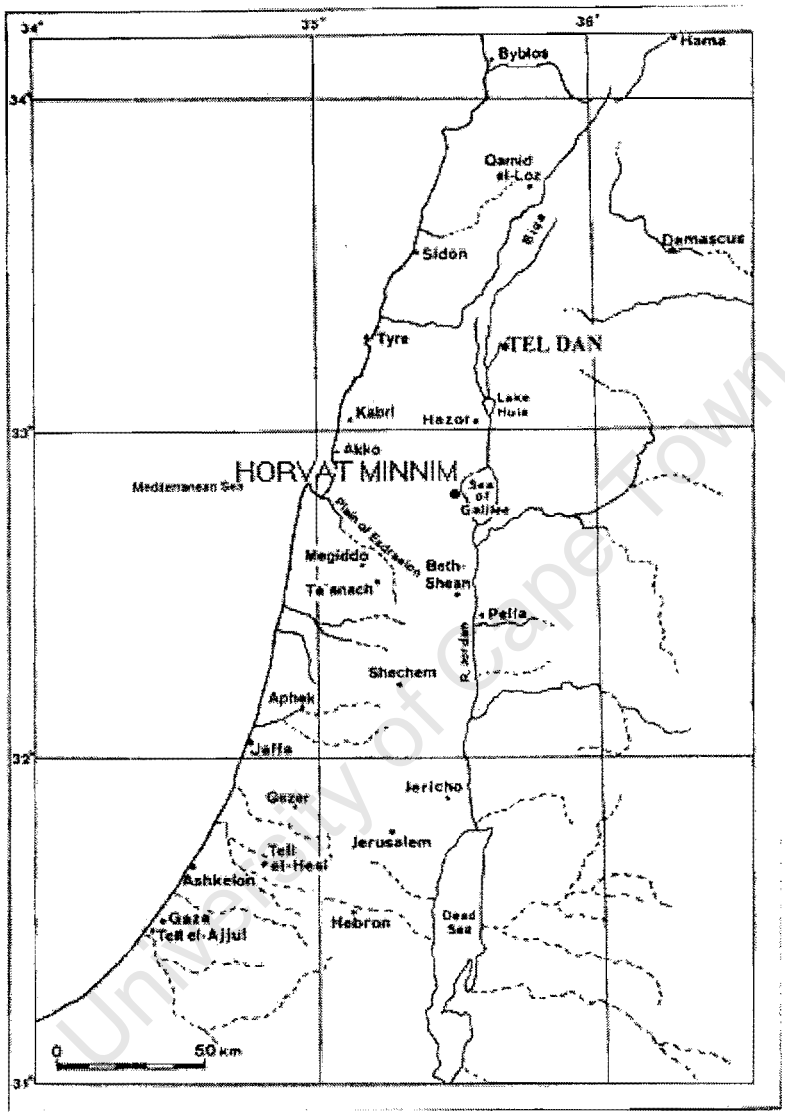

Figure 1.1 Israel and the location of Horvat Minnim (Biran *et al*, 1996)

The palace is located some 2 km north of Kibbutz Ginosar on the west shore of Lake Galilee, Israel (see Figure 1.1). The lower courses of the building illustrate the use of basalt as a feature of northern architecture in Israel. It is probably one of the best examples of this particular architecture. Dating from the earliest stages of this architectural period, Horvat Minnim describes the essence, or represents what one may call the basic formula, of this architecture, both in its plan and in the architectural

decoration that completes the compound. In this respect it precedes the majority of the Umayyad Palaces outside the country.

Some significant aspects of the palace:

- Horvat Minnim is unique in being the only Umayyad palace in Israel.
- The palace retains much of its original architectural integrity, with little significant alteration of the design during later periods.
- The palace is an excellent example of northern architectural styles in its use of basalt and may be seen as a precursor of Islamic palace architecture.
- The mosaic floors preserved in the building are a fine and rare example of the end of the long tradition of mosaics in the eastern Mediterranean.
- The site has potential significance for the local community and the Arab population of Israel as a unique example of Islamic architecture and art.

1.4. Objectives and Limitations

The objectives of this thesis are:

1. Production of DSMs of the complete Horvat Minnim palace, modelling the structure as closely as possible;
2. Production of orthophotos of each stereo-model from the DSMs produced;
3. Comparison with other 3D models (CAD-based and line drawing); and
4. Visualisation of the palace, or part thereof, using suitable software.

As mentioned previously, the realisation of a complete 3D GIS is beyond the scope of this thesis. The focus here is on generating a 3D model of a structure where accuracy is paramount and a replication as close to the truth as possible is achieved. It is hoped that this will form a basis for the realisation of a 3D GIS.

In terms of actually visualising 3D objects, existing software needed to be identified and used. Many programs are being developed and have been developed both commercially and in the academic world. These programs are often very limited in their scope, having been developed to meet a specific need of the programmer or

organisation under which they are developed. To develop another such limited program was deemed unnecessary, but rather an investigation into the visualisation of 3D objects using existing software was carried out. A review of some of the available software can be found in section 3.3.

Since this thesis has architectural and archaeological as well as photogrammetric relevance, it has been written for the photogrammetrist and non-photogrammetrist alike. In this regard, CHAPTER 2 deals exclusively with the theory behind digital photogrammetry, surface reconstruction and visualisation.

CHAPTER 2
Digital Photogrammetry

2.1. Definitions

In the fourth edition of the *Manual of Photogrammetry*, "photogrammetry" was defined as "the art, science and technology of obtaining reliable information about physical objects and the environment through processes of recording, measuring and interpreting photographic images and patterns of electromagnetic radiant energy and other phenomena" (Thompson & Gruner, 1980). With the relatively recent advent of advanced computer techniques and the ability to capture, scan and/or process digital images, photogrammetry has advanced into the digital world. Image measurement is now done in terms of pixels (discrete picture elements, see section 2.2.1) instead of points.

The conversion from analytical to digital photogrammetry is well under way. Schenk (1994) describes digital photogrammetry as "the most intensively researched area of photogrammetry". Karara (1989) describes it further as "... essentially a sequential process in which ... the digital data are processed in computers without human assistance. As such, digital photogrammetry involve[s] the practice of using pixels and image processing techniques to arrive at geometric information."

Schenk (1994) identifies four levels under which all digital photogrammetric tasks and processes can be grouped; these are summarised in Table 2.1. The rest of our discussion on digital photogrammetry will be centred on these four levels. According to Schenk, the majority of research has been directed toward the first two levels. This thesis focuses on levels two and three.

1. *System-level tasks.* The display and storage of digital images are the main system-level tasks, a crucial factor being the file size of the digital images. Magnification and stereographic display of images are dealt with at the system-level.

2. *Low-level tasks.* Image processing tasks and most photogrammetric operations, from orientation to digital model generation and orthophoto production, are included here.

3. *Middle-level tasks.* Surface and feature reconstructions are the typical middle-level tasks. Unlike in the generation of digital models, where emphasis is placed on the accurate and dense reconstruction of a surface, surface reconstruction here is as explicit as possible, for the purpose of guiding subsequent vision processes (such as object recognition).

4. *High-level tasks.* Image understanding is essential for many machine vision applications, but its role in photogrammetry is less important. Tasks such as analysing objects and their interrelationships have relevance in a GIS environment. Since the development of GIS is a topical subject at present, further research is warranted at this level.

Table 2.1 Classification of photogrammetric processes and tasks (Schenk, 1994).

Category	Processes, algorithms	Tasks
1. System-level	Store, access and display images	Manipulate digital imagery; Stereo display
2. Low-level	Process and match features; Extract data	Image processing, orientation, triangulation, DEM generation, orthophoto production
3. Middle-level	Group and segment images	Surface and feature reconstruction
4. High-level	Understand images	Object recognition; Image interpretation

2.2. System-Level Tasks

Digital image storage and compression will be discussed. For a description of the display of stereo images, the reader is referred to LaPrade *et al* (1980), who discuss the theory of stereoscopy, and Gulch (1996), who gives a summary of the different techniques for displaying digital images in stereo.

2.2.1. Digital Images

Digital images differ from hard-copy, continuous-tone images in that they are made up of many small, discrete picture elements, or pixels. Kraus (1993) defines a digital image as a two dimensional matrix G, for which every element g_{ij} represents the pixel area. The pixel dimensions are given by $\Delta\xi$ and $\Delta\eta$ in Figure 2.1.

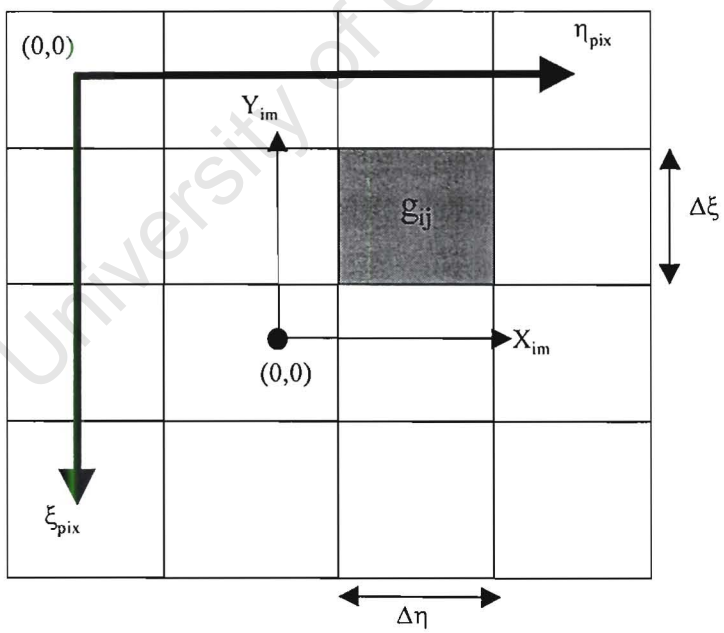

Figure 2.1 Definition of a digital image, showing pixel vs. image co-ordinates

Figure 2.1 also illustrates the relationship between the pixel and the image co-ordinate systems. (For clarity, the axes describing the image co-ordinate system have been offset from their origin.) The image co-ordinate system provides positions of points in

a system related to the principal point, in metric units (Mikhail, 1989). It is this system that is assumed in all of the equations relating to the geometry of image and object space. The pixel co-ordinate system has its origin at the centre of the top, left pixel, and positions of points are given in terms of pixels.

Conventional, film-based cameras still provide unsurpassed photographic resolution (Streilein, 1994). The pixel dimensions, $\Delta\xi$ and $\Delta\eta$, of a digital image, although very small, cannot compete with film in terms of depth of resolution. Modern techniques are simply incapable of capturing and storing digital images that can match film-based images in this regard, although the quality of the processed data is comparable, and some tasks can be performed more efficiently with digital devices (Bacher, 1998).

2.2.2. Compression and Storage

Toth (1996) proposes that, without advancements in storage and data compression technology, the usefulness of digital photogrammetry would have been limited to academic research alone. Compression is certainly necessary, when we consider that every pixel g_{ij} in a black and white image requires 8 or more bits of storage space (24 or more bits for a colour image). To improve the quality of an image, $\Delta\xi$ and $\Delta\eta$ (the pixel dimensions) are reduced with a corresponding increase in the number of pixels in an image.

For an average colour, aerial photo with a standard format of 23 cm x 23 cm and a pixel size of about 7,5 μm, the resultant, uncompressed file size will be of the order of 2,7 Gigabytes. Fortunately, images contain a large amount of redundant data (every pixel g_{ij}, although unique in position, is not unique in value) and so they compress well.

2.3. Low-Level Tasks

2.3.1. Image Processing

One of the advantages of working with digital imagery is the ease with which it can be enhanced, corrected and manipulated. Kraus (1997) discusses various image processing techniques by which digital images can be improved. Lillesand & Kiefer (1994) categorise digital image processing into the following five broad categories:

1. *Image rectification and restoration.* Distorted or degraded image data is corrected in such a way as to create a more geometrically correct representation of the original scene.

2. *Image enhancement.* The objective of image enhancement is to create a new image from the original image, increasing the amount of information that can be visually obtained from the data.

3. *Image classification.* The intent of the classification process is to group all the pixels in a digital image which describe a particular object, surface type or land-use, into various classes or themes (e.g. lakes, roads, industry, wetlands, etc.).

4. *Data merging and GIS integration.* The combination of image data with other spatially referenced data for the same area falls under this category.

5. *Biophysical modelling.* The objective here is to relate the remotely sensed digital data to the biophysical features and phenomena measured at the surface. This usually applies to satellite imagery.

Most digital photogrammetric workstations commercially available today come with an image processing package capable of, at least, the first two operations listed above. Data merging is a subject that will be touched on in section 2.4 and again in CHAPTER 4. Image classification and biophysical modelling are not addressed in this thesis.

2.3.2. Orientation

2.3.2.1. Interior Orientation

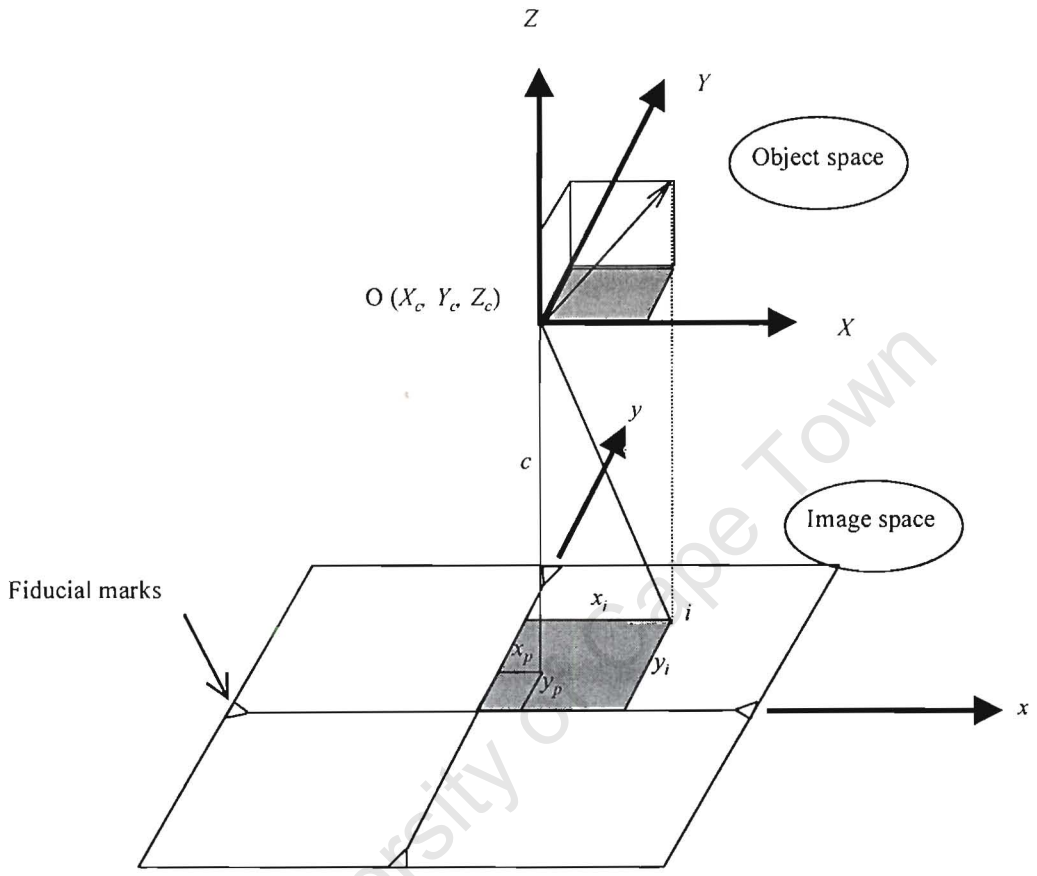

Figure 2.2 Image and object co-ordinate systems (Wong, 1980).

The *Manual of Photogrammetry* (1980) describes interior orientation as the determination of the interior perspective of the photograph as it was at the instant of exposure. McGlone (1989) identifies two sets of parameters to be determined. The first set consists of the geometric parameters of the camera itself: the principal distance and the co-ordinates of the principal point. The second set consists of parameters describing systematic errors (distortions) within the camera. These parameters can be determined by calibration either in the field or laboratory.

The perspective projection is the mathematical model in which an object in three-dimensional space (object space) is projected, through a perspective centre, onto a

two-dimensional plane (image space). Object space is where the object, be it a book, a building or a landscape, exists. Image space is where the photograph itself is found, at the moment of photography.

Referring to Figure 2.2, the perspective centre, O, is defined as the internal centre of the lens through which light from the object passes in order to be projected onto the image. The projection of the perspective centre onto the image is the principal point. This does not fall exactly in the centre of the image, and so the image co-ordinates of the principal point, x_p, y_p, have to be determined. The perpendicular distance between the perspective centre and the image plane is the focal length. The principal distance, c, is a computed value which minimises lens distortion such that c = *focal length* + *distortion correction.*

Systematic errors (the second set of parameters to be determined) can be grouped into the four categories of radial lens distortion, decentering distortion, focal plane unflatness and focal plane distortion. The reader is referred to McGlone (1989) for a description of these errors. They are modelled through camera calibration and are thus accounted for and can be removed from subsequent calculations.

2.3.2.2. Exterior Orientation

Exterior orientation refers to the position of the camera (perspective centre) when the image was taken, and to the angular relationship between the image and object space co-ordinate systems (McGlone, 1989). The exterior orientation of a single image can be determined, but for the purposes of this thesis only the stereo case will be considered. Following the pattern of most forms of photogrammetric software, exterior orientation consists of two parts:

- **Relative Orientation.** Wong (1980) defines relative orientation as the determination of the relative position and attitude of two photographs in a stereo pair, with respect to each other. The primary purpose of relative orientation is to orient the photographs so that each corresponding pair of rays from the two photographs intersect in object space. In effect, this is to satisfy the co-planarity condition. This states that the base vector between the two perspective centres

and the vectors from the two exposure stations to a point on the object, must all lie in the same plane.

- **Absolute Orientation.** In order to relate the images to the object, the model must be scaled, translated and rotated with respect to the object reference co-ordinate system (Wong, 1980). This process is absolute orientation, and may be defined simply as a problem of co-ordinate transformation. A minimum of two (pre-surveyed) control points, with known x, y, and z co-ordinates, and one further z co-ordinate, is required to solve for the scale factor, translation and rotation parameters.

The co-ordinate systems are defined as per Figure 2.2. The transformation from a point (x_i, y_i) in image space to (X_i, Y_i, Z_i) in object space can be modelled by a scale factor and three translations or shifts (absolute orientation), and three rotations (relative orientation). This is represented by:

$$\begin{bmatrix} x_i - x_p \\ y_i - y_p \\ c \end{bmatrix} = sR \begin{bmatrix} X_i - X_c \\ Y_i - Y_c \\ Z_i - Z_c \end{bmatrix}$$

Equation 2-1

where s is the scale factor which relates the relative distances between the two systems;
R is an orthogonal rotation matrix describing the rotations of the image plane about the three-dimensional co-ordinate system in object space; and
X_c, Y_c, Z_c are the object co-ordinates of the perspective centre.

This equation is based on a fundamental principle of image geometry: that any object point, the perspective centre and its image point all lie on a straight line (the collinearity condition). Equation 2-1 can be reduced to the two collinearity equations of Equation 2-2:

$$x - x_p + \Delta x = c\frac{r_{11}(X - X_0) + r_{21}(Y - Y_0) + r_{31}(Z - Z_0)}{r_{13}(X - X_0) + r_{23}(Y - Y_0) + r_{33}(Z - Z_0)}$$

$$y - y_p + \Delta y = c\frac{r_{12}(X - X_0) + r_{22}(Y - Y_0) + r_{32}(Z - Z_0)}{r_{13}(X - X_0) + r_{23}(Y - Y_0) + r_{33}(Z - Z_0)}$$

Equation 2-2

where: r_{ij} are the elements of the rotation matrix R, describing the attitude, in space of, the original photograph relative to the object co-ordinate system;
c is the principal distance of the camera;
x, y are the image co-ordinates of the point in image space, often to sub-pixel accuracy;
x_p, y_p are the image co-ordinates of the principal point;
Δx, Δy are distortion parameters;
X, Y, Z, are the object co-ordinates of the rectified pixel; and
X_0, Y_0, Z_0 are object co-ordinates of the camera centre.

2.3.3. Epipolar Geometry

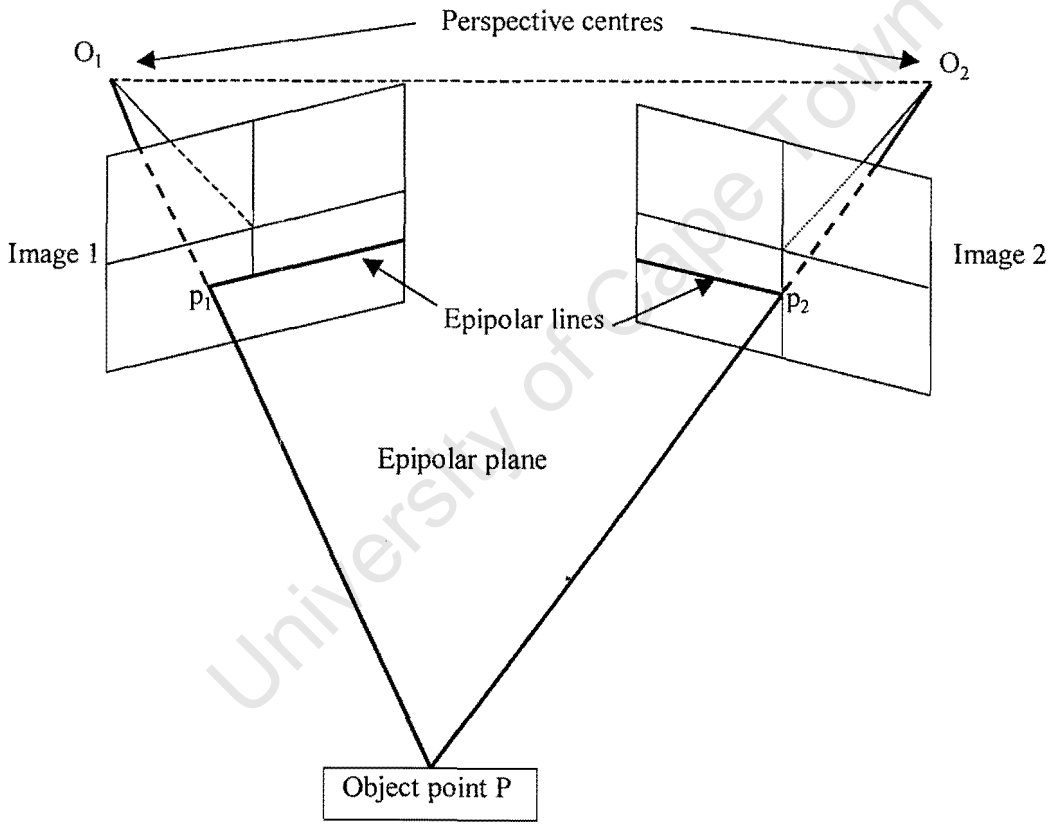

Figure 2.3 Epipolar Geometry

Assuming the two images have been oriented relative to each other, the collinearity condition (and hence the coplanarity condition) is satisfied. Referring to Figure 2.3, we have the object point, P, the two image points, p_1 and p_2, and the two perspective centres, O_1 and O_2, defining the epipolar plane. This plane intersects the two image planes in the epipolar lines. All epipolar lines in an image are parallel. For

a given point in one image, the epipolar line in the corresponding image can be computed. The corresponding image point must lie along this line, reducing the image matching problem (section 2.3.4.3) from a 2D to a 1D task (Heipke, 1996).

Additionally, the two images can be transformed into the normal case, whereby all the epipolar lines in an image lie horizontally. This further simplifies the image matching problem by constraining the solution to lie in one (horizontal) direction only. A drawback of this technique, however, is that the images must be resampled. This degrades the images and consequently can lead to an impaired image matching

2.3.4. Generating a Digital Model

Although the automatic generation of digital models is a complex process, the underlying algorithms are still "low vision" problems (Schenk, 1994) and as such are grouped here under the low-level tasks of photogrammetry. Closely linked to the generation of digital models is surface reconstruction, which is a middle-level task to be dealt with in section 2.4.

Before beginning a discussion of how digital models are generated, it is necessary to define some of the terms used to describe the various types of digital model.

2.3.4.1. Definitions concerning digital models

(a) Types of Model

Maune (1996) gives definitions of some of the types of digital models, which are illustrated in Figure 2.4.

Strictly speaking, a **Digital Elevation Model (DEM)** is defined as a "digital cartographic representation" of the elevation (z value) of land at regularly spaced intervals in x and y. The term is used generically to describe the representation of the earth in any form, be it a regular grid or irregular point cloud format.

Digital Terrain Models (DTMs) incorporate the elevations of significant features on the land as well as breaklines, irregularly spaced to better characterise the shape of the terrain. **Breaklines** are linear features that describe changes in the continuity of a surface (such as ridges).

Triangulated Irregular Networks (TINs) are a set of adjacent, non-overlapping triangles computed from irregularly spaced points with x, y and z co-ordinates. Fewer data points are usually required than for DEMs or DTMs. Breaklines define terrain discontinuities to model the surface closely.

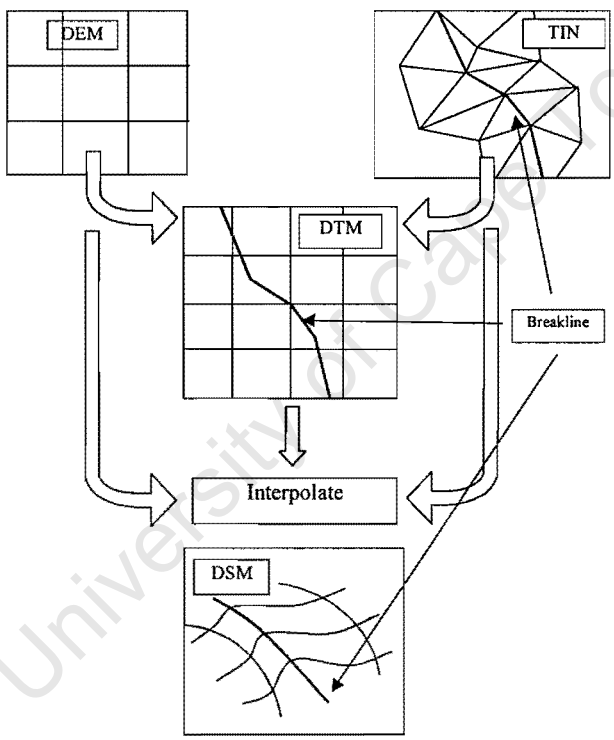

Figure 2.4 Types of digital model

TINs can be converted to DEMs and DTMs, and vice versa, but this usually results in a loss of information or accuracy of the model.

A **Digital Surface Model (DSM)** can be constructed from a DEM, DTM or TIN model by interpolating between the data points to define a continuous surface (Kraus, 1997). A more detailed discussion of DSMs follows in 2.3.4.4(a).

(b) Dimensionality

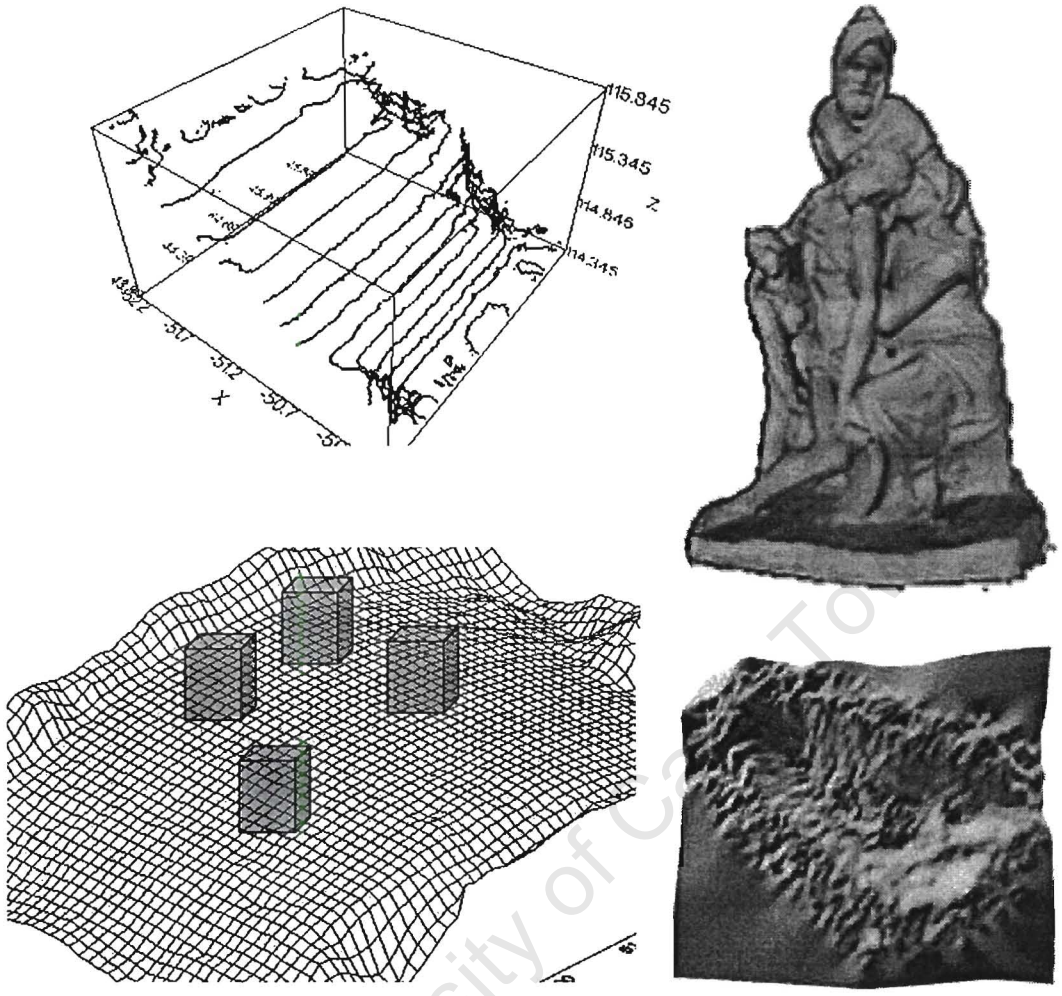

Figure 2.5 3D models: line-model (top left), surface-model according to Kraus (Christensen, 1999) (top right), surface-model according to Bill & Fritsch (1991) (bottom right), volume-model (bottom left).

Dimensionality in digital models is an area that can cause confusion if the terms are not appropriately defined. Bill & Fritsch (1991), Kraus (1997) and Scott (*n.d.*) address this issue, the latter in an Internet article concerning Geographic Information Systems (GIS). We can distinguish between 2D, 2.5D and 3D data.

2D data can be expressed in the form (x, y, a) where a is an attribute (e.g. corner beacon of a plot of land).

2.5D models have (x, y, $z[a]$), where height (z) is actually an attribute. These are often (incorrectly) referred to as 3D models. Kraus (1997) further describes 2.5D surface models as a 2D grid with a z co-ordinate attached to each grid point, with the proviso that there exists only one z for every x, y position.

According to Scott (*n.d.*), 3D models are defined by (x, y, z, a) and are represented by a system of volumes. Bill & Fritsch distinguish between three different 3D models (see Figure 2.5). 3D line-models may be described as 3D contour plots. 3D surface-models consist of small polygon entities such as squares or triangles. Kraus (1997) describes a 3D surface-model as having potentially more than one z co-ordinate for every x, y position. This type of model is often referred to as having full 3D extent (Boochs *et al*, 1998). 3D volume-models can be described as a surface-model with added data on the surface describing 3D structures (such as buildings) by means of primitive entities. In addition Bill & Fritsch (1991) define a 2D+1D model which has 2D attribute data as described previously with a 3D line-model included. Using this model a surface is described which includes structures on the surface as part of the surface (as opposed to a 3D volume-model which includes them separately from the surface).

Scott (*n.d.*) proposes a nomenclature to be used in describing models and multi-dimensional GIS, in preference to a reference to the dimensionality of the model or GIS. This is outlined in Table 2.2.

Table 2.2 Dimensionality nomenclature for digital models (Scott, *n.d.*)

Existing Nomenclature	Mathematical Expression	Proposed Nomenclature
2D	(x, y, attribute)	Plane / Planar
2.5D	(x, y, z[attribute])	Surface / Surficial
3D	(x, y, z, attribute)	Volume / Volumetric

For the purposes of this thesis, a **DSM (Digital Surface Model)** will be defined as a group of interrelated points which can be used to define a (2.5D, according to Kraus, 1997) surface. The points may be organised in a grid structure with a specific post spacing, or in an irregular pattern which lends itself to the generation of TINs. A

detail to note is that the surfaces generated in this project do not represent terrains but vertical walls. Where a set of adjacent surface models is brought together in one co-ordinate system to describe, for example, a tower in its full 3D extent, more than one z value can exist for each x and y co-ordinate as described in Kraus' definition of a 3D surface model.

2.3.4.2. Definitions concerning image matching

In photogrammetry and remote sensing, 'matching' can be defined as "the establishment of the correspondence between various data sets" (Heipke, 1996). Schenk (1996) gives the following definitions for terms pertinent to image matching:

A **conjugate entity** is a general term used to describe representations of object space features occurring in two or more images, including points, lines and areas. A **matching entity** is a primitive that is compared with primitives in other images in order to find conjugate entities. The primitives include grey levels, features or symbolic descriptions. A **similarity measure** is a quantitative measure indicating how well the matching entities correspond to each other. The **matching method** performs the similarity measure, while a **matching strategy** is an overall concept or scheme for the solution to the image matching problem.

2.3.4.3. Image Matching Techniques

The production of orthophotos relies on the generation of digital models, which are the products of image matching. Since orthophoto production is a major part of this thesis, it is necessary to explore the methods used in extracting 3D points from the photographs.

The process of surface reconstruction is not limited to measurement alone; it involves object interpretation and image understanding as well. This makes automating surface measurement an extremely difficult task. The process of finding matching points, lines or areas between two or more images, which a human operator does intuitively, without much effort, is certainly not trivial in digital image processing (Kraus, 1997).

Schenk (1996) sums this up by saying that if a human operator can solve something without conscious effort, that does not necessarily mean that the task is easy. Heipke (1996) adds that matching "is one of the most challenging tasks in photogrammetric research and development." Why is this so difficult? To answer the question, we must look at the subject matter which the computer would use to perform the match.

The theoretically ideal case would be to find a match for every single pixel. This is certainly not feasible (Heipke, 1996); we saw previously in section 2.2.2 that each pixel grey value is not unique. There will, therefore, be many identical pixels in one image, any one of which could be a match for the search pixel. In addition, Kraus (1997) gives the following three reasons why finding a match for every single pixel cannot be achieved or makes no sense in practise:

- The computing time necessary with such a large quantity of data will be too high;
- Such large quantities of data are difficult to manage;
- It is impossible to measure such a point density as unfavourable surface conditions, radiometric differences, occlusions and strong shadows cause image matching techniques to fail.

It is preferred, then, to use entities (groups of pixels relating to the same area) over single pixels. There will still not be a match for every pixel using this method due to the third reason given above (occlusions, shadows, etc.). The size of the entity chosen becomes a crucial factor as too large an entity may not have a close match, and too small an entity may not be unique enough. An incorrect choice of entity size and bad initial approximations of the position of the conjugate entity can lead to the following two problems (Schenk, 1996):

- A *combinatorial explosion* occurs if the similarity measure between matching entities is computed over the entire image. The matching procedure will then find multiple matches for a conjugate entity, when only one is the true match. The search space needs to be restricted by making accurate initial approximations of the position of the match.
- *Ambiguity* occurs if the matching entity is not unique enough. Then, again, multiple matches may be found in the corresponding image. To ensure a unique matching entity exists the size of the entity must be carefully chosen.

Depending on what assumptions are introduced to the problem, different image matching techniques have been developed to combat these pitfalls. An overview of these techniques follows below. (For a more detailed description, the reader is referred to Baltsavias (1991), Geenfeld & Schenk (1989), Schenk (1996), Heipke (1996) and Kraus (1997).)

The techniques can be grouped into two broad categories: area-based and feature-based matching, based on the entities used. Baltsavias (1991) uses a combination of the two categories in his Multiphoto Geometrically Constrained matching technique, increasing the precision and reliability of conventional matching techniques through the introduction of *a priori* known geometric information and more than two images. Since only stereo-models (comprising two images) were matched, this technique has no application here and will not be addressed further.

All techniques follow four basic steps, which summarise the problem of image matching (Schenk, 1996):

1) Select a matching entity in one image.
2) Find a conjugate in the other image.
3) Compute the 3D location of the matched entity in object space.
4) Assess the quality of the match.

(a) Area-Based Matching

The matching entity used in area-based matching is a window or image patch of pixel grey values. This remains fixed in one image, centred on the point to be matched. A search window is defined as the search space in an image within which matching entities in the corresponding image are compared with the conjugate entity. The matching entity is shifted pixel by pixel in the search image until a conjugate entity is found. Problems arise when occlusions are encountered in one image, and when the radiometric differences between images is significant. Poor or repetitive texture also leads to errors.

Two types of algorithm have been developed: area-based matching by correlation and by least squares. Rosenholm (1987) extends the least squares matching algorithm to

include multiple points, to combat bad texture and large radiometric differences. We will briefly look at his multi-point image matching technique too.

... by Correlation

In area-based matching by correlation, a correlation factor is computed which measures the similarity of the template to the matching entity. The similarity between templates is defined as a function of the differences between the corresponding grey values. This function is a cross-correlation factor, computed for each position of the matching entity within the search window.

Defining the criteria for a good match obviously plays a crucial part in determining the success of the algorithm. Where the cross-correlation factor reaches a maximum, the best match between the template and the search window has been found. However, the spatial variation of the cross correlation co-efficient can be extensive, making it difficult to find the maximum: ambiguous solutions are often encountered. Fortunately the central perspective projection, which is assumed when dealing with photographic images, provides a powerful constraint: epipolar geometry (see section 2.3.3). This constraint is not specific to correlation only.

... by Least Squares

Here the similarity function is the sum of the squares of the grey value differences or gradients between the conjugate entity and the matching entity. This is minimised by adjusting the position and shape of the matching entity, using an affine transformation. A good match is defined by that set of parameters for which the sum of the squares of the differences or gradients is a minimum.

An advantage of least squares matching over matching by correlation is its high accuracy and reliability. A disadvantage is the need for accurate approximate values for the position of the search template (to within a few pixels). A larger tolerance for the approximate values can be achieved through low-pass filtering, at the cost of degradation to the matching accuracy.

To obtain close approximate values, image pyramids may be used. This reduces the ambiguity problem and extends the pull-in range of the matching algorithm. An image pyramid is constructed by taking the same image and resampling it at smaller and smaller scales (decreased by a factor of 2 from one level to the next). Then, by finding matches first at the coarse (high) levels of the pyramid, these results can be used as approximations for subsequent levels. Local disturbances, such as occlusions, become less of a problem.

... Using Multiple Points

According to Rosenholm (1987), the results obtained using least squares matching as described above are not reliable enough and gross errors are insufficiently detected. A limitation is the difficulty of making measurements in areas of low signal content (this is true of manual measurements, too).

Multi-point matching is regarded as an extension of the single point least squares technique, whereby a group of points in a regular grid are matched simultaneously. The grid points are connected in a bilinear function with smoothness constraints on the object surface imposed on the solution. The problem is then to minimise the differences between the two matching images under the smoothness constraints (Li, 1991).

When working with architectural data, continuity of surfaces cannot be assumed (see section 2.3.4.4(b), and Hanke and Ebrahim (1997a)). For surfaces which are not smooth, or discontinuous, the inclusion of breaklines to the original formulation is possible. Another possibility is to include a discontinuity explicitly and to use two different, unknown parallaxes at each discontinuity point (Rosenholm, 1987). However, Rosenholm (1987) and Li (1989) both state that multi-point matching performs weakly in the cases of breaklines, discontinuities and occlusions. These are some of the most critical points of image matching. Rosenholm claims that multi-point matching increases the reliability of a match when compared to least squares matching, but Baltsavias (1991) disagrees, stating that no comparison between the two techniques proves that multi-point matching is better.

(b) Feature-Based Matching

The conjugate entities are features within the original grey level image. Features may be points, edges or areas. Edges are the most widely used and correspond to a difference in brightness between adjacent areas in the images. As a prerequisite to matching, the image is often smoothed to eliminate noise.

Features are usually extracted *a-priori* in each image. They should be distinct with respect to their neighbourhood, invariant with respect to geometric and radiometric influences, stable with respect to noise, and unique with respect to other features (Förstner, 1986). The result of feature extraction is a list containing the features and their descriptions for each image.

Defining a similarity measure for feature-based matching is complicated. Usually the geometric and radiometric differences between the images are combined in order to compute a similarity measure called either a cost or a benefit function. To achieve a good match, a cost function must be minimised and a benefit function maximised. Corresponding edges usually have a slightly different shape due to the perspective projection. Thus images are often normalised before matching features is attempted.

In this context, matching is a selection process whereby edges are paired according to measures of similarity and consistency, taking into account the similarity measure. For each given feature in one image, a small search area is defined in the other image and an exhaustive search is undertaken to match the features. To reduce the search space, compliance with epipolar geometry can be introduced as a constraint to the process.

Multiple matches may be encountered and eliminated through global consistency checks. The first check is on the vertical disparity (y parallax) of the matches, assuming a zero rotation between images. The second check is on the azimuth and distance between pairs of matched vertices. Van der Merwe (1995) suggests verifying the most probable feature matches by examining the topology between relevant features. This is achieved by searching for triangles formed between the centre of mass points of adjacent features. Finally, relative orientation between the images is

computed by least squares and the residuals checked for errors. Large residuals indicate incorrect matches.

2.3.4.4. Surface fitting

The points or features obtained through image matching are not uniformly distributed and do not exactly represent the surface of the object. Due to the reasons given in section 2.3.4.3 for the impossibility of matching every pixel, 3D points must be interpolated to represent the entire surface without holes (missing data). This is termed surface fitting: the process of finding a function which agrees with the data points and behaves reasonably between them.

The methods of surface fitting can be classified according to reliability of fit, extent of support, or type of mathematical model (Schenk, 1996). Tests have shown that, with optimal data acquisition, the different interpolation methods have similar performance. Different results are obtained in terms of accuracy and performance if data acquisition is not optimal (Ackermann, 1996). Gaps between data points and a generally poor point distribution would not qualify as being optimal.

(a) Digital Surface Models

DSMs may be interpolated from existing DEM, DTM or TIN data (Kraus, 1997). From a DEM, where data points occur at regular X, Y positions forming a grid, the surface between the points can be approximated by a hyperbolic paraboloid:

$$Z = a_0 + a_1 X + a_2 Y + a_3 XY$$

Equation 2-3

where the coefficients a_i are given by:

$$\begin{bmatrix} Z_1 \\ Z_2 \\ Z_3 \\ Z_4 \end{bmatrix} = \begin{bmatrix} 1 & 0 & 0 & 0 \\ 1 & \Delta d & 0 & 0 \\ 1 & 0 & \Delta d & 0 \\ 1 & \Delta d & \Delta d & \Delta d^2 \end{bmatrix} \begin{bmatrix} a_0 \\ a_1 \\ a_2 \\ a_3 \end{bmatrix}$$

Equation 2-4

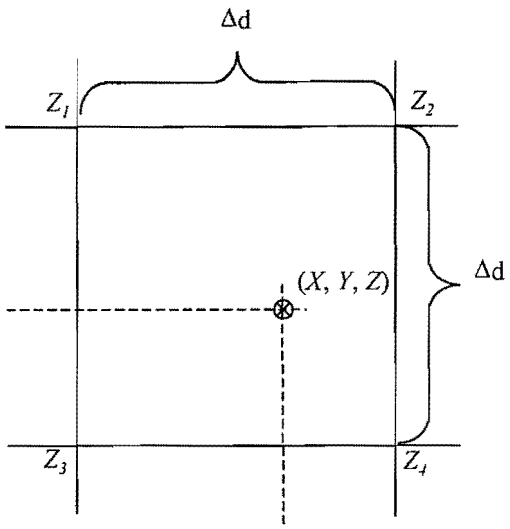

Figure 2.6 Relationship between parameters involved in DSM interpolation from grids

Z_i are the Z co-ordinates of the four points defining a grid square, and Δd is the length of a side, shown in Figure 2.6. From Equation 2-4, then, Z for any point X, Y within a grid square can be calculated once a_i are known. Figure 2.7 shows an example of this type of surface model.

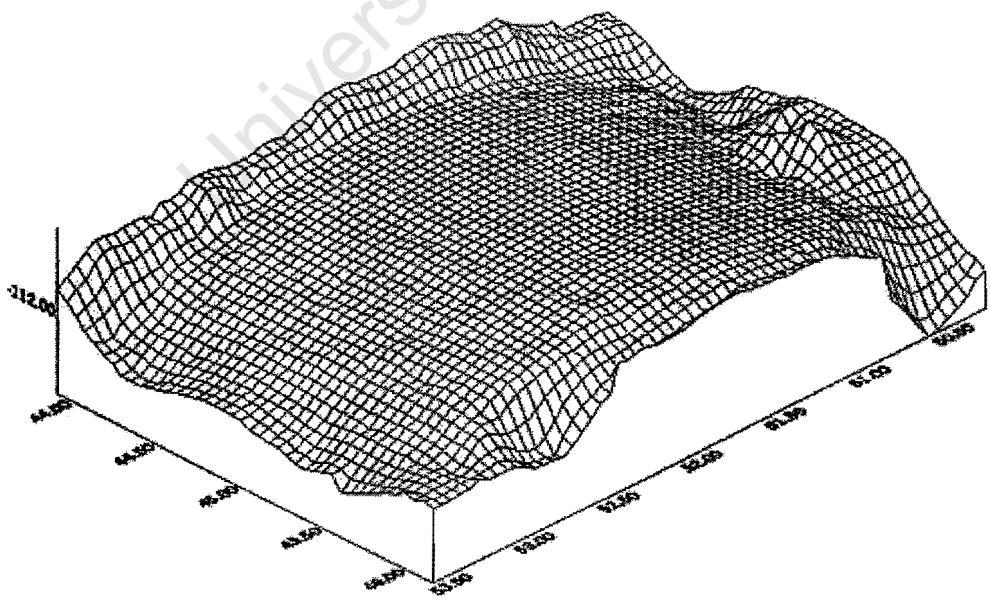

Figure 2.7 Example of a DSM

If an irregular distribution of points is used (TIN), or if breaklines and spot heights are included (DTM), the surface between the points can be approximated by inclined triangles with common edges. The equation of such an inclined plane is:

$$Z = a_0 + a_1 X + a_2 Y$$

Equation 2-5

where the coefficients a_i are given by:

$$\begin{bmatrix} Z_1 \\ Z_2 \\ Z_3 \end{bmatrix} = \begin{bmatrix} 1 & 0 & 0 \\ 1 & X_2 & Y_2 \\ 1 & X_3 & Y_3 \end{bmatrix} \begin{bmatrix} a_0 \\ a_1 \\ a_2 \end{bmatrix}$$

Equation 2-6

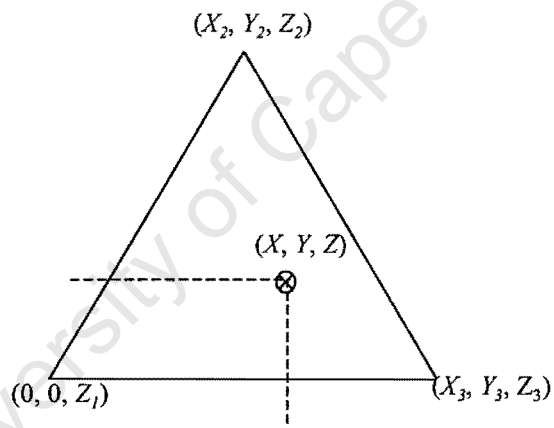

Figure 2.8 Relationship between parameters involved in DSM interpolation from triangles

X_i, Y_i are the co-ordinates of the vertices of the triangles, illustrated in Figure 2.8. In both of the above examples, the X, Y co-ordinates are referenced to one of the data points making up the grid square or triangle.

(b) The Architectural Case

The preceding discussion on interpolation and surface fitting presumes a continuous surface, as given by Equation 2-3 and Equation 2-5, where $z = f(x, y)$. These surface

functions are smooth mathematical functions of the x and y co-ordinates, and are not given to abrupt changes in elevation such as often occur on building facades.

Consequently, no DEM post can be used as an approximation for its neighbour when interpolating between posts: the difference in 'elevation' (depth) between the two points could be several metres. Also, due to the presence on building façades of alcoves and protrusions which hide other features (or are themselves hidden), every smoothing and interpolation algorithm must fail (Hanke & Ebrahim, 1997a).

Architectural photogrammetry is a special case that requires its own methods and techniques. Like image matching, many different techniques have been proposed, each with its own successes and failures. A discussion of some of these techniques follows in section 2.4.

2.3.5. Orthophoto Production

In many instances, it may be necessary or desirable to use photographic- instead of line maps, as greater insight can often be gained from a photographic image than from a symbolic representation of a scene. However, photography, be it metric or non-metric, is subject to distortion. This distortion arises from the tilt of the photo and displacements in the image due to relief, in a central perspective projection. Before a photograph can be used in place of a map, these distortions must be eliminated and the image corrected to an orthographic projection (see Figure 2.9).

An orthophoto is an image showing objects in their true orthographic (x, y) positions and is, therefore, geometrically equivalent to a map. This means that it can be used for direct angular, distance, area and position measurements without making corrections for image displacements. The principal difference between an orthophoto and a map is that the former uses actual images of objects or features, while the latter utilises lines and symbols to represent objects and features.

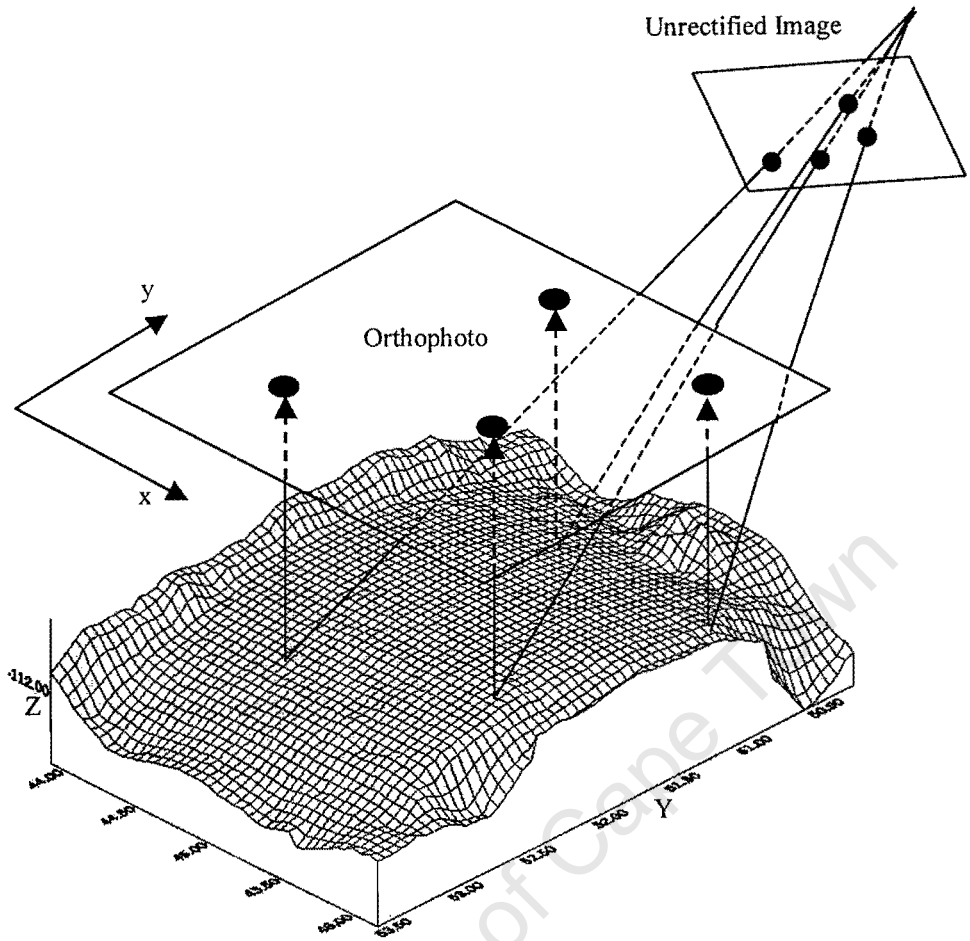

Figure 2.9 Theory of orthophoto production

The production of digital orthophotos is accomplished through a process called differential rectification, whereby displacements due to tilt and relief are corrected as best as possible. There are four basic steps which describe an indirect transformation from the orthophoto (to be produced) back to the original image (a direct transformation is also possible, with worse results):

1. Create a grid for the orthophoto, the grid squares corresponding to pixels, and select a point in the orthophoto grid;
2. Interpolate the terrain height for the point from the DEM, DTM or TIN;
3. Using an affine transformation, find the corresponding point in the original image;
4. Interpolate the grey value in the original image and transfer this to the digital ortho-image.

For the transformation from orthophoto to original image, the Z co-ordinates of every orthophoto pixel-centre are required. Working pixel-by-pixel (step 1) the Z co-ordinates can be obtained from the relevant digital model by interpolation using Equation 2-3 or Equation 2-5 (step 2). The equations of central projection (Equation 2-2, the collinearity equations), give the mathematical relationship for the transformation (step 3).

The question of how to assign pixel grey values in the resultant, rectified image, which match the grey values in the corresponding positions of the original image, is best solved using standard image processing techniques (step 4). The most common image processing techniques are:

- Nearest-neighbour, the simplest, which adopts the density of that pixel whose centre is closest to the transformed position. This can result in pixels in the resultant image being shifted by up to half a pixel from their correct positions. It also yields a very coarse, 'blocky' appearance;
- Bilinear, which interpolates linearly between the four closest pixels, first by rows and then by columns. Bilinear interpolation results in an improvement in image quality over nearest-neighbour interpolation, but may still result in smoothing effects that are unsatisfactory; and
- Bicubic, which applies a piecewise polynomial function to a 4 x 4 neighbourhood of nearby points and preserves the fine detail present in the source image. It is, however, the most time-consuming method.

2.4. Middle-Level Tasks

At the middle-level of photogrammetric tasks lie the topics of surface and feature reconstruction. The preceding section dealt with digital surface models which were accurately constructed from points obtained through image matching techniques. The techniques of surface reconstruction described in this section rely less on the exact geometric model and more on the visual or pictorial quality of the model.

The primary goal of surface reconstruction is to guide subsequent vision processes such as object recognition. Unlike in the generation of digital models, where an

accurate representation of the surface is achieved using a dense distribution of points, surface reconstruction is concerned with as explicit a representation of the surface as possible (Schenk, 1994). In other words the appearance of the model is considered more important than its underlying structure (Daniels, 1997).

Two types of surface models are identified: those based on DSMs and those constructed from surface primitives. The former are those models dealt with in the preceding sections; the latter are models constructed from planes, cylinders etc. (CAD models). The two types meet different requirements and have different purposes. They cannot, generally, be used interchangeably. What we need to identify at the outset is the role the model will be playing:

- Will it be quantitative (i.e. for scientific or research purposes), or
- Will it be qualitative (i.e. used in marketing, education and public awareness)?

The latter has little need for the high accuracy requirements of the former, while the former may become caught up with too much detail. A model designed to teach scholars or students about past eras will not need highly accurate data as its base (such as a DSM), as long as it conveys the necessary information. However, if the purpose of the model is as accurate a portrayal as possible of the structure as it now stands, the data base is of paramount importance.

Feature reconstruction is not discussed here because it has no relevance to this thesis.

2.4.1. Techniques for Models Having Full 3D Extent

Instead of constructing a surface from a cloud of 3D points (regular grid or irregular TIN) as discussed previously in section 2.3.4.4, it is generally preferred to work with continuous patches or segments of a surface which can be grouped to represent the entire exterior of the object (Schenk, 1994). Kraus (1997) gives two examples of how this may be done, referring specifically to structures having full 3D extent.

Firstly, a 3D surface model (or volumetric DSM, to use Scott's nomenclature – see section 2.3.4.1) can be constructed using a 3D-grid, the basic element of which is a cube (or voxel: volume element). These voxels may be used as the basis on which to

perform mathematical or logical operations, an important consideration in the design of a volumetric GIS (Scott, *n.d.*). Within these cubes are planar triangles which describe the surface (Figure 2.10). The quality of the surface description using this technique is dependant on the mesh size (or the size of the individual voxels). A decrease in voxel size leads to an increase in quality, at the expense of a rapid increase in storage requirements and computing effort. If the voxel size is small enough, complex surfaces can be described and processed very efficiently.

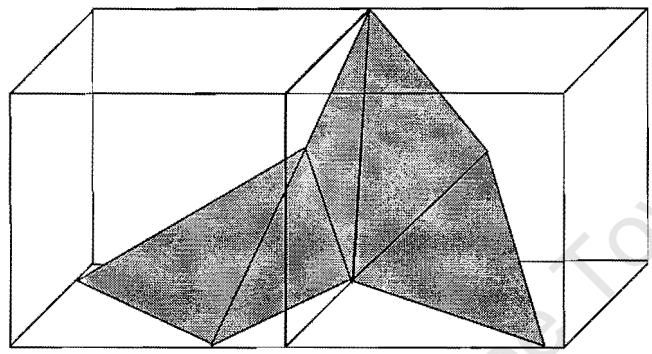

Figure 2.10 Partial surface reconstruction using small, inclined triangles within cubic elements (after Kraus (1997))

The second method used to reconstruct surfaces having full 3D extent is by using partial surfaces positioned in 3D space. Referring to Figure 2.11, each partial surface is defined in a local co-ordinate system (X_{Li}, Y_{Li}, Z_{Li}) such that, for example, the Z_{Li} co-ordinate always represents depth. These may then be rotated and translated in a global co-ordinate system (X_G, Y_G, Z_G) to position them correctly in relation to each other.

By partitioning the surface in this way, it is possible to construct a series of individual surfaces using a TIN, DTM or DEM structure, preserving the $z = f(x, y)$ relationship (Equation 2-3 and Equation 2-5). The surface will need to be divided into sections as fine as necessary to maintain this relationship, without having more than one z-value for each x, y. The more complicated the surface, the more subdivisions will be needed (Boochs *et al.*, 1998).

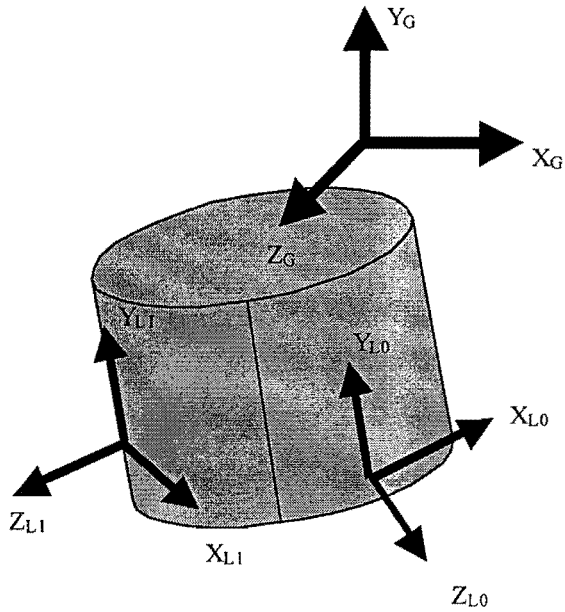

Figure 2.11 The relationship between partial surfaces and their (local) co-ordinate systems, in a global co-ordinate system.

2.4.2. 3D Photo-models

Orthophotos have the disadvantage that they contain no information about depth in an image. Depth is important for human interpretation of the image contents. This disadvantage can be partially offset by the addition of contour lines, resulting in a so-called orthophoto-map. A more general solution, however, lies in projecting each pixel of the image contents onto the DSM (interpolated surface model), creating a 3D photo-model. Colombo (1998) proposes that this could become a "standard for presentation aspects." Kraus (1997) gives a concise description of how this is done using an indirect image transformation. El-Hakim *et al.* (1998) identify the following algorithm:

1. Select an image in which a specific TIN triangle *t* (or grid square *g*) appears;
2. Using the exterior orientation parameters, determine the correspondence between the 3D triangle or grid square vertex co-ordinates in space and the 2D co-ordinates in the image;
3. Specify 3D and texture co-ordinates in a modelling language such as VRML (Virtual Reality Modelling Language); and
4. View the scene using standard 3D viewer software.

2.4.3. CAD-Based Object Reconstruction

Depending on the level of detail required, or the purpose of the reconstruction, a digital model of the object may not be necessary. Instead the object can be represented by a series of primitive 3D shapes (planes, spheres, cylinders, pyramids, cubes etc.) with or without photo-texture. An assembly of these shapes in a CAD environment can be used to approximate the shape of the object in 3D space. Then, with photo-texture applied, a visually realistic (if not entirely geometrically correct) portrayal of the object is achieved.

Figure 2.12 CAD-based surface reconstruction using intersecting planes and photo-texture (Hoffman, 1996).

Since photogrammetry generally records all data as a series of 3D co-ordinates, it makes a natural partner for the modern, 3D CAD systems. By marrying the two, Streilein (1994) proposes that photogrammetric data acquisition and processing can be improved, 3D objects can be geometrically described and a photo-realistic visualisation achieved. Many of the problems of insufficient storage space and

computer efficiency can be overcome by using CAD models instead of dense DSMs, while maintaining an accurate and realistic reconstruction of the object.

Figure 2.12 is an example of such a technique (Hoffman, 1996): a series of intersecting planes is used to represent a house, onto which 77 geometrically referenced images (from 6 different photographs) are mapped. The positions of the surfaces making up the model were obtained through photogrammetric measurement. Steps 3 and 4 from the previous section are then carried out as the model is assembled using VRML and then viewed using CosmoWorlds software.

Photo-realism does not necessarily require the use of actual photography. In reconstructing structures from a bygone era, a realistic portrayal can be achieved using suitable, synthetic textures, as shown in Figure 2.13 (Haval, 1999). Using a geometrical model of an object or objects, which can be constructed from photogrammetric measurements, and texture-mapping suitable colours and lighting effects onto it, a CAD-based 3D model of the structure is constructed. It should be evident from Figure 2.13 that complex surfaces can be constructed using CAD so that, although not every part of the object surface has been measured, a comprehensive model can be built.

Figure 2.13 CAD-based surface reconstruction using artificial lighting and texture (Haval, 1999).

There are two main categories of models used in architectural and archaeological visualisation of monuments, each with associated benefits and drawbacks. Daniels (1997) gives a detailed summary which is outlined below and tabulated in Table 2.3.

Table 2.3 A summary of the types of models used in visualisation.

Type of model	Composition	Advantages	Disadvantages
Surface Models			
Wireframe	Points and lines	Simple	Visualisation is difficult. No interior detail.
True surface	Points, lines and faces	Visualisation is easy	Computationally expensive. No interior detail.
Solid Models			
B rep	Boundary faces, edges and vertices	Holds interior information.	Computationally very expensive. Needs much storage space.
CSG	Primitives	Holds interior information. Numerical stability	Computationally very expensive and difficult to manage. Needs much storage space.
Spatial subdivision	Simple cells	Holds interior information.	Computationally very expensive. Needs much storage space.

2.4.3.1. Surface Models

Surface modelling may be performed using either a simple wire frame or true surface model (Figure 2.14). Visualisation is difficult on the former since the model deals only with the edges of entities rather than surfaces. Details which should be obscured by objects nearer the viewer are not hidden (i.e. the model is transparent) and visual properties such as colour and shadow cannot be applied to the surface, as per Figure 2.13.

True surface models are composed of points, lines and faces. Their limitations compared to other models are that they are more computationally expensive than wireframe models, have no physical property besides surface area, and they have no interior detail (i.e. they do not allow sections to be taken through them, a common practise in archaeology). The *xyz* co-ordinates of the vertices and information about the surfaces are all that is stored (Wood *et al*, 1992). Lighting effects and texture can be applied as in Figure 2.12 and Figure 2.13.

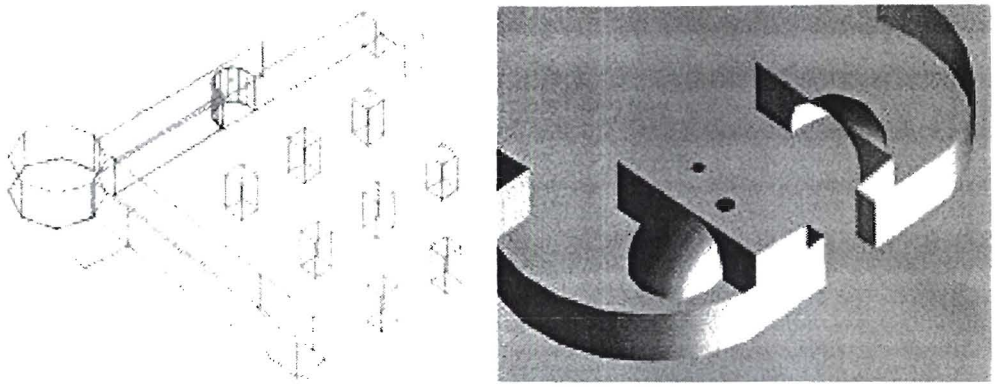

Figure 2.14 Wire frame model of part of Horvat Minnim (left); surface model of entrance to Horvat Minnim (right).

The type of model generated in this thesis is a surface model: there is no information about the interior of the walls of the structures. The techniques of photogrammetry can only be used to record and measure surface data, producing a hollow shell with an enormous amount of surface detail. For purposes of completeness, a description of solid modellers follows.

2.4.3.2. Solid Models

Modelling structure is better performed with a solid modeller, which can be used to help answer questions about the physical properties and economics of construction of a structure. In a surface model we only have information about the outer edge of the walls; a solid model can hold information about the interior of the structure (e.g. the composition of walls such as the dimensions of each stone and the materials used) in 3D. The main disadvantage is that such models are computationally very expensive and take up much more storage space than surface models.

Most solid modelling systems have adopted either constructive solid geometry (CSG) or boundary representation (B Rep) as representations of solids (Daniels, 1997; Vuoskoski, 1996). In addition, Daniels (1997) includes spatial subdivision as a method of representing solids. CSG modellers work with objects made up of primitive solids, such as spheres, cubes and cones, as discussed previously. They have the greatest numerical stability of the three models, although they are computationally

more difficult to manage. B Rep models represent solids using boundary faces, edges and vertices linked together to form a structure. In spatial subdivision models, the model is decomposed into cells, each with a simple structure. The cubic voxels discussed in section 2.4.1 are examples of this.

CHAPTER 3

Review of Related Topics

3.1. Why Photogrammetry?

E. H. Thompson (1962) placed a number of conditions on the beneficial use of photogrammetry for recording and measurement. He stated that photogrammetric methods of measurement are useful only in any of the following circumstances:

1. When the object to be measured is inaccessible or difficult to access;
2. When the object is not rigid and its instantaneous dimensions are required;
3. When it is not certain whether the measurements will be needed;
4. When it is not certain what measurements are required;
5. When contours of the surface are required;
6. When the object is very small (microscopic); or
7. When direct measurement by some other means (theodolite, tape, etc) is impossible, impractical or uneconomical.

Looking at the application of digital photogrammetry to archaeology and architecture, we can see that in some circumstances condition 1 applies: structures and objects of archaeological significance are often fragile and / or difficult to reach. Conditions 3 and 4 almost definitely apply in a number of circumstances; photogrammetry allows a relatively easy way of gathering a large amount of data, which may be processed in various different ways. Contours, or at least, DSMs formed the core of the research done in this thesis; thus condition 5 is fulfilled. Condition 7 is also readily fulfilled here: it would be nearly impossible, definitely impractical, and quite uneconomical for the survey to have been carried out 'by hand', using a theodolite, EDM (Electronic Distance Measurement) or tape. Conditions 2 and 6 do not apply. Following Thompson's conditions, then, photogrammetry is (at least) a useful method of obtaining measurements of archaeological buildings.

As we have seen from CHAPTER 2, photogrammetry concerns the accurate measurement and analysis of photographic images. Originally developed for aerial mapping, it can equally well be used at ground level to record, in three dimensions, the form of structures both natural and man-made (Biddle, 1991). Through the continuous development of digital photogrammetric methods the application of photogrammetry to archaeology has been positively affected by providing a means for the rapid and satisfactory geometric documentation of monuments (buildings, ruins, statues etc.) (Ioannidis *et al*, 1997).

Regarding archaeology, the discipline is concerned with material culture and has a great need for visual information in describing its data (Daniels, 1997). Human communication and orientation naturally rely heavily on visual information. Consequently an objective, visual representation and description of the actual state of the buildings or structures under investigation forms a necessary basis for all subsequent investigation, including work for conserving and restoring these historic structures (Heckes & Hornschuch, 1997). Photogrammetry provides such a visual basis.

Considering architecture, terrestrial photogrammetric techniques are used to provide an inventory of important historic buildings for conservation, development and restoration work. Graphically, this is done through line drawings and controlled photo mosaics. The former emphasises the object geometry, allowing the interpretation of the architectural history and construction features. By using original photography, the latter shows the actual record of a façade in more detail and with less need for interpretation. A combination of both line drawings and photo mosaics allows a better perception of the building as a whole (Marten *et al*, 1994), permitting us to analyse both its architectural structure as a building and the rate of decay of the building over time.

From the preceding arguments, then, photogrammetry is seen to be a meritorious candidate for the 3D documentation of structures both archaeological and architectural. An overview of some of the work done in this field, both previously and currently underway, follows in the rest of this chapter.

3.2. The 3D Documentation of Structures

According to Reilly and Rahtz (1992), as the quality of recording in the archaeology of buildings improves, and the questioning of data becomes more demanding in terms of accuracy of detail, the traditional 2D methods of representation of this data are proving inadequate. With the growth in both quantity and complexity of data, they propose a corresponding increase in the sophistication of analysis and display techniques called upon in investigations. These will help researchers to explore and understand the form, structure and content of objects. The methods of display may comprise of simple 2D graphics and scatter charts, 2D slices derived from 3D assemblages, 3D interactive, object-oriented graphics, or full 3D interactive visualisation systems including volume renderers.

With regard to architectural construction and preservation, Xu & Zhu (1998) stress the importance of utilising 3D models in the design phase, construction phase and the documentation of the completed structure. They stress that interpretations of 2D blueprints are subject to ambiguity and may differ from one designer to the next. Chalmers *et al* (1996) share the same view: static images are useful for providing impressions of a site, but far greater insight can be obtained by interactive, 3D visualisation. Daniels (1997) supports the call for 3D representation of data, both for publication of results and for recording and research, saying that it is becoming both desirable and, often, necessary. Since the archaeological discipline has a great need for visual information in describing its data, the enhanced ability to conceptualise data using three dimensions is obviously of great benefit to the discipline. In fact, Daniels goes on to say that "... it is very difficult, and often dangerous, to manipulate three-dimensional data unless one can visualise it in some way". In other words, misinterpretation is easy.

Sims (1997) discusses the relevance of 3D archaeological / architectural modelling. He begins by asking, "are architectural reconstructions in computer graphics a helpful research tool, or just pretty pictures...?" For example, a virtual model of Stonehenge serves not only as an educational tool, but it aids in research as well. A similar reconstruction of part of a library in Ephesus assists in the partial, physical

reconstruction of the building. Using these two examples, Sims supports virtual reality reconstructions both for education and research. Mathur (1997) discusses this topic further. Regarding the benefits of virtual reality and visualisation and their application to archaeology, he cautions that artificially reconstructed models can serve only as tools for developing new hypotheses or extending existing ideas. "No one model … can unlock the mysteries of the past." It is also possible to become misled by reconstructions that look good but are inaccurate. Computer graphics can fool the scientist and lay person alike into believing that speculations and hypotheses are proven fact. Mathur acknowledges the importance of GIS in archaeology and shows that the emergence of virtual reality visualisation systems has positively impacted this field.

As we saw in section 2.4, there are different types of 3D models with varying degrees of simplification, some of which will not be accurate enough for use in the measurement of ancient buildings. These may still suffice for building documentation and in gaining understanding of how our ancestors lived. Various examples can be found on the Internet: see for example Baum *et al* (1998) and Chalmers *et al* (1996), as compared to Hoffman (1996).

Of the texts reviewed (and in the opinion of the author) all authors concur that 3D modelling and visualisation of artefacts gives far greater insight and is more useful on the whole than 2D representations of the data. There are pitfalls with regards inaccuracy, as identified by Mathur (1997), Sims (1997) and Chalmers *et al* (1996), among others, and it is important that the user of the model be made aware of these.

In the following sections, some examples of work done using different model types will be presented. This review is not all-inclusive, but serves as an illustration of what is possible.

3.2.1. Modelling of Architectural Structures

Possibly the simplest, quickest and easiest way of reconstructing an object in 3D is by using so-called CAD-based methods of reconstruction. As we have seen in section

2.4.3, these involve the use of primitive shapes and artificial texture and lighting in order to create a realistic impression. Actual photography may also be used, where this is available, to give an even more convincing effect. Examples of both of these cases will be given below. Buildings can generally be approximated by primitive entities such as planes and, occasionally, curved shapes too; this makes the documentation of architectural structures a natural candidate for CAD-based photogrammetric measurement.

Xu & Zhu (1998) describe their efforts of building a 3D digital documentation of a large-scale timber structure, the Chi Lin Nunnery in Hong Kong. 3D simulation of the physical reconstruction and quality control during construction were also effected. Additionally, they looked at the pros and cons of various software packages in terms of reconstruction. After the photogrammetric survey, AutoCAD with AutoLISP programming language, was used to recreate components of the structure in 3D, using line frame and solid body modelling. Where the CAD system could not adequately represent the intricacies of the surfaces, Adobe Photoshop was used to merge colour photography of the structures with the CAD model. A 'digital reconstruction' was carried out prior to the physical reconstruction to check for errors in design and inaccuracies in construction, and to plan the sequence of reconstruction. A significant problem encountered was the quantity of data to be processed and presented by the computer, which could be extremely time-consuming.

The high degree of description afforded through the use of photo-realistic or ortho-image texture data cannot be achieved using standard vector data. Colombo (1998) uses this fact to reinforce the benefit of using raster data for the representation of building façades. He created a photo-textured virtual model of a mansion, the "House of Harlequin", in North Italy, using a CAD modeller. Some details could not be reconstructed photogrammetrically (see section 2.3.4.4(b)) and these were filled in by direct measurements with artificial texture applied. The façades were assumed to be

planar and so 'orthoginalisation' of the images was carried out using simple rectifications (so-called 'rubber sheeting'[2]).

The aim of the model is as a reference for linking historical, architectural and thematic hypertexts within an Internet or Intranet database. Colombo envisages this as eventually leading to inclusion in a GIS compilation. He, too, mentioned access time and data transfer rate as a hindrance to the process (using Pentium II 333 MHz processors, as used by the author for this thesis).

Similar projects were carried out by Mason and Streilein (1996) and Henrickson *et al* (1996), although on a larger scale. They looked at methods of reconstructing entire cities in 3D. In terms of visualisation, such a 3D city model would be useful for planning, property management, emergency services, environmental analyses as well as reconstruction of past cityscapes. The models may also be used as components in GIS for information management.

The technique described by Mason and Streilein differs from those mentioned above in that aerial photogrammetry is a first step. A DSM of the entire area to be modelled is generated from aerial imagery; this includes the buildings as part of the model (a 3D volume model as per Bill & Fritsch (1991), see section 2.3.4.1(b)). Each major planar roof component was measured separately using a Wild AC3 analytical plotter. This was output to AutoCAD in DXF format. Building walls were inferred by projecting the roof boundaries down onto the underlying DTM. Mason and Streilein identify four different techniques by which this may be accomplished:

1. *Façade reconstruction by roof boundary projection:* each wall is inferred by vertically projecting the two vertices of each roof boundary line onto the DTM. Eaves can be modelled by offsetting the inferred wall, assuming verticality.
2. *Façade reconstruction by ground plan projection:* building plan boundary lines are projected vertically to intersect with the associated roof models.
3. *Façade reconstruction by vectorial densification of simple façade models:* terrestrial imagery can be applied to either of the above two models, adding vectorial information to the façade. Mason and Streilein used this method.

[2] 'Rubber-sheeting' is the process whereby images are stretched to fit to a surface usually described by primitive entities. The topography of the surface is not taken into consideration during the rectification process, and so a 'rubber-sheeted' image is not a true ortho-image.

4. *Façade reconstruction by 3D photogrammetric measurement:* the connection of roof models to reconstructed façades is made via measurement of common point features in a common datum. The façades are reconstructed photogrammetrically using stereo or convergent terrestrial imagery. This is the type of reconstruction carried out in this thesis (using stereo photography and without the roof model).

The texture data was referenced to the façade reconstructions by a series of surveyed control points. The boundaries of the texture data have to correspond exactly to the geometry of the surface onto which it is mapped if the texture model is to be geometrically correct.

Henrickson *et al* (1996) describe two automated methods for building reconstruction from aerial images. TOBAGO (Topology Builder for the Automated Generation of 3D Objects from Point Clouds) is a semi-automatic routine requiring complete and accurately measured 3D points, a building model catalogue, and an operator capable of subdividing complex roofs into manageable roof units. ARUBA (Automatic Reconstruction of Sub-Urban Buildings from Aerial Images) is a fully automatic building reconstruction system which makes effective use of the known 2D and 3D information present in several images of a site. The final result is a complete CAD model of the building roof and walls. Problems arise in areas of shadow and for complex roof structures.

Besides the need for higher levels of automation and greater computing power, Mason and Streilein also identified protrusions such as window sills and balconies as a difficulty in creating texture-mapped façades. Marten *et al* (1994) propose splitting façades into different planes which can be projected independently. The object geometry for digital rectification of the images was provided by analytical stereo measurements combined with a CAD system to define the planar wall structure. Ortho-images are generated by 'rubber-sheeting'. The errors incurred should not be too great using the technique of Marten *et al* because, by splitting the surface up into sections, each segment can be individually modelled by a plane. The smaller the segment, the less the inaccuracy due to 'rubber-sheeting' of the image.

The methods described above are examples of work done using CAD to help create a 3D representation of an object (besides the latter which addresses a particular problem common to all architectural photogrammetry). To follow is a description of instances

where CAD-based techniques form an integral part of not only the 3D reconstruction, but processes of feature extraction and compilation as well.

Streilein (1994) states that "as photogrammetry generally records all data as a series of three-dimensional coordinates [*sic*], it makes a natural partner for today's three-dimensional CAD systems." The team at the Institute of Geodesy and Photogrammetry of ETH Zurich have used this relationship in the development of their Digital Photogrammetry and Architectural Design (DIPAD) system. A description of DIPAD can be found in section 3.3.1.

Streilein and Niederöst (1998) used the DIPAD technique to document the ancient, 7th century monastery of Disentis, in Switzerland. They used a total of 49 images to cover the entire structure, including 19 taken from a helicopter platform. The monastery has a more or less rectangular form, with two rectangular towers at one end. As an initial approximation for the DIPAD program, a CAD model consisting of a cuboid with the approximate dimensions of the building, and two vertical cuboids defining the towers, was created. Successive iterations produced a refined CAD model of the building.

Another hybrid, low-cost photogrammetric system is presented by Luhmann (1998), also described in section 3.3.1. The historic Powder Tower of Oldenburg was one of the structures photogrammetrically surveyed and 3D points were intersected on the exterior walls using PHIDIAS software. The results were transferred to AutoCAD for further processing, and 2D drawings and a cylindrical projection (see section 4.3.1 for an example related to this thesis) were derived therefrom.

Hanke and Ebrahim (1997a) have developed an approach to creating 3D, CAD-based models from photogrammetric data, which they call a "digital projector". The concept involves an object-oriented 3D restitution of the whole object aimed at reversing the situation during exposure. There are three main steps:

1. The interior and exterior orientation of the camera are found, and the building's outlines and faces are reconstructed from the bundle adjustment and / or from an analytical plotter.
2. This framework is edited within a CAD environment and additional measurements (tape, theodolite, etc.) are added where necessary. The wireframe model will then

be converted to a surface model, the faces of which will serve as "projection screens".

3. The photographs are projected onto the faces of the surface model using the camera's interior geometry and relative position, creating a complete 3D computer model.

With this method, it is not difficult to combine photography from different sources or at different scales, as long as it is projected onto the surface model using the correct parameters. It also becomes easy to combine inner and outer walls into one model. The authors claim to be able to create ortho-images of single façades from the 3D model, but they do not describe how this is done. Henrickson *et al* (1996) maintain that this procedure of projecting images onto façades is equivalent to digital rectification and that ortho-images are produced.

Departing from the CAD-based techniques described above, Koch (1994) has developed a model-based 3D scene analysis system using stereoscopic imagery. The system analyses scenes from an arbitrarily moving stereoscopic video system, and segments them into smooth surfaces. These it stores in a 3D scene model, including surface texture. Image matching is done by correlation on the basis of grey level gradients between patches. The likelihood of matches being correct is displayed in a confidence map, and the disparity value obtained for each candidate is likewise displayed in a disparity map (based on local depth measurement only). From the disparities, similarity measures are computed whereby the scene is divided into continuous surfaces. Gaps are filled by interpolation. The 2D depth map is converted into a 3D surface description by spanning a triangular wireframe in space for each segmented object surface. For each triangular patch, the corresponding image texture is stored and used to synthesise computer-generated views.

The Internet hosts many examples of the use of computer modelling to create virtual 3D models, mostly CAD-based. See for example Miliano (1999), who uses the advanced visualisation capabilities of a 3D game engine to create 3D architectural models; and Campbell & Wells (1994), who discuss how virtual reality can be implemented into the architectural design process, identifying some of the benefits and shortcomings of the use of virtual reality in the design process.

3.2.2. Modelling of Archaeological Structures

It is not always possible to assume that an object is made up of regular shapes when dealing with archaeological subjects. Consequently, the predominantly CAD-based techniques described in the previous section will not be as applicable here. Modelling of archaeological structures takes on varying forms, depending on the purpose of the model. For our purposes, it will be split into modelling of the structure as it stands today (section 3.2.2.1, as per section 4.3.3), and recreating the structure as it may once have existed, based on existing data (section 3.2.2.2, as per section 4.3.2). To a large degree, the two go hand in hand.

3.2.2.1. Documenting Existing Structures

Heckes & Hornschuch (1997) give five examples from their experience of documenting existing structures. The first three, the Bahla Fortress in the Sultanate of Oman, the Siwa Oasis in Egypt, and the imperial burial mound Yongding-Ling in China, represent examples of objects with a very irregular surface. For accurate documentation of these sites, dense elevation models were required. On the other hand, the Kaiserdom at Köningslutter in Germany and an image map of the town Linzi, China, represent examples where surfaces can be described by simple geometrical forms (a CAD model) as discussed previously.

For the Bahla Fortress a surface model with a grid spacing of 10 cm was measured across the outer wall using an analytical plotter, after which orthophotos were created. Automatic DEM generation was used for the oracle temple on Mount Arghumi at the Siwa Oasis. To preserve this important feature, a reconstruction of the entire oracle area was planned, requiring large-scale maps. The irregularity of the terrain, including existing structures and eroded hillsides, posed a serious difficulty for image matching. Heckes and Hornschuch state that "those matching procedures available today do not offer sufficiently reliable data for close range applications when dealing with abrupt changes in curvature." Consequently, some areas had to be filled in manually or, where possible, interpolated from the surrounding data.

In reconstructing the northern transept of the Kaiserdom, geometric information was supplied by analytical photogrammetric techniques and additional

geodetic measurements. A volume model was created and used in an object information system along with documentation of damage sustained to the building. Documentation of earlier restoration works were also integrated into the information system. A photo-realistic presentation of the current state of the building was achieved through texture-mapping of the rectified images onto the model. Heckes and Hornschuch hope to continue work on this project, creating an information system that can be used and extended by different scientific disciplines.

Ioannidis *et al* (1997) used line drawings as the predominant means of documenting the aged structures of the Castle of Nerajia on the island of Kos, the Castle of the City of Chios and the Monastery of the 'Nea Moni' on the island of Chios. Vector plan compilations were selected over photomosaics and orthophotomaps as these were not considered a suitable basis for further processing; i.e. they do not accept the inclusion of additional vector information that must go into special architectural plans. For the compilation of the plans, two methods were used:

- Digital rectification was applied to flat surfaces where the accuracy of the detailed restoration was not certain;
- For curved surfaces (towers, domed structures etc.) stereo-restitution in a digital photogrammetric system was chosen.

AutoCAD was used as the CAD package in which the line drawings were compiled. The façades were projected onto pre-defined planes and not compiled in a 3D visualisation as to do so, using primitive shapes, would have led to distortion of the drawings. This serves as an example of a case where the traditional, 2D method of representation is deemed more beneficial than a 3D visualisation.

Similar works to those described above have been done by Eckstein (1997), who describes efforts of recording and restoring stone sculptures, and Adolfsson (1997), with respect to an ancient fortress and the Swedish National Art Museum. The survey and representation of curved surfaces and domes are described by Guerra (1997) and Karras *et al* (1997), as well as Bacigalupo *et al* (1997, 1998); their work will be discussed in section 3.2.3.

Christensen (1999) describes the efforts of a team from IBM at modelling Michelangelo's Florentine Pietà. Michelangelo began work on the statue while in his 70s, but never completed it. Two years after he had stopped working on it, he attacked the statue with a sledgehammer. Through 3D computer reconstruction, the IBM team hopes to be able to distinguish between the work of Michelangelo and the later addition of his apprentice, and to propose an hypothesis as to why Michelangelo tried to destroy the statue. Abouaf (1999) gives a detailed account of how the survey was carried out and the digital reconstruction begun. A six-lens Virtuoso camera was used to capture a true, 3D model of the structure (as per Kraus (1997), see section 2.3.4.1(b)).

A pattern of stripes was projected onto the sculpture to provide texture for matching. Six images of each region of the statue were captured simultaneously using the Virtuoso camera. A 2 mm point spacing was used in order to model the structure accurately. These points were triangulated into a TIN surface, and each TIN surface was combined into one smooth model. With texture data supplied by the cameras, a realistic impression of the statue was achieved to sub-millimetre accuracy: enough detail to be able to see the tool marks left by Michelangelo.

Five benefits associated with the application of digital technology to the mapping of the statue are given by Abouaf:

1. Convenience and interaction: people can view the statue through the 3D computer model in ways otherwise not available;
2. Precision: the recording method used gave precision of the order of 1 mm in the digital model;
3. Problem solving: identifying which parts of the sculpture are original and which have been added at a later stage;
4. Documentation;
5. Stimulating new research.

Whether a CAD-based description is used, line drawings, or a DEM with image data texture-mapped onto it, the documentation of existing archaeological structures is a difficult and on-going task. In the next section, the presentation of structures as they may once have existed, is discussed.

3.2.2.2. Recreating Structures from Archaeological Evidence

According to Chalmers *et al* (1996), by combining archaeology and computer science expertise, 3D computer reconstructions and interactive photo-realistic visualisations of archaeological sites may be realised. These will "enable archaeologists to evaluate hypotheses concerning ritual performances, site utilisation, structure, contents and development of the area." Mathur (1997) states that the new and developing computer technologies allow for better and more efficient analysis and display of archaeological data.

For example, Nikihilesh Haval (1999) records a process of documenting and visualising the ancient royal residence of Fatehpur Sikri in India (Figure 2.13 and Figure 4.38). The necessary data was provided through detailed plans, elevations, sections and photographs of this world famous heritage building. The CAD models of this complex were utilised to prepare a real time virtual walkthrough. Haval identifies one of the main difficulties he encountered as being computer processing time and memory restrictions. The first four of the twenty-one structures were reconstructed using PC level computers (Pentium-II 300 MHz with 128 MB RAM). Although the level of detail was satisfactory for still images and animations, faster computers were required to complete the whole palace complex. Due to the high complexity of the model, the hardware used was upgraded to computers with specifications like Dual Pentium-II 400 MHz with 512 MB RAM and Dual Pentium-II 300 MHz with 384 MB RAM.

These types of reconstructions are also useful from a tourism point of view. The Roman civic bath complex in the city of Bath is one of the most visited monuments in England, with around one million visitors each year. A computerised model has been developed which helps visitors comprehend what it is they're looking at (Reilly, 1992). Their experience of the site is enhanced as they can both see the ruins as they stand today and get a feel for what it must have been like when the complex was originally built. The model was created by a team led by J. Woodwark in the 1980s. They used solid modelling to create the model, with only one primitive solid: the planar half-space. Woodwark (1991) reports that this may have been the first application of solid modelling to archaeological reconstruction.

Chalmers *et al* take the reconstruction process one step further by adding artificial lighting and effects such as smoke and dust. By using these effects, hypotheses can be made by archaeologists concerning the utilisation and purpose of ancient sites. The various stages of construction can also be investigated using digital models. Chalmers *et al* give the example of the Ggantija temple in Malta, whereby "the intervisibility and spatial interaction of the participating audience and various priests can only be assessed through alternative reconstructions of the contemporary architecture, ritual furniture and liturgical artefacts." With interactive visualisations, ritual hypotheses can consequently be tested.

The Internet hosts many more examples of archaeological visualisation. See for example Heine (1999), who looks at the visualisation and documentation of ancient Maya sites.

3.2.3. Other Surface Measurement Techniques

Photogrammetry alone is not always sufficient for the documentation of structures. It is not always the most efficient method available due to physical and/or time constraints. A review of some literature concerning the use of photogrammetry in conjunction with other techniques for the 3D documentation of structures, particularly laser-mapping, follows below. The techniques described rely on photogrammetry to provide realistic texture data for orthophotos etc., but use other methods to derive 3D point or surface data.

The survey of historic monuments and sites generally requires a large amount of manual processing, even when photogrammetric techniques are used. Kleiner and Wehr (1993) sought to speed up the process of object measurement and created their 4D-LaserScanner (4D-LS) system that directly measures the 3D co-ordinates of a surface. By measuring the phase difference between a transmitted and a received laser signal and the direction to the surface, the distance to the surface can be calculated in three dimensions. The fourth dimension is given by the intensity of the returning signal, from which an image of the surface can be derived. Although this is not a

realistic image, orthographic projections of the image and 3D points can be used to create orthophotos of a scene.

El-Hakim *et al* (1998) use a similar technique incorporating texture data as well. They have designed a Data Collection and Registration (DCR) system consisting of a 233 MHz Pentium computer, 12 CCD (charged couple device) cameras, 1 laser sensor mounted on a computer-controlled pan-tilt unit, and 1 digital still colour camera similarly mounted. Range and texture data are acquired simultaneously for the entire object surface and a triangulated mesh generated. During registration, the images and 3D data are positioned and oriented in the same co-ordinate system, after which the images from either the CCD sensors or digital camera are mapped onto the geometric model. An important consideration was obtaining as realistic a representation as possible, both geometrically and in terms of texture, while allowing real-time interaction in terms of visualisation of the models. The size of the geometrical model therefore had to be kept manageable.

Balletti and Pilot (1998), Guerra (1997), Karras *et al* (1997), and Bacigalupo *et al* (1997, 1998) describe methods of documenting aged architectural structures which are difficult to access or present difficult surfaces for photogrammetric mapping. The Torazzo of Cremona, Italy, was surveyed by Balletti and Pilot using laser ranging combined with conventional topographic and photogrammetric surveys. Laser ranging was used to provide co-ordinates of points on the exterior of the tower as well as photogrammetric control points on the walls. In this way, nearly 20000 points were surveyed. The interior surfaces were also surveyed using laser ranging. Image texture was applied to the model by rectifying ('rubber-sheeting') and mosaicking images of the exterior tower walls.

Bacigalupo *et al* describe the process of documenting domed structures in Uzbekistan. An exact, geometrical construction of the domes represents a tool of "fundamental importance" for understanding the design and construction of these complex structures (Bacigalupo *et al*, 1998). They did not have sufficient room for a complete, stereoscopic, photogrammetric survey of some of the domes; the geometrical configuration of the classical stereo photogrammetry is not suitable because of short bases, sloping sights and acute angles. They hence integrated

geodetic and photogrammetric techniques that helped with the monitoring of structural disruptions.

3.3. Software

In any project the choice of software is important and may greatly influence the results of the analysis. For this reason, a description of some of the available software for photogrammetric processing is given below. Bearing in mind the rate at which software are being improved or upgraded and new software developed, this is not a comprehensive review. An overview of close-range photogrammetric software available in 1989 is given by Rüther (1989), which serves to aid both the photogrammetrist interested in purchasing software, and the programmer interested in writing a new package. Although now a decade old, this review still shows the plethora of photogrammetric software available and highlights the large degree of choice on hand. The reasons behind the choice of software that was made for this project are given in section 4.1.2.

The review below is divided into two sections. Section 3.3.1 deals with both commercial and "in-house" photogrammetric systems such as those described by Rüther (1989). Section 3.3.2 deals with Digital Photogrammetric Workstations, which are designed primarily for large aerial photogrammetry projects

3.3.1. Photogrammetric Software

DIPAD, developed at the Institute of Geodesy and Photogrammetry, ETH Zurich (Streilein, 1994), aims to:

- improve photogrammetric data acquisition and processing,
- improve the creation of 3D geometric object descriptions, and
- create a photo-realistic visualisation and guided architectural processing.

Architects work nowadays with digital models instead of plans. In many cases line drawings are not sufficient for the representation of an architectural object. The photogrammetric analysis which DIPAD delivers is a 3D geometric and semantic

object description. This allows the automatic creation of what Streilein (1995) calls a Digital Surface Model in a CAAD (Computer Aided Architectural Design) environment, which represents the object by surfaces instead of lines. The CAAD system pre-processes the data and stores it in databases adapted to architectural purposes. The system allows efficient data transformations into other representations and is suitable for documentation and visualisation, and for complex simulations, manipulations and analysis of the object.

The operator performs the 3D reconstruction without any manual measurements; his job is to interpret the scene qualitatively and select features to be measured. Measurement and data management are done by the computer using two different, semi-automatic measurement routines: least squares matching (section 2.3.4.3(a)) and CAD-based 3D feature extraction (briefly described below). The former measures the precise position of pre-defined points, and the latter measures architectural features.

The idea behind CAD-based 3D feature extraction is to reverse the designing process of the architect by locating the edges of features to be measured and then deriving vertices as intersections of the appropriate lines. Input to the system comes in the form of digital images and *a priori* architectural knowledge of the system as a coarse CAD model. The CAD model is iteratively refined as feature extraction progresses. The photogrammetric processing results are converted into a CAAD format via AutoLISP. The CAAD system is used for documentation and visualisation, as well as simulations and analysis of the object.

Luhmann's (1998) system is designed for the recording of large engineering objects in characteristically complex environments. It aims at:

- Recording of large objects;
- Processing of natural, non-targeted objects;
- Medium accuracy requirements;
- Difficult environmental conditions; and
- Results processed as 3D CAD data.

Image acquisition is analogue, digitisation coming in the form of low-cost, desktop scanners. Image processing is performed interactively in a CAD environment which incorporates photogrammetric solutions. PHIDIAS, PHIDIAS-MS and Rollei

CDW multi-image compiling systems were used. An image database was also developed to help keep track of the many images required to record large structures.

PHAUST (Photogrammetrische Auswertestation für digitale Bilder) is a photogrammetric evaluation system for digital images developed at the Institut für Photogrammetrie und Bildverarbeitung (Woytowicz, 1993). It is somewhat out of date as it works on a 486, DOS-based PC, but in terms of performance and results it is not yet obsolete. It has applications in architectural photogrammetry, where image rectification is an essential feature, and in accident scenes, an application of multi-image rectification.

Kempa & Schlüter (1993) compare the performance of Facets Stereo Vision, developed by Wrobel (1987), with that of a photogrammetric operator using the LEICA AC3 analytical plotter. The test objects were parts of a cross column on an aged monastery. The resultant DEMs were compared and it was found that those produced by Facets Stereo Vision were smoother than those produced by the operator. Qualitatively, the surface topographies corresponded. Kempa and Schlüter concluded that Facets Stereo Vision was capable of performing with the same accuracy as a photogrammetric operator.

The low cost, photogrammetric, softcopy, close-range program, PhotoModeler, developed by EOS Systems, is reviewed by Hanke and Ebrahim (1997b). The test field was two brick walls with good contrast and a 120° intersection. The investigation aimed at obtaining the accuracy of the software in architectural and archaeological applications. Hanke and Ebrahim reported that PhotoModeler "showed its competence for a wide area of photogrammetric applications". Collins (1998) describes it as "a viable tool for architectural photogrammetry", although he admits that it is not a "true" photogrammetric system (i.e. not stereo-photogrammetry). The production of orthophotos is also possible using PhotoModeler, although the orthophoto is created using a surface model created by the user in PhotoModeler. The more detailed and accurate the surface model drawn by the user, the better the orthophoto will look. This is not like the orthophotos created by topographic photogrammetric systems that use dense point DEMs. It is designed primarily for

man-made objects with surfaces that can be described well by large triangular elements.

3D-Builder is a low-cost "photogrammetric" tool which combines information from a large number of photographs of simple or complicated objects, extracts information and merges data into a single, 3D model for export to a range of applications (Patias *et al*, 1998). It was tested against the strict photogrammetric close-range multi-photo software, Rollei CDW-2000, the test field being an archaeological wall. Patias *et al* report that the kinds of accuracies attainable suit the needs of architects and archaeologists who regularly map at scales of 1:25, even though the attainable accuracy was much worse than for the Rollei system. They conclude that 3D-Builder "and the software of this kind should not be underestimated by [photogrammetrists] since their functionality is quite adequate for a range of close range applications."

3.3.2. Digital Photogrammetric Workstations (DPWs)

The *Proceedings of the OEEPE - Workshop on Application of Digital Photogrammetric Workstations* (1996) gives a good account of the operation, user-friendliness and application of DPWs. Kölbl (1996a) begins with a broad summary of the use of DPWs in practice. He stresses the applicability of photogrammetry to GIS and highlights the growing need for DPWs to perform data extraction and integration into GIS, as well as the traditional photogrammetric operations. The difficulty of spatial (3D) representation in this regard is mentioned. The benefits of using DPWs are discussed, bearing in mind the difficulty and time delay associated with learning new software, as compared to an experienced photogrammetrist using an analogue plotter.

Kölbl (1996b) goes on to give an overview of commercial software products for digital, aerial triangulation. He compares

- the DCCS software of Helava,
- the DPW aerial triangulation package HATS (Helava Aerial Triangulation Software) incorporated into SOCET SET, and
- the software of the ImageStation of Intergraph.

Kölbl's experiences with regard to HATS are verified by Kersten and O'Sullivan (1996). Kersten and O'Sullivan identified extreme height differences, among other factors, as a problem for the correlation algorithm. In contrast, aerial triangulation on the ImageStation was described by Kölbl as "very efficient". The only drawback described is that image correlation for points transfer was unreliable and led to several mismatches. Kölbl concludes that the cumbersome error correction of HATS eliminates the advantages offered by this system, although Kersten and O'Sullivan recommend it for use in production. The latter authors also recommend extensive training and the use of well documented user manuals if operators are to reap the benefits of the software. The Intergraph approach, although "more primitive" (Kölbl, 1996b), is more efficient. The DCCS has fallen into disuse and so is not described here.

After triangulation, the natural next step is DTM generation. Dupéret (1996) and Torre & Ruiz (1996) discuss this process with regards SOCET SET of Helava and MATCH-T of Intergraph respectively. Dupéret carried out a case study of aerial photogrammetry on different terrains to produce DTMs. The terrains chosen were flat without trees, rolling with hedges, and flat using images of average quality, respectively. The editing of the DTMs is described in some detail. He concludes that:

- ground obstructions can be easily removed,
- data merging allows the creation of a DTM which describes the surface properly, and,
- although correlation gives a good description of the ground surface, editing is imperative.

Gasior (1996) concludes that the Helava system is "one of the most interesting and versatile systems ... that can be obtained on the market."

Torre and Ruiz (1996) perform similar tests using MATCH-T. They found that, even with the inclusion of breaklines, it was difficult to obtain cartographic-quality contours.

The discussion concerning MATCH-T is continued by Ackermann (1996), who focuses on general image matching problems and solutions and explains how these are dealt with using MATCH-T. He recommends feature-based matching over area-

based matching for DEM generation, unless the accuracy of individual points is essential. Concerning the problem of vegetation and occlusion, he recommends a multi-sensor approach as "the only feasible solution" (see section 3.2.3).

Bacher (1998) reviews the DPW770 of Leica-Helava, of which SOCET SET is the software component. He compares Adaptive and Non-Adaptive Automatic Terrain Extraction techniques, concluding that the Adaptive technique is the best under the test conditions. He also identifies areas of vegetation and very steep terrain, as well as built-up regions, as problem areas. The results can be improved by filtering, but he states that manual post-editing is almost always necessary in these cases.

A thorough comparison of four DPWs is carried out by Baltsavias and Käser (1998). The Leica-Helava DPW770, Zeiss PHODIS, Autometric Softplotter and INPHO MATCH-T are evaluated in terms of DTM generation and, in the case of the first three, orthophoto production. As far as DTM generation is concerned, the results differed significantly between systems, relying heavily on the choice of many poorly explained matching parameters. Time consuming manual editing of points was necessary in each case. In ortho-image generation, Baltsavias and Käser reported that the radiometric differences between the different systems' respective output were higher than expected.

CHAPTER 4

Presentation of Results

4.1. Preliminary Information

According to the requirement of the Getty Conservation Institute, the following surveys of Horvat Minnim had to be carried out:

- Close-range-photogrammetric survey of the remaining wall wherever possible and where significant sections of the wall are visible;
- Topographic survey of the area of the ruins as well as the area surrounding the ruins.

To this end, the following deliverables were required:

1. Scanned UMK stereo images (scanning resolution: 50 micron);
2. Contour maps of all recorded walls;
3. Stone-by-stone line-drawings of all recorded walls;
4. Ortho-images of all recorded walls;
5. A topographic map of the excavated area and surrounds showing all walls and features not covered by vegetation or otherwise obscured.

4.1.1. Photogrammetric Control Survey

4.1.1.1. Data acquisition and analysis procedures

1. The survey design took the following into account:
   - Positioning of the photogrammetric base lines, taking care to cover all visible and significant walls with photography;
   - Positioning of control points both on the walls and around the site;
   - Design of reference network.
2. Data acquisition, both survey and photogrammetric, incorporated:

⇒ Survey

- Survey of reference network (27 reference points, Δ in Figure 4.1);
- Position survey of control points (450 points);
- Vertical angle measurements (triangulation).

⇒ Photogrammetry

- Stereo-photography with UMK (approximately 100 baselines, T in Figure 4.1, or approximately 200 photographs);
- Fill-in photography with DCS;
- Supporting photography with conventional 35 mm camera;
- Survey of base line end points;
- Tacheometric survey.

3. The data analysis undertaken involved:

⇒ Survey

- Least squares adjustment of the reference network;
- Adjustment of levelling network;
- Computation of positions and heights of:
  - control point positions (accurate to less than 0,5 cm in x and y),
  - camera baseline endpoints,
  - tacheometric points (walls, structures, vegetation, terrain);
- Production of topographic map in AutoCAD format.

⇒ Photogrammetry

- Image scanning;
- Relative orientation;
- Absolute orientation;
- Line drawings in 3D-format and transfer to AutoCAD format;
- Editing of line drawings;
- Image matching;
- DSM generation;
- Ortho-image generation.

The camera positions for all stereo pairs were established with the aid of a handheld view-finder to guarantee full coverage of all significant features. The baseline points

were later surveyed at a low accuracy (± 5 cm) in order to provide provisional co-ordinates for a bundle adjustment. The positions of the baselines (T in Figure 4.1) were chosen at an average distance of 4 m from the wall (image scale 1 in 40) varying from 3 m (i.e. 1 in 30) to 12 m (i.e. 1 in 120). The base/height ratio (the ratio of the distance between camera stations and the distance from the wall) was chosen to be between 1 in 5 and 1 in 10, with most overlaps being taken with a 1:5 ratio. Difficulties were experienced in the selection of some of the base lines as a result of space limitation; this was especially difficult in the west section of the structure with its small rooms and high walls (the top end of Figure 4.1).

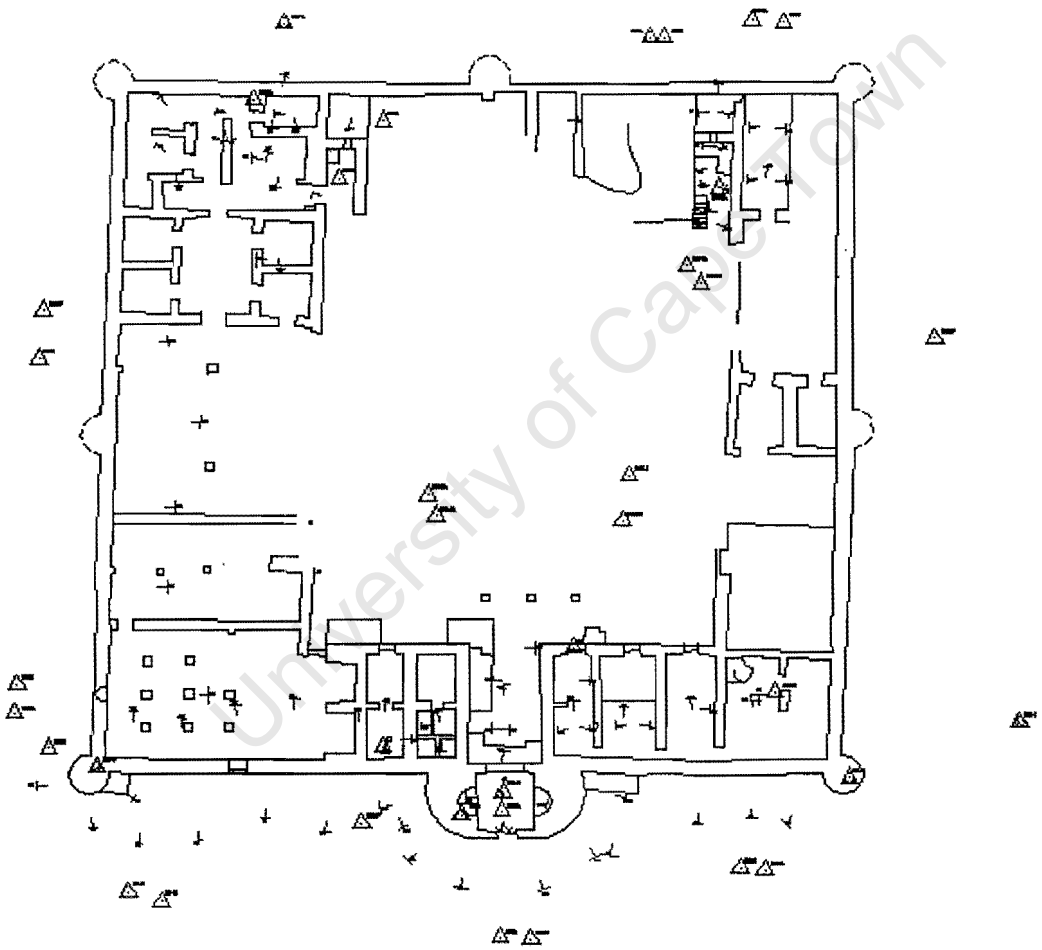

Figure 4.1 Horvat Minnim plan showing survey control points (Δ) and camera baselines (T).

Once the base lines were established a total of 450 control points was placed in suitable positions. A minimum of three control points, with known co-ordinates, per overlap is required for an absolute orientation, a fourth point is considered essential as

a check. SOCET SET requires at least 5 points. Where possible for this project, six control points were surveyed per stereo-model. The control points were retro-reflective circles on a black cardboard background. Circle diameters varied from 8 mm to 12 mm with a few targets of 10 cm diameter to allow for varying camera object distances. Targets were attached to the walls of the site with wood glue and left in place after completion of the survey as possible damage to the site was feared if the targets were removed[3].

A difficulty with respect to control points (as well as relative orientation) arose when images were taken of the lower wall sections, or taken with the cameras further away from the wall than normal. These contained substantial sections of the surrounding walls, not covered with control, as well as sky. This made relative and absolute orientation difficult if not impossible. To overcome this difficulty, the large (10 cm diameter) targets were attached to 6-foot long wooden stakes and placed on the mounds surrounding the site. For the same reason medium and large targets were attached to the trunks of palm trees and small targets were attached to short wooden pegs placed in front of the problematic wall sections. These additional control points above and below the walls provided a significantly improved control point geometry.

Between the photography and the control point survey, a number of control points were removed through vandalism, making it impossible to use these points in the orientation process. In addition to the missing wall targets at least one of the stake targets was removed. This caused additional survey work and delayed the survey. A more serious difficulty arose from the possibility that some of the survey targets attached to stakes might have been moved without this being noticed. This would result in a poor absolute orientation and thus a poor positioning of the wall section in the overall survey network. However, due to the large number of additional control points, no unsolvable problems were encountered during the data processing stage. It was even possible to find a solution to the triangulation of some stereo-models using

[3] The survey team removed some of the markers after completion of the survey to test the possible damage to the wall, and found that these points could be removed without notable damage. The approximately 450 attached targets obscure a combined area of 0.30 m x 0.30 m; their impact is thus minimal. Final removal of the targets was accomplished by the GCI field team.

either the ADAM TopoCart or Intergraph workstation where SOCET SET could not (due to its requiring more than the minimum number of control points). This solution was then either imported into SOCET SET or, failing this, additional points were manually measured using the systems mentioned and treated as additional control in SOCET SET.

4.1.1.2. Reference co-ordinate system

A local co-ordinate system was defined for the photogrammetric and topographical survey of the site. The origin was chosen as an existing survey point on top of the South 'tower' of the entrance to the site (A in Figure 4.2) which appeared sufficiently stable. A new point, C, was established on the north-east corner tower of the site using a fence post. The direction from point A to point C was adopted as the positive *y* axis of the co-ordinate system (approximate south-to-north axis), thus fully defining the reference system with its origin in A and the positive *x* axis at a right angle to the A-C line (Figure 4.2).

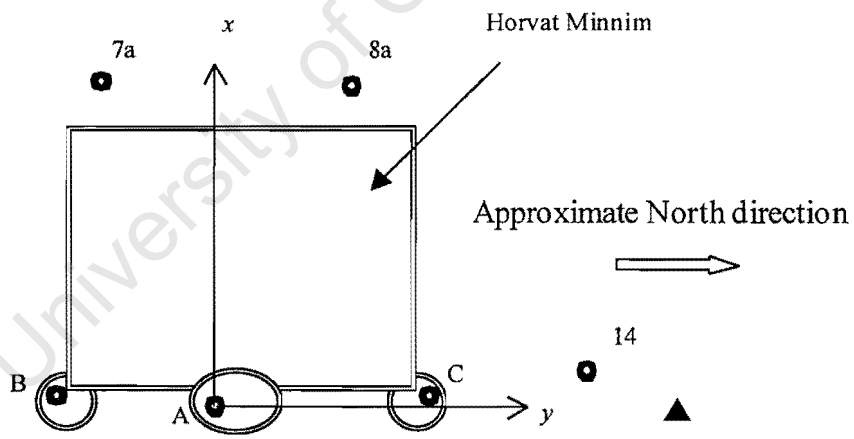

Figure 4.2 Horvat Minnim reference network origin

X, *y* co-ordinate values of 100,00 m and an arbitrary height (*z* co-ordinate) of 50,00 m were adopted for point A. A least-squares adjustment of the entire reference network was based on these co-ordinate values. The standard deviation of all of the points in the reference network (20 in total) from the least squares adjustment, are given in APPENDIX C.

The axis, as defined by points A and C, could not be maintained for all stereo-models in the photogrammetric survey due to the lack of parallelism between the co-ordinate system and the predominant wall direction. In order to produce meaningful and interpretable contours of a wall, it is necessary to refer the contours to a plane which runs approximately parallel to the wall (such that z, distance from the wall, is a function of x and y, distance across the wall and height of the wall respectively). This set-up is also required for DSM generation and can be achieved by aligning the co-ordinate system with the direction of the wall. In Horvat Minnim, this was easily accomplished as all walls were built at approximately right angles to each other (see Figure 4.1). It was therefore possible to rotate the reference system through 90°, or some multiple thereof, and arrive at a situation where $z = f(x, y)$ again. In some cases, stereo-photography was taken of both sides of a wall, necessitating a 180° rotation of the co-ordinate system.

4.1.2. Processing the Data

4.1.2.1. Choice of Digital Photogrammetric Workstation

At the disposal of the author were both the Softcopy Exploitation Tool Set (SOCET SET 4.0.9) DPW of LH Systems, and the Intergraph Image Station Z. DSMs were initially to be created and orthophotos produced using the Image Station Z; however the image matching software, MATCH-T, was not designed to match photography of less then 1:1000 scale. As mentioned in section 4.1.1.1, the images taken of the palace were at a close range and a much larger scale than provided for by MATCH-T. The Image Station Z was therefore unable to create DSMs of the walls, but it was able to triangulate the palace data.

Since a requirement of the project was the extraction of 3D line drawings from the photographs, this was manually attempted using the triangulated models in the Image Station Z, with some success. However, when these line drawings were imported into AutoCAD, they were totally unsatisfactory: lines did not intersect as they should. It was ascertained that neither software package was at fault; the file formats were simply not compatible. An ADAM Topocart was then used for the manual extraction

of 3D line drawings, and these were converted into AutoCAD drawings using an automated scripting function. The entrance and tower sections line drawings are shown in Figure 4.3.

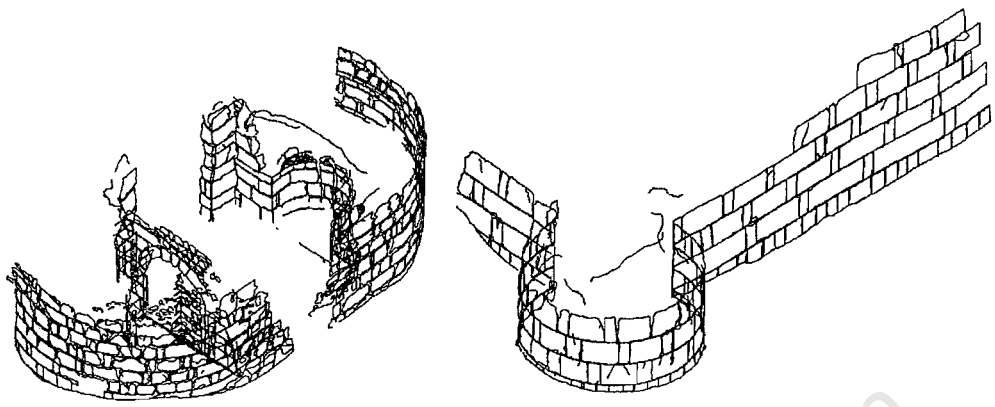

Figure 4.3 Line drawings of Horvat Minnim: entrance (left) and tower (right).

SOCET SET was able to both triangulate the models and extract 'terrain' data (3D points and breaklines) from the images. The DSMs produced were done to a satisfactory accuracy and precision (see section 4.2), and orthophotos were easily created therefrom.

4.1.2.2. Choice of CAD package

Table 4.1 Choice of CAD package

Software	Visualisation	Design	Importing data
MicroStation	Good	Difficult	Fair
AutoCAD	Fair	Easy	Good

In creating a CAD model of the palace, both MicroStation and AutoCAD 2000 were available. The pros and cons of these design packages, according to the requirements of the project, are laid out in Table 4.1. MicroStation proved very good at creating a visualisation of the palace: it was easy to add texture and lighting effects to the planes and cylinders representing the walls. In AutoCAD, this was possible but more tedious. However, creating the planes and cylinders in AutoCAD was very easy, as was the importing of line drawings (DXF files) and images (TIFF files). On this basis,

AutoCAD was adopted as the design package used in creating a simple virtual model of the palace.

4.1.2.3. Visualisation

Accurate 3D models of parts of the palace Horvat Minnim were created using VRML and ArcView. The former is a 3D file interchange format for describing interactive 3D objects and worlds delivered across the Internet. A Visual Basic program for converting DEM data into a format recognised by VRML was developed at the Department of Geomatics, UCT (Taylor, 2000). With this program, it was possible to visualise portions of the palace walls in an interactive, 3D environment, with orthophotos texture-mapped to the walls. It would be possible to visualise an entire archaeological or architectural structure in this way, even to the extent of creating 'fly-throughs'. With the number of points per stereo-model ranging from about 10000 to 35000, an average computer with a Pentium II processor would not, however, be able to produce a visualisation of all 100 stereo-models. A severe limitation is computing power and speed.

ArcView is a GIS program with visualisation capabilities in its '3D Analyst' extension. The '3D Analyst', however, is limited to 2.5D visualisations. It was not possible to represent an object's full 3D extent using ArcView's 3D Analyst (as was possible using VRML), but ArcView has the advantage of allowing measurements to be made on the surfaces represented.

The issues of visualisation with respect to CAD and GIS are dealt with in more detail in section 4.3.

4.2. DSM and Orthophoto Production

This section presents a selection of results from the image processing (extraction of DSMs and production of orthophotos) done on Horvat Minnim. As the algorithms used for generating digital models from correlation are proprietary to LH Systems (Olander, 1999, *pers. comm.*), the author was unable to ascertain exactly why image

matching sometimes failed and at other times was successful. Some theories are proposed, drawing on the background of section 2.3.4.3, but these remain unsubstantiated. All that is presented are the results from the author's own experience of using SOCET SET 4.0.9 for Windows NT to create DSMs and orthophotos of archaeological buildings.

4.2.1. Creating the DSMs

Experimentation was the key in producing orthophotos and DSMs of the walls of Horvat Minnim. SOCET SET gives the user a choice of matching 'strategy', the best of which had to be chosen, using that combination of parameters that proved most successful. This was not always the same between different stereo-models; the strategy that worked for one model often produced errors in a similar model. Factors such as the graininess of the walls, the amount of shadow on the walls, the distribution of control points and the changes in depth of the walls played a large role in determining the success or failure of a certain strategy.

The SOCET SET strategy files were designed for the aerial case of photogrammetry. The subject, on which image matching was performed, architectural structures, does not adhere closely to this basis. In some cases, the building walls are badly eroded, weathered and/or damaged, presenting a rough 'terrain' with rapid and excessive changes in elevation. Other parts of the buildings exhibit smooth, well-preserved surfaces. Both scenarios present difficulties for image matching using area-based techniques: the former due to the unexpected elevation differences where smoothing between matched points can lead to errors; the latter because the uniformity of the surface can make it difficult for a match to be found. Where possible and when necessary, the algorithms were edited to conform as closely as possible to the conditions of the project: close-range, horizontal photography.

Three different Horvat Minnim stereo-models will be analysed in sections 4.2.1.2 to 4.2.1.4 as examples of the performance of SOCET SET's matching strategies on different wall types. Section 4.2.1.1 is a description of the matching strategies and their operation.

4.2.1.1. Matching Strategies

The following is a list of the strategy files used by SOCET SET's Automatic Terrain Extraction (ATE) describing how and when the files are used, according to Drollinger and Miller (1995). The terms 'flat', 'rolling' and 'steep' are relative depending on the scale of the imagery.

Flat.strat is used for stereo-models with flat terrain, or very small x-parallax. The criterion for maximum slope is set low (20 degrees) and spikes and pits (matching errors) are also detected at low thresholds. It uses a larger correlation window (see Figure 4.4) and will perform faster than rolling and steep strategies.

Rolling.strat is used for rolling terrain (hills and valleys with gentle slopes) and permits slopes up to 30 degrees.

Steep.strat is a more time consuming strategy and will allow slopes up to 50 degrees. It generally works well for all terrain types.

Strategies **flat_1.strat**, **rolling_1.strat**, and **steep_1.strat** can be used similarly to the ones described above but tend to run slower and produce more accurate data. These strategies use the 1:1 minification level whereas the ones above stop at the 2:1 reduced resolution level. If the imagery is very poor or very noisy, these strategies may produce worse data.

Strategies **flat_plus.strat**, **rolling_plus.strat**, and **steep_plus.strat** are similar to the above strategies, but perform additional filtering to remove trees and buildings and additional smoothing in non critical points in the DSM. (Critical points are those describing a breakline or the edge of the DSM.) They were not used much in this project as, besides being undesirable, there was little need for additional smoothing.

Strategies **flat_dense.strat**, **rolling_dense.strat**, and **steep_dense.strat** are similar to the **_plus.strat** strategies described above but skip non critical points to perform more rapid extraction when doing very dense grids.

Strategies **flat_dense.strat**, **rolling_dense.strat**, and **steep_dense.strat** are similar to the **_plus.strat** strategies described above but skip non critical points to perform more rapid extraction when doing very dense grids.

Iterative Orthophoto Refinement (IOR) strategies all use the naming convention "**ior_X_YYY_Z.strat**", where X is the number of passes, YYY is a descriptive term, and Z is the minification level of the input imagery which will be used for correlation. The IOR strategies failed to produce any meaningful results, and have in fact been discontinued by LH Systems in subsequent versions of SOCET SET as tests showed very little benefits for their customers (Miller, 1999, *pers. comm.*).

All of the above strategies are designed for Non-Adaptive ATE, whereby the chosen strategies are used over an area that is assumed to be homogeneous. **Adapt.strat** is a general purpose strategy file used for Adaptive ATE: an inference engine is used to generate image correlation strategies adaptively according to the immediate terrain type (flat, rolling, steep) and apply them as needed (Helava Associates Inc., 1997).

An example of the adapt.strat, flat.strat, rolling.strat and steep.strat files is given in Appendices B.1 to B.4. A description of each strategy parameter in the strategy files, from Miller and Drollinger (1995), is found in APPENDIX A. Figure 4.4 illustrates some of the parameters associated with the matching entities. The matching entity used by SOCET SET is here called the "master patch" with square dimensions given by the CORR_AREA_2D parameter in pixels. The size of this entity is iteratively expanded if the computed signal power of the master patch is too low. Signal power is computed as the sum of the squares of the grey levels divided by the number of grey levels within the correlation area. Once the entity size reaches MAX_CORR_AREA_2D, or once the signal power exceeds the minimum threshold, the entity expansion ceases.

U_SRCH_DIST and V_SRCH_DIST are the distances, in pixels, in the epipolar u and v directions respectively within which a match is searched for. U_SRCH_MAX and V_SRCH_MAX are the maximum distances to which the search area can be iteratively expanded if a possible match is found at the edge of the search area.

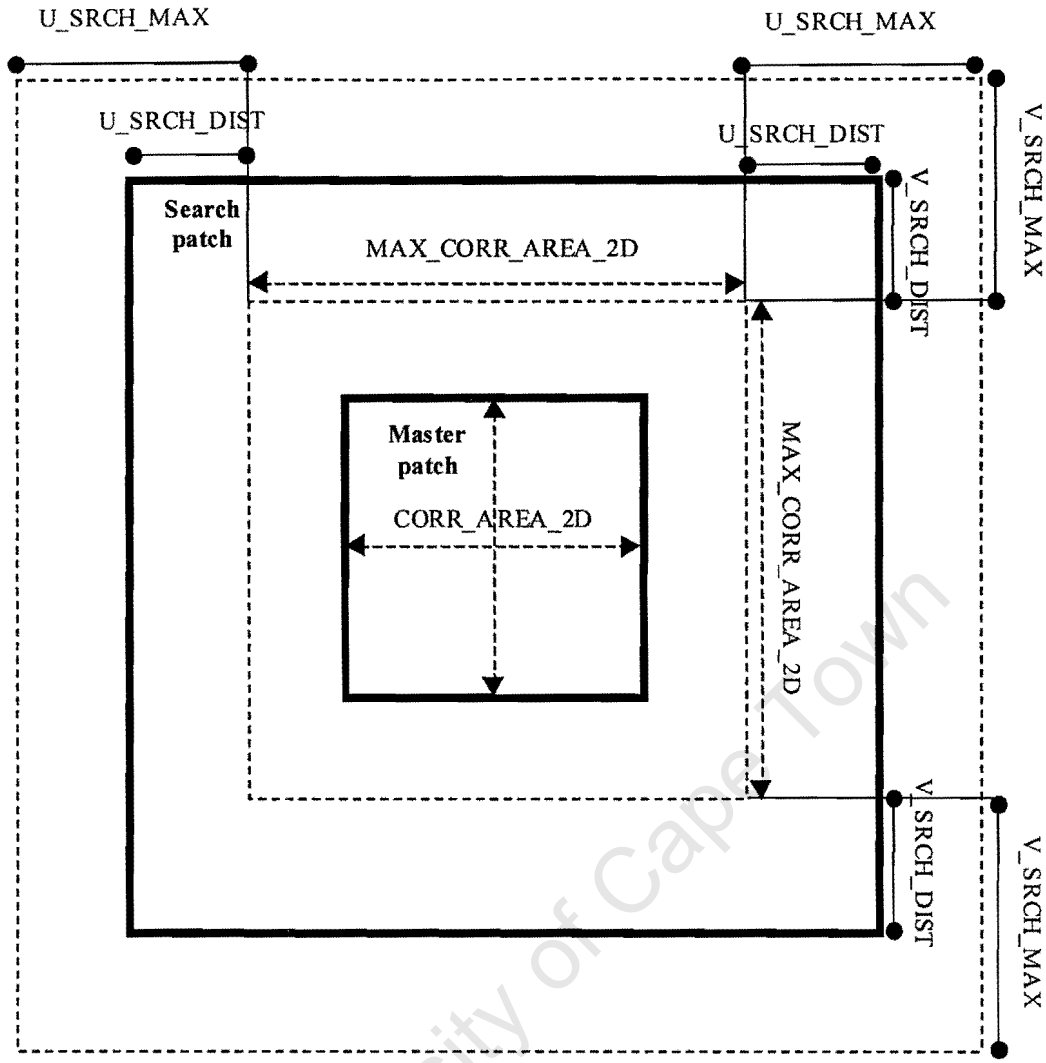

Figure 4.4 Geometric parameters used in matching strategies.

By adjusting these parameters in the strategy file, the likelihood of finding a match is increased or decreased: one can either avoid or encounter the two problems alluded to in Section 2.3.4.3 (after Schenk (1996)), i.e. combinatorial explosion and ambiguity. The parameters SLOPE_LIMIT and SPIKE_LIMIT can also be adjusted so that a match is accepted or rejected by enforcing a certain terrain type: for flat terrain a small SLOPE_LIMIT and SPIKE_LIMIT are chosen; rough, level terrain may suit a small SLOPE_LIMIT and large SPIKE_LIMIT, etc.

4.2.1.2. Experimental Results – 7a

Figure 4.5 Stereo-model 7a.

The stereo-model 7a, illustrated in Figure 4.5, is a flat, more or less uniform wall with no protrusions and little shadow across its surface. The only aspect of the wall that may make matching difficult is that it has a fairly repetitive or featureless texture. A series of tests were performed on this model using different matching strategies to try to produce an error free DSM and distortion free orthophoto of the wall. It was found that Adaptive ATE with either a TIN or a grid did not work for this model. Non-Adaptive ATE worked with a varying degree of success depending on the strategy file chosen.

The first strategy attempted was the Adaptive ATE using the adapt.strat strategy file (see Appendix B.1). According to the description in the previous section, this strategy should work well regardless of the terrain / wall type. It ceased to function before completion of the matching process, however, leaving no DSM data and no means of creating an orthophoto. Identical results were obtained regardless of whether a TIN or a grid was generated. The reason for the failure of this matching strategy was not ascertained, but it may have less to do with SOCET SET and more to do with the Windows NT operating system.

Two Non-Adaptive ATE strategies were attempted, all using the grid format required by SOCET SET for this style of matching (Appendices B.2 and B.4). Since the wall in model 7a is flat and uniform, the flat.strat strategy file was the first attempted, with

satisfactory results. Steep.strat is reputed to work well on all terrain types and so the final strategy attempted was this one, which produced good results.

Numerically, the accuracy of the DSMs can be checked by referring to the control points: SOCET SET measures the difference in *z* value (horizontal distance from the wall) between the control points and the DSM. The results of these measurements are presented in Table 4.2 for the two Non-Adaptive ATE strategies used. The units of measurement are metres, and the *z* differences are calculated as control points minus DSM. Figure 4.5 gives the positions of the control points on the wall. Figure 4.7 and Figure 4.8 show the DSMs.

Points 138, 139 and 140 exhibit large errors in both DSMs. A look at Figure 4.7 and Figure 4.8 shows a rough DSM texture in the area of these control points, indicative of DSM errors. Although the DSM created using steep.strat gives the smallest average *z* difference, a look at the standard deviation shows that flat.strat actually performed better at the control points. In fact, the standard deviation of the elevations of all the points in the flat.strat DSM is 0,1516 m while that for the steep.strat DSM is 0,2384 m. This confirms that flat.strat gives the output which most closely models the planar wall surface.

Table 4.2 Z Differences between control points and DSM

Point ID	Z Diff in metres	
	(flat.strat)	(steep.strat)
136	0.0311	0.0444
137	0.0214	0.0212
138	-0.0666	-0.0540
139	-0.0714	-0.0787
140	0.0508	0.0867
Avg Z diff	-0.0070	0.0039
Std Dev	0.0576	0.0689

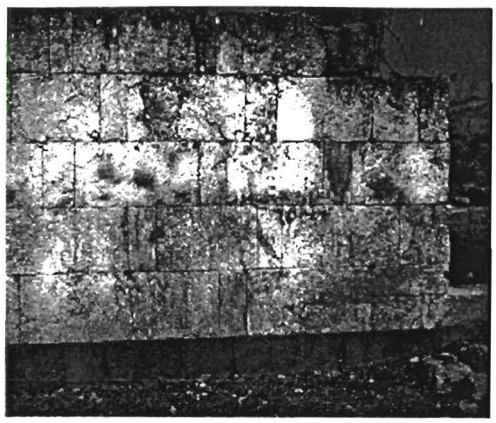

Figure 4.6 Original image.

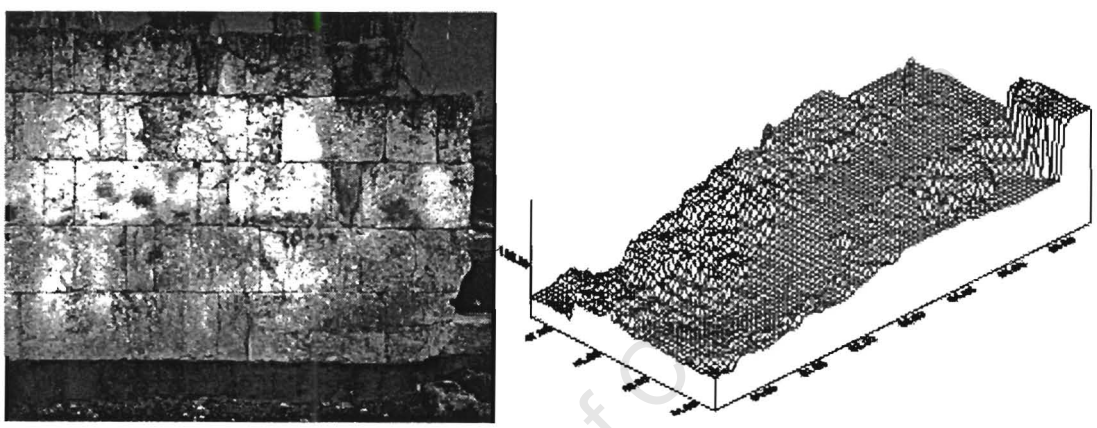

Figure 4.7 Flat.strat orthophoto (left) and DSM (right)

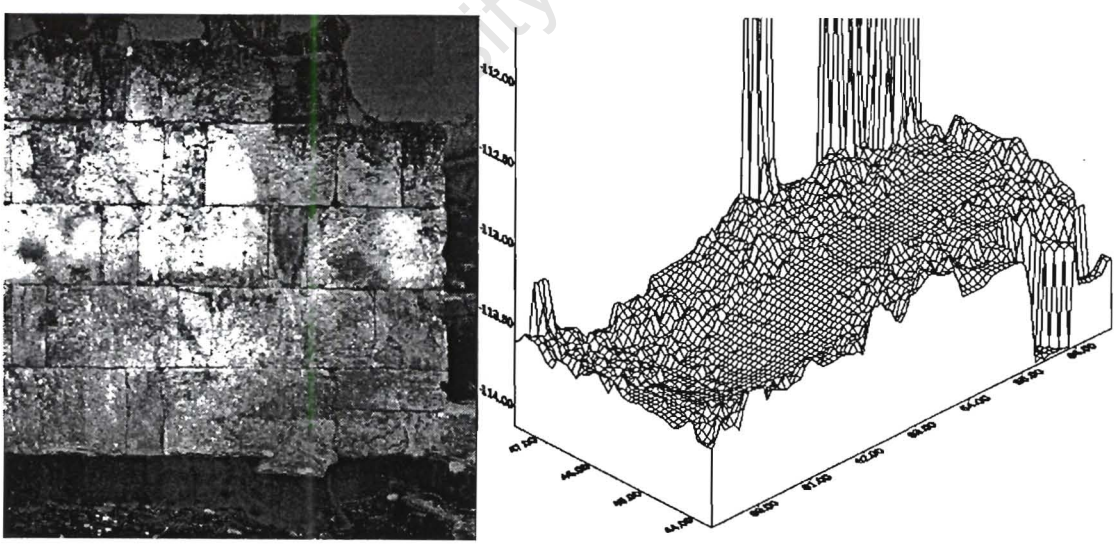

Figure 4.8 Steep.strat orthophoto (left) and DSM (right).

An indication of the effects of the errors in these DSMs is given by the orthophotos produced therefrom. Excessive changes in elevation in the DSM cause the pixel grey values of the original image to be shifted with respect to their correct x and y

positions. This is evident in Figure 4.7 and Figure 4.8, particularly in the lower right corner of the figures (the right edge of the wall should be straight, as per Figure 4.6, and the edges of bricks should line up). To eliminate these distortion effects, editing of the DSMs is necessary; this is covered in section 4.2.2.

A numerical analysis of the accuracy of the orthophotos is possible using the control points. By zooming in by up to a factor of 5, the positions of the control points in the images can be accurately measured using SOCET SET's co-ordinate measurement tool. These measurements are then compared to their actual, 'ground' co-ordinates. The differences are laid out in Table 4.3 (again, the differences are calculated as control point 'ground' x and y minus the corresponding measured values). Differences of a few millimetres up to 3 cm (the post spacing) are acceptable.

Table 4.3 Orthophoto control point x and y differences.

Point ID	X Diff (m) (Flat.strat)	Y Diff	X Diff (m) (Steep.strat)	Y Diff
136	0.000	0.000	0.000	0.003
137	0.001	0.004	0.002	0.003
138	0.002	-0.021	0.002	-0.019
139	0.013	0.015	0.011	0.013
140	0.025	0.009	0.041	0.017
Avg diff	0.008	0.001	0.011	0.003
Std dev	0.011	0.014	0.017	0.014

From the above analysis, it would appear that the flat.strat strategy gives marginally more accurate results of the two methods, for this stereo-model.

4.2.1.3. Experimental Results – 50a

The stereo-model 50a consists of two relatively flat, uniform portions of wall, separated by a singular protrusion. This protrusion breaks the uniformity of the wall, and hence makes this model unsuitable for matching using a single Non-Adaptive

ATE strategy as done previously for model 7a. A series of strategies was attempted over the entire wall using Adaptive ATE, as well as Non-Adaptive ATE for comparative means, with little success on both counts. Finally the wall was split into three separate regions (A, B and C in Figure 4.9) and each was dealt with separately before merging the generated DSMs to create the final orthophoto. These final results, and some of the preliminary results, are presented below.

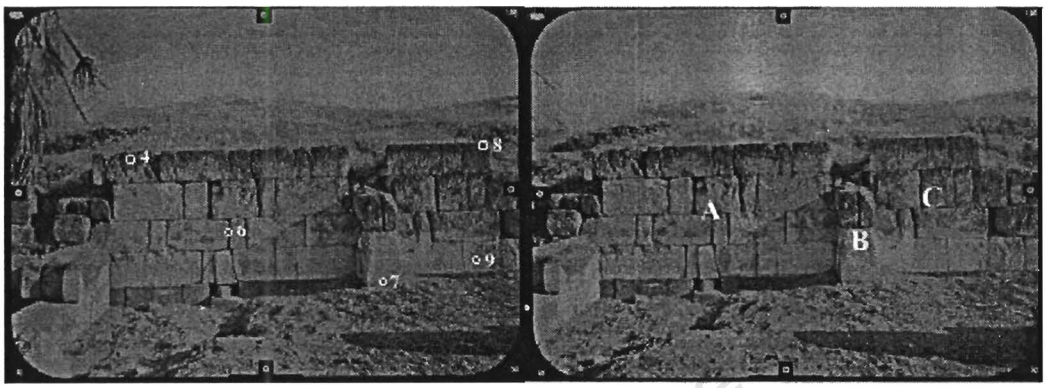

Figure 4.9 Stereo-model 50a.

Performing adaptive ATE over the entire wall surface, using a TIN to accurately model the changing elevation on the wall, produced the DSM shown in Figure 4.10. Figure 4.11, the orthophoto corresponding to this DSM, illustrates the degree of success of this matching strategy on this particular surface. From Figure 4.10, which is a view of the DSM inclined on its side with the top of the wall at bottom left and the left hand side of the wall at bottom right, it is not difficult to make out the protrusion from the wall (region B, to the upper left of the figure) and the flat portion to the left (region A, lower right of the figure). The flat portion to the right, however, is not well modelled at all (region C, top left of the figure). Spikes and pits are evident in the DSM and their influence is clearly observable in the corresponding orthophoto as smearing on the right hand side.

From Figure 4.9 it is clear that there is no image data in either photo of the stereo-model for the region immediately to the right of the central protrusion. The result of this occlusion on the orthophoto (Figure 4.11) is a confused area where the image data has been smeared across what should be a gap in the image. As an orthophoto, this is unsatisfactory as it is not a true reflection of the subject.

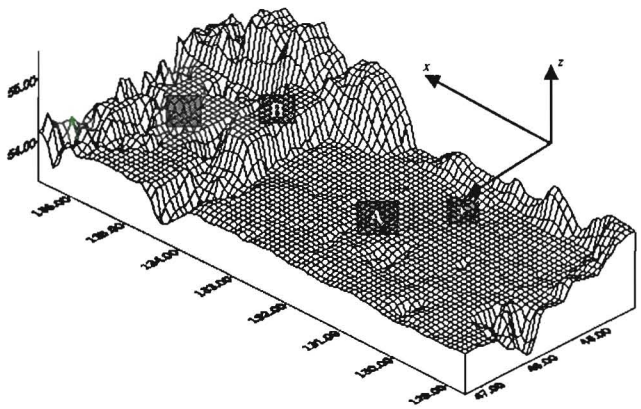

Figure 4.10 DSM of model 50a using Adaptive ATE

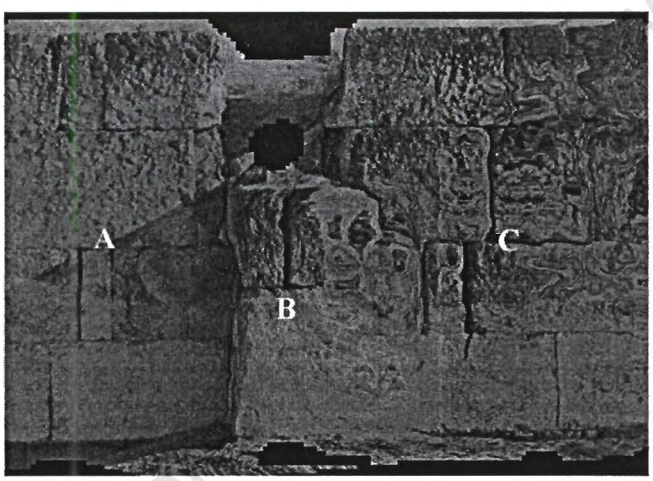

Figure 4.11 Centre portion of orthophoto of model 50a using Adaptive ATE

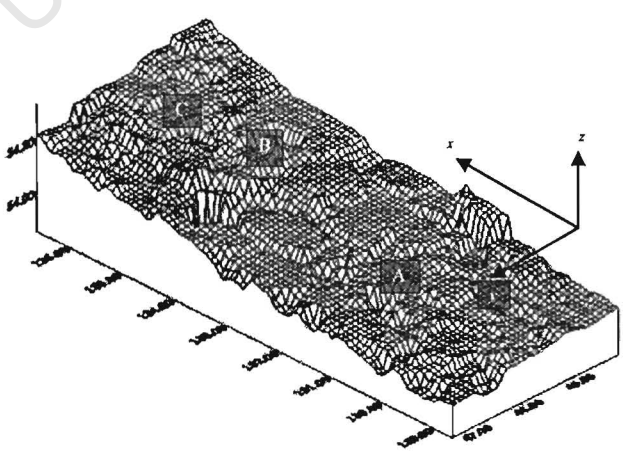

Figure 4.12 DSM of model 50a using Non-Adaptive ATE strategy flat_dense.strat

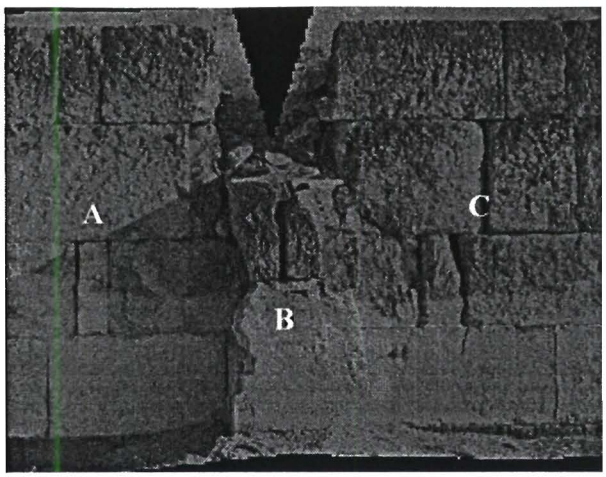

Figure 4.13 Centre portion of orthophoto of model 50a using Non-Adaptive ATE flat_dense.strat

Table 4.4 Control point and DSM Z differences for model 50a

Point ID	Z Diff (m)		
	(adapt.strat)	(flat_dense.strat)	(Combined DSM)
4	0.0365	0.0324	0.0113
6	0.0055	0.0281	0.0192
7	0.0081	0.5477	0.0008
8	0.1040	0.0015	0.0067
9	0.3952	0.0146	0.0037
avg Z diff	0.1099	0.1249	0.0083
Std dev	0.1644	0.2367	0.0072

To try and improve on the results, the same area was matched using the Non-Adaptive ATE strategy, flat_dense.strat. The resulting DSM and orthophoto are presented in Figure 4.12 and Figure 4.13 respectively. Although the right hand side of the DSM, viewed here in the same orientation as Figure 4.10, shows improved results compared to the same region in Figure 4.10, on the whole this DSM models the wall less accurately. This is confirmed when the control point *z* co-ordinates are compared for the two DSMs as per Table 4.4.

The positions of the points are given in Figure 4.9. The average *z* difference and standard deviation of the second DSM are higher. Since the model created using flat_dense.strat does not model the protrusion well, a large error is incurred on point ID 7. The model created using adapt.strat does not model the right hand area well, and so larger errors are obtained for point IDs 8 and 9 than for 4, 6 and 7 for this model.

From the above two examples, it should be evident that it is not possible to create an accurate orthophoto of this stereo-model using a single strategy for the entire wall. Large errors are incurred over some of the control points, and the occluded region to the right of the central protrusion will not be modelled correctly unless the wall is split into separate regions which are each dealt with individually.

Using the Non-Adaptive strategy, flat_plus.strat, the DSM of the flat, left portion of wall (region A), illustrated in Figure 4.14, was created. The average *z* difference of this DSM is 0,0152 m. The standard deviation is 0,0056 m. These figures show that the DSM is accurate at the control points, and a manual comparison (using stereoscopic viewers) confirms that it is a true portrayal of the wall's shape.

The central region (region B) was matched using Adaptive ATE in a TIN format, the DSM of which is presented in Figure 4.15 in a grid format. Non-Adaptive strategies such as steep.strat did not perform as well as expected, possibly due to the excessive changes in elevation in this region which are unlike any natural terrain. The region chosen included some of the flat area to the left, to ensure continuity was maintained where it was applicable, and stopped on the right hand side of the protrusion. It was not extended onto the flat region to the right as this would have resulted in smearing in the orthophoto across the occluded area, as per Figure 4.11 and Figure 4.13. The TIN encompasses only one control point, point ID 7, the error in elevation of which is 0,0008 metres.

Finally, the right hand portion of the model (region C) was matched using Adaptive ATE in a TIN format without an obstruction filter and with an OVER_COLLECT filter (see APPENDIX A) on the last pass. Points 8 and 9 fell within this model and

exhibited *z* differences of 0,0067 m and 0,0037 m respectively, which are entirely satisfactory. Figure 4.16 shows the DSM in a grid format.

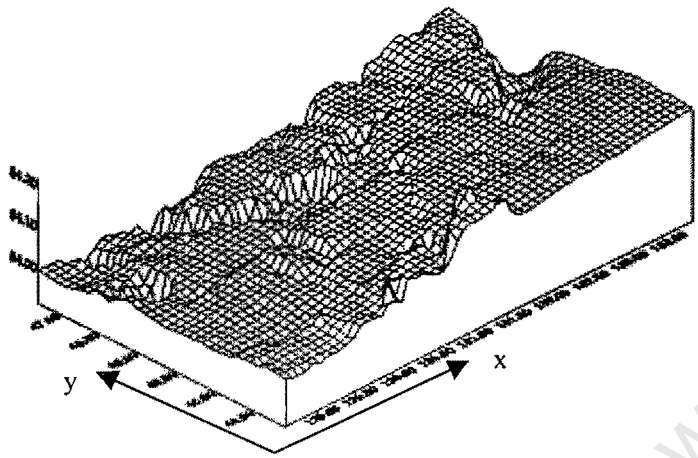

Figure 4.14 Left portion of model 50a (region A) created using flat_plus.strat

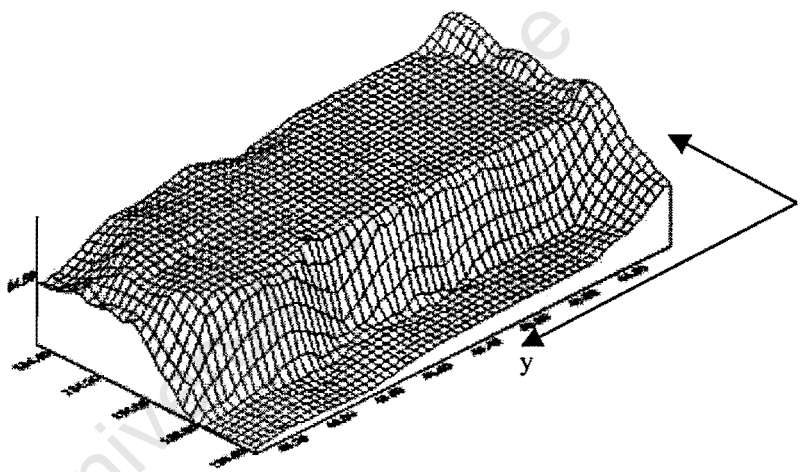

Figure 4.15 DSM of protrusion (region B), 50a

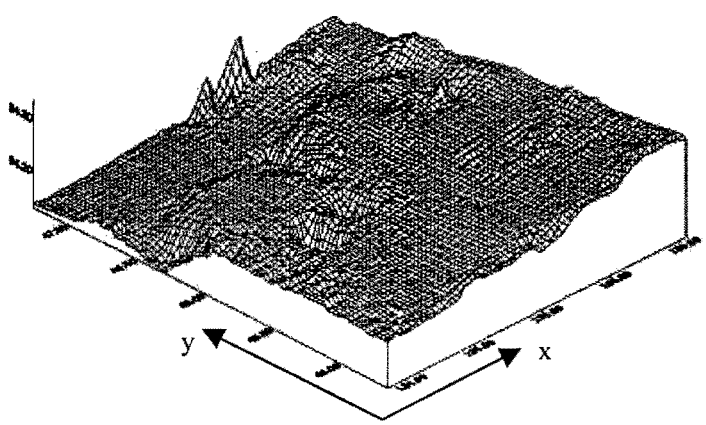

Figure 4.16 DSM of right portion of 50a (region C), created using Adaptive ATE

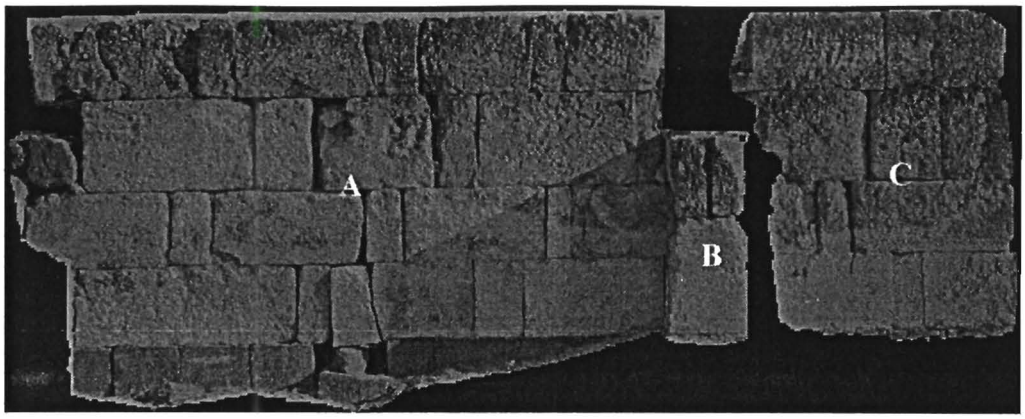

Figure 4.17 Combined orthophoto – 50a

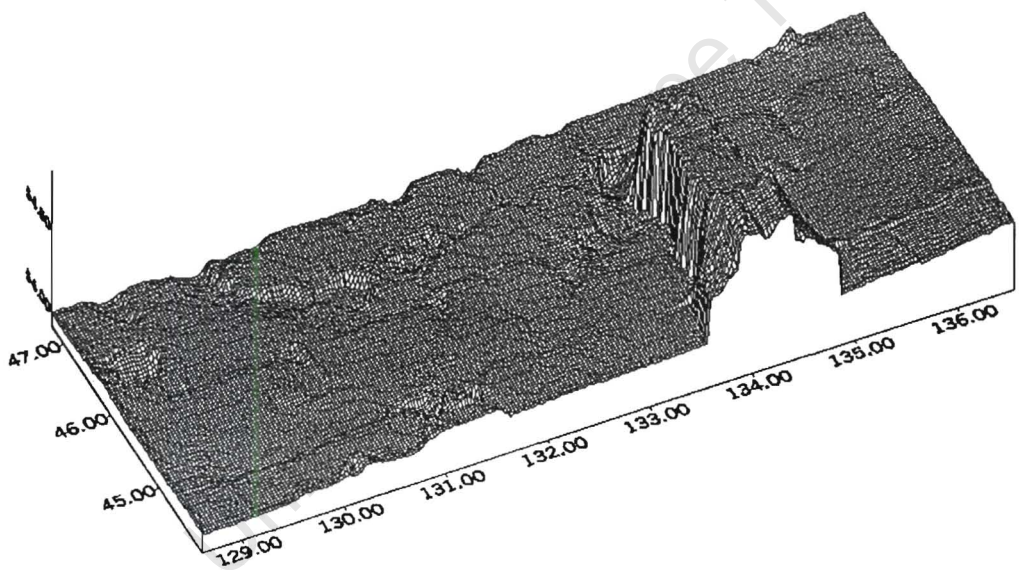

Figure 4.18 Combined DSM 50a

The three DSMs described above were then merged using SOCET SET (Figure 4.18) and the corresponding orthophotos mosaicked onto the combined DSM (Figure 4.17). It was necessary to mosaic the separate orthophotos because, if one orthophoto had been created from the combined DSM, the pixels would still have been stretched across the gap in the data. In this way, the occluded region was maintained as such, without incorrect interpolation across the gap.

4.2.1.4. Experimental Results – 4a

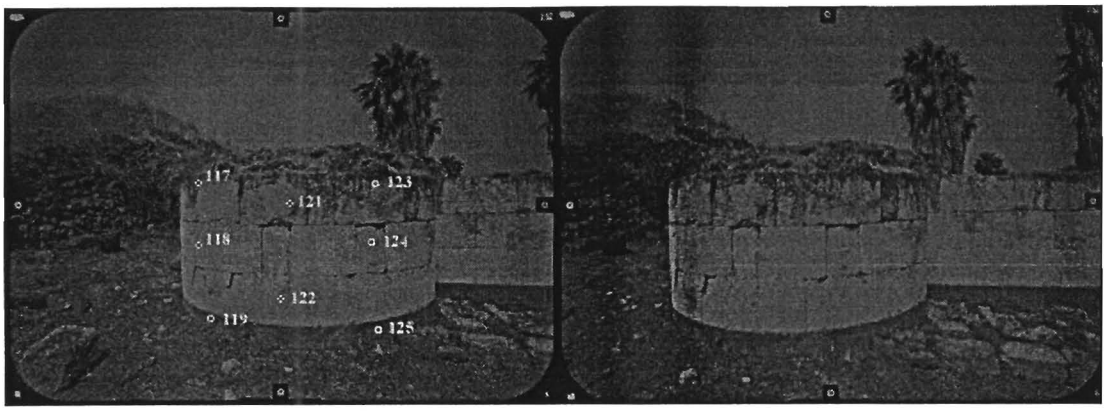

Figure 4.19 Stereo model 4a.

The curved surfaces presented by stereo models 2a, 3a, 4a and 5a (which describe one of the tower structures, shown in Figure 4.19) required a different matching strategy again. Flat.strat would not have worked on any of these sections, and so rolling.strat (refer to Figure 4.20 and Appendix B.3) and steep.strat (refer to Figure 4.21 and Appendix B.4) were attempted for the Non-Adaptive mode of terrain extraction. It was found that Adaptive ATE using a TIN (refer to Figure 4.25) with the inclusion of breaklines (refer to Figure 4.24) generated the most satisfactory surface reconstruction, although editing was still necessary (dealt with in the next section). Table 4.5 is illustrative of the precision of the different strategies.

Comparing Figure 4.20 and Figure 4.21, the most obvious difference between the two DSMs is the large elevation differences towards the top and bottom of the latter figure. Whereas the rolling strategies tend to interpolate across such areas, the steep strategies are designed for abruptly changing or mountainous terrain; they will try to find a match where other strategies would not. This makes the steep strategies more robust than the flat or rolling strategies and allows them to model the surface more closely. This can be confirmed by comparing the two 'top' views of Figure 4.20 and Figure 4.21, shown in Figure 4.22 and Figure 4.23, respectively. The semi-circular surface of the tower (represented by an offset, semi-circular arc in the two figures) is represented more closely by Figure 4.23, generated using steep.strat, than by Figure 4.22, generated using rolling.strat.

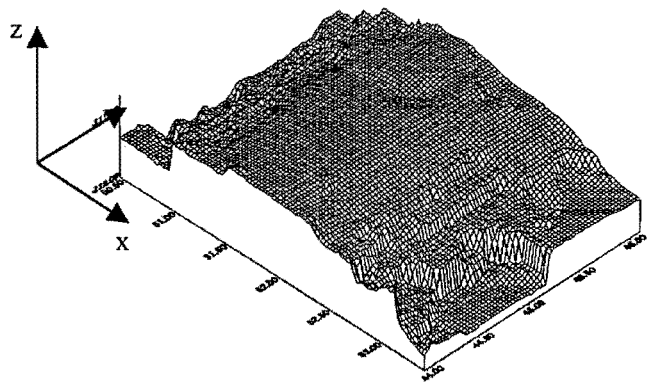

Figure 4.20 Model 4a generated using rolling.strat

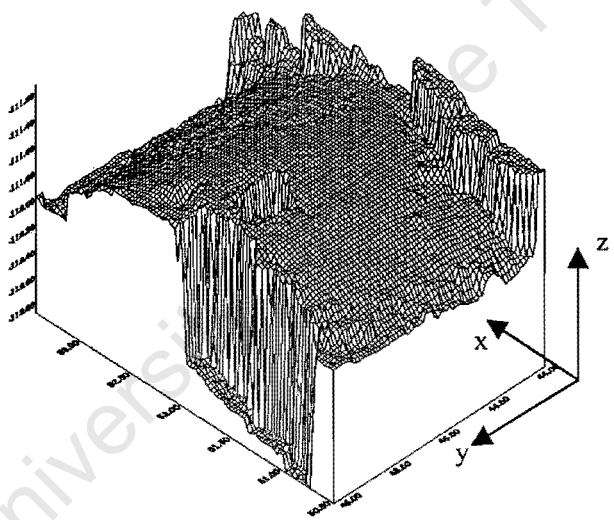

Figure 4.21 Model 4a generated using steep.strat

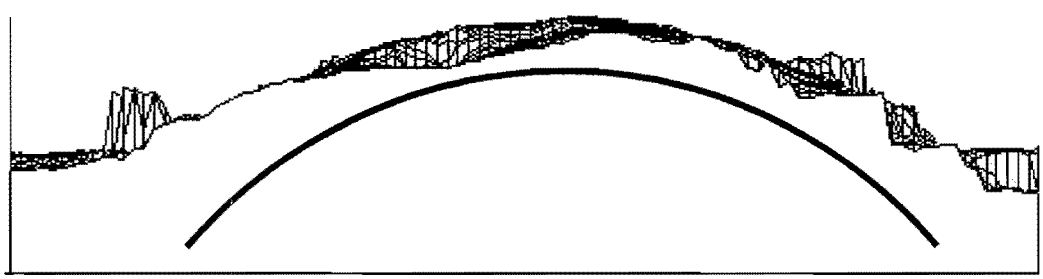

Figure 4.22 'Top' view of model 4a generated using rolling.strat

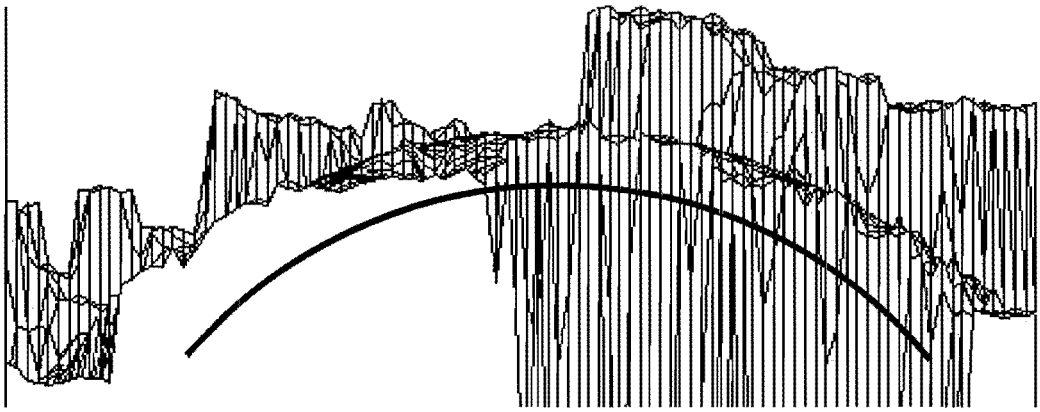

Figure 4.23 'Top' view of model 4a generated using steep.strat

Table 4.5 Control point and DSM Z differences for model 4a

Point ID	Z Diff (m)			
	Non-Adaptive ATE		Adaptive ATE	
	(Rolling.strat)	(Steep.strat)	(With breaklines)	(Without breaklines)
117	-0.0252	0.0102	-0.0045	N/A
118	0.0007	0.0013	0.0031	0.0060
119	0.0281	0.0462	-0.0010	0.0057
121	0.0004	0.6519	0.0033	-0.0004
122	0.0035	0.0008	0.0069	0.0070
123	0.0008	0.0032	0.0094	0.0081
124	0.0069	0.0157	0.0105	0.0109
125	0.0313	0.0134	0.0093	0.0090
Avg Z Diff	0.0058	0.0928	0.0046	0.0066
Std dev	0.0177	0.2264	0.0054	0.0036

Comparing the differences in elevation between the control points and the DSMs (Table 4.5), however, we can see that rolling.strat gives the numerically superior results: both the mean and the standard deviation of the differences are significantly less. The results of matching using steep.strat, however, have been skewed by the inclusion of a significant outlier: point ID 121 has a *z* difference of 65 cm, which is greatly in excess of the other points' *z* differences. A comparison of the z differences,

excluding point 121, gives a standard deviation of 16 cm which is practically equal to that for rolling.strat (17 cm). A comparison of all the other points' *z* differences reveals very little in terms of which strategy performed best. We can conclude, therefore, that rolling.strat and steep.strat perform equally well for this model (at least, for our purposes).

Referring again to Table 4.5, there is little numerical difference between the two DSMs generated using Adaptive ATE, shown in Figure 4.24 and Figure 4.25. A proposed reason for this is that the control points are not in the areas affected by the inclusion of breaklines. From the two figures, it is evident that a better approximation of the tower surface is achieved by including breaklines (Figure 4.24). The DSM is constrained to the wall surface in difficult areas, particularly at the top edge of the wall. A description of the use of breaklines follows in section 4.2.2.1, with particular reference to model 4a.

The results of matching using Adaptive ATE, either with or without breaklines, are better than those attained using Non-Adaptive ATE. A comparison of the standard deviations in Table 4.5 confirms this: the error distribution is the least by an order of magnitude for Adaptive ATE without breaklines (mm as compared to cm).

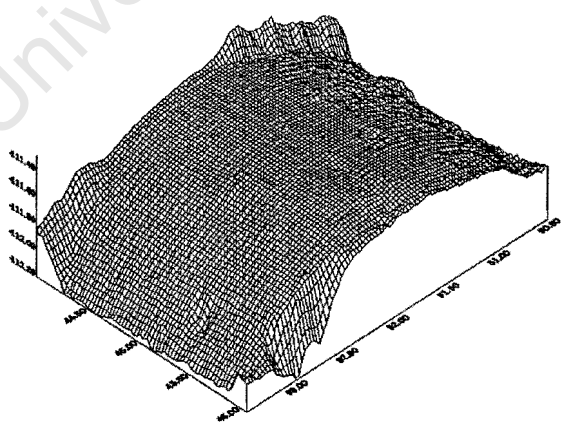

Figure 4.24 Model 4a generated using Adaptive ATE and including breaklines

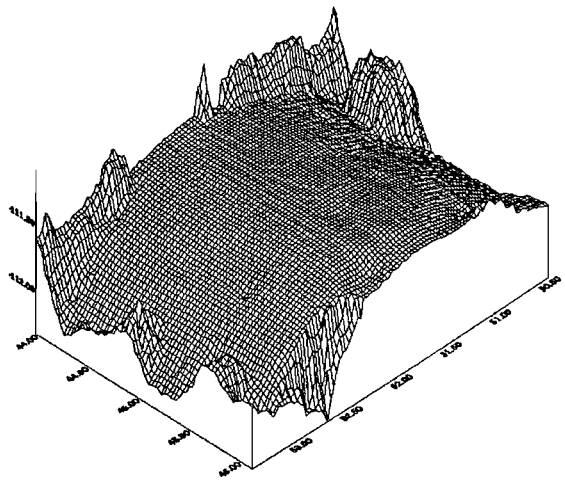

Figure 4.25 Model 4a generated using Adaptive ATE without breaklines

4.2.2. Editing

Regardless of the matching strategy used, errors are incurred in the production of DSMs. Editing of the DSMs is therefore a necessary part of the process of creating an accurate model of a structure and a distortion free orthophoto. Three different types of editing were performed on the SOCET SET DSMs: two automatic, or program-driven, and one manual.

4.2.2.1. Manual Editing

Manual editing consists of viewing the surface in stereo on the DPW, SOCET SET, and placing a floating point on the surfaces of the walls. The floating point is used to define additional DSM points and insert breaklines where necessary. Although a time-consuming process, it was the author's experience that this gave the most accurate results, especially when using a TIN model. The perceptual abilities of the human brain still far exceed those of a computer and so, through manual editing, points could be placed precisely where required and their elevations adjusted to model the wall accurately.

When using TIN models, SOCET SET allows the manual inclusion or deletion of points and the adjustment of their elevations. Since models exhibiting a grid format

have fixed x and y positions for every point, based on the post spacing, only their elevations may be modified. Breaklines can be added to constrain the model to fit to the wall in difficult areas. This is done more effectively using a TIN model than a grid. The types of breakline offered for grids are designed for the inclusion of roads and ditches into a terrain model, as illustrated in Figure 4.26. For TIN models, breaklines constrain the surface to ridges, drains, toes of slopes, or crests. An 'undefined' option also exists by which points are constrained to lie along a polyline (a series of joined line segments, such as the terrain profiles in Figure 4.26). The 'hardness' or 'softness' of the breaklines can also be specified, referring to the extent by which the breakline breaks from the surrounding terrain. For example, a steep, sharp ridge jutting out of an otherwise flat landscape would merit a 'hard' description.

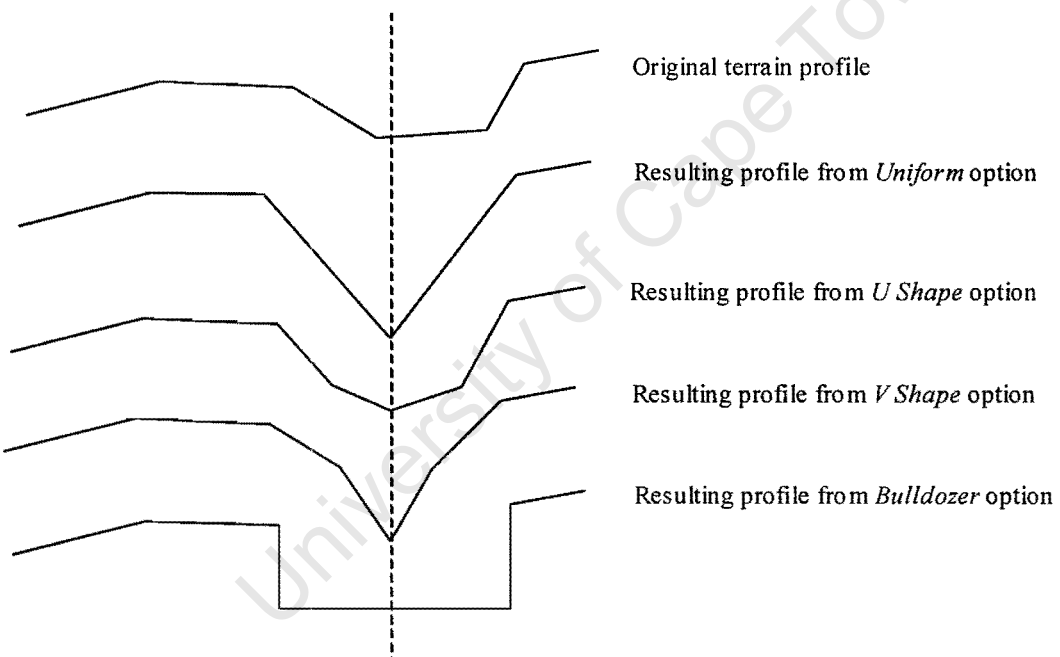

Figure 4.26 Grid format breaklines offered by SOCET SET.

Adding breaklines offered flexibility in defining wall shapes, especially where the wall surface was rough and broken. Figure 4.27 shows two orthophotos of model 4a developed without using breaklines (top), and with breaklines (bottom). The orthophotos were created using the DSMs illustrated in Figure 4.25 and Figure 4.24 respectively. From Figure 4.27, it is easy to see that the inclusion of well-placed breaklines aids in the surface description. The region to the bottom left of the wall is badly modelled without breaklines, as is the entire top edge of the wall.

Figure 4.27 Effect on orthophotos of including breaklines: without breaklines (top) and with breaklines (bottom). Arrows show areas of distortion.

Breaklines with a 'ridge' description were used to model the edges of cracks, while 'drains' were used for the middle of cracks or large gaps between bricks. The 'crest' option was chosen for the edges of bricks where one side was obscured from view (e.g. the top edge of the wall). An 'undefined' option exists whereby points can simply be made to lie along a line, against the wall surface.

4.2.2.2. Automatic Editing

(a) Standard Deviation Threshold

Automatic editing was performed using two different programs developed at the Department of Geomatics, UCT. The first, developed by the author using Microsoft Visual Basic 5.0, used a calculation of the standard deviation of the elevation of all the points on the wall, given by Equation 4-1:

$$\sigma = \sqrt{\frac{n\sum Z^2 - \left(\sum Z\right)^2}{n(n-1)}}$$

Equation 4-1

σ is the standard deviation of the elevations of the points;
n is the total number of points; and
Z is the elevation of the points in the DSM.

Two options were available to the user. A 'mean wall elevation' could be calculated using either:

1. the mean elevation of all of the DSM points, or
2. the mean elevation of the control points.

The choice would depend on the shape of the particular wall and on the distribution of the control points.

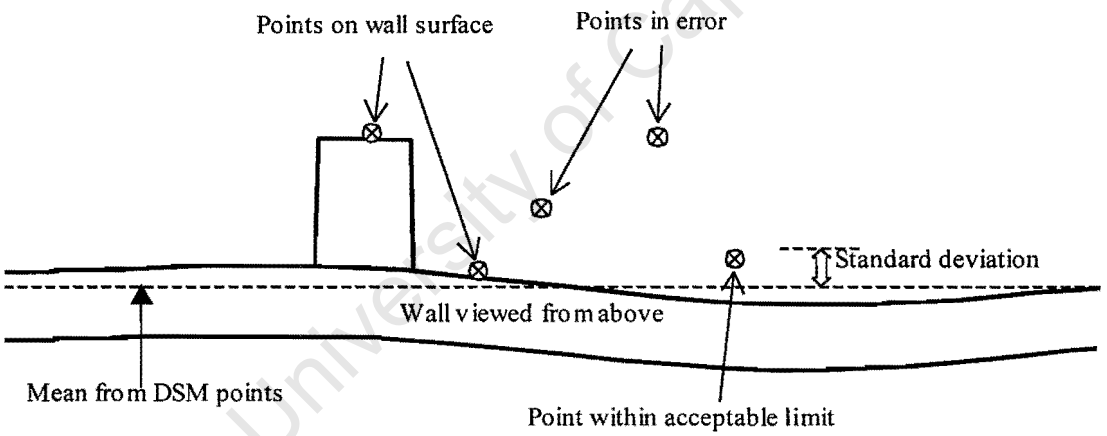

Figure 4.28 Theory of DSM editing using standard deviation as threshold.

Points lying between $s\sigma$, where s is an integer typically from 1 to 3, and the mean elevation were accepted. Points exceeding this threshold were most likely spikes or pits and hence excluded from the DSM. Figure 4.28 illustrates this process. Although the generally accepted exclusion level for outliers is 3σ, it was the author's experience that this was often insufficient: too many errors were still included in the DSM. Consequently, 2σ and even σ were used. Manual editing was always necessary to both correct mismatches remaining after the threshold test, and fill in areas where points had been deleted (see Figure 4.29).

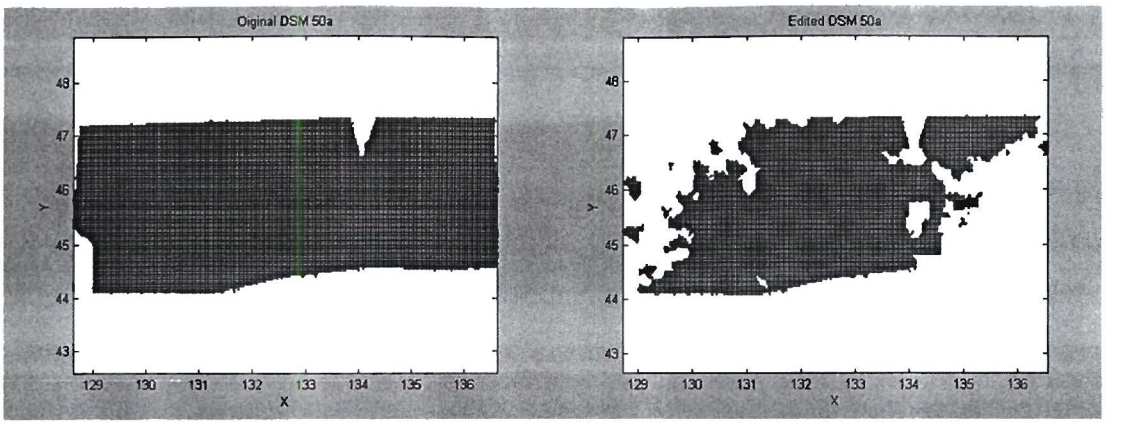

Figure 4.29 Original *x*, *y* point scatter, DSM 50a before editing (left) and after editing (right)

An assumption made was that the wall surface is relatively flat (planar). Excessive protrusions, such as illustrated in Figure 4.28 and described in section 4.2.1.3, would be modelled by points mostly exceeding σ, and possibly 2σ as well. Consequently these regions would be eliminated by the editing process, which is an undesirable result. Curved surfaces, such as those presented by the towers described in 4.2.1.4, present a large standard deviation due to their curved nature. The points in error, lying off the wall, are not represented by the standard deviation calculation, and so a different algorithm was required for dealing with these surfaces. This is discussed in 4.2.2.2(b) below.

The effect of eliminating points lying outside of σ is graphically evident from Figure 4.29. The standard deviation of all the points in the DSM of model 50a created using flat_dense.strat, Non-Adaptive ATE (Figure 4.12 and Figure 4.13) is 0,0845 metres. There were 25325 points in the original DSM, and only 15822 points in the edited DSM. Figure 4.29 shows the uniform distribution of points in the grid illustrated in three dimensions by Figure 4.12. In a case such as this, where a large number of points have been eliminated, manual editing becomes necessary to replace points in appropriate positions. This is generally performed quickly and easily, as only the minimum points required to model the structure accurately are added[4]. The original

[4] During automatic DEM generation, a computer measures a large number of redundant points. A human operator using an analytical plotter measures only those points necessary to model the surface adequately.

grid format DSM then needs to be saved in a TIN format as the post spacing is no longer uniform throughout the model.

(b) Incidence Angle Threshold

Davey (1999) of the Department of Geomatics, UCT, developed a technique for eliminating mismatches on curved surfaces. Oblique surface orientation was identified by Baltsavias (1991) as one of many factors leading to mismatching. Davey (1999) consequently proposed that, if a method of identifying and eradicating these mismatches can be developed, a better representation of a mapped surface can be achieved.

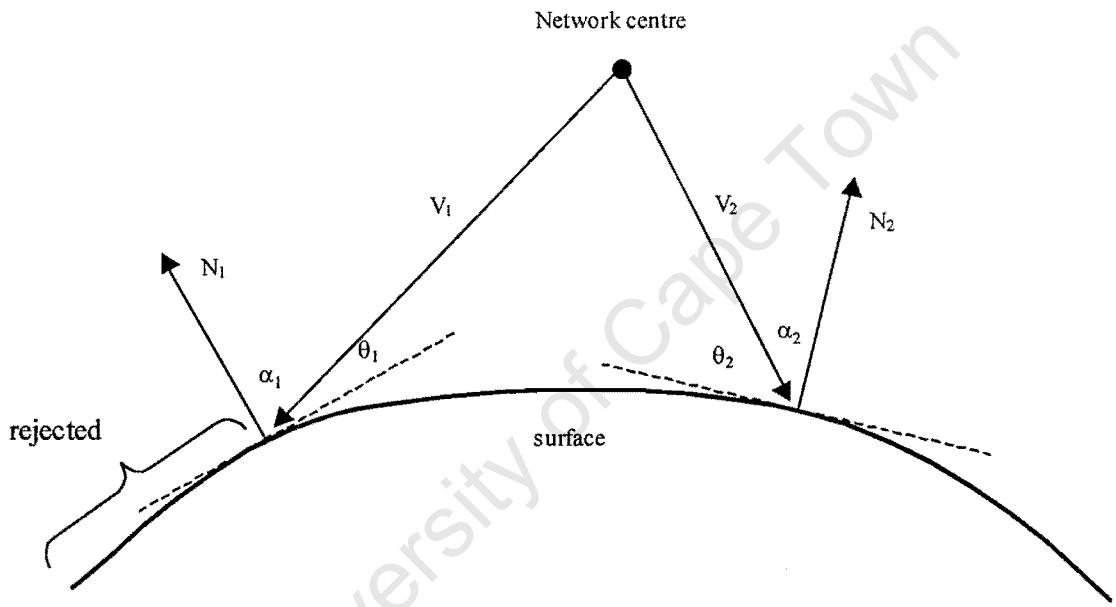

Figure 4.30 Theory of DSM editing using incidence angle threshold (Davey, 1999): θ_1 is the threshold angle.

Using C++, a program was written whereby a best-fitting plane was calculated through every point using, typically, five neighbouring points. The normal to this plane was then calculated at every point. The angle between the normal and the vector from the point to the network centre (the mean position of the cameras used) was then obtained using:

$$\cos\alpha = \frac{\vec{V} \bullet \vec{N}}{\|\vec{V}\|\|\vec{N}\|}$$

Equation 4-2

where α is the angle;
V is the vector from the point to the network centre; and
N is the normal.

The incidence angle (θ_i in Figure 4.30) was calculated as the complement to α and compared with a threshold value. Points with an incidence angle below the threshold were discarded and the remaining points were written to a new file.

In Figure 4.30, V_i are the vectors from the DSM point to the network centre. N_i are the normals to the plane through the DSM point, at the DSM point. θ_i are the incidence angles, where θ_1 is the threshold value. All those points with a smaller incidence angle than the threshold are rejected. The threshold value needs to be determined empirically and the procedure applied with caution (Davey, 1999). A practical example of this is given by Figure 4.31 below.

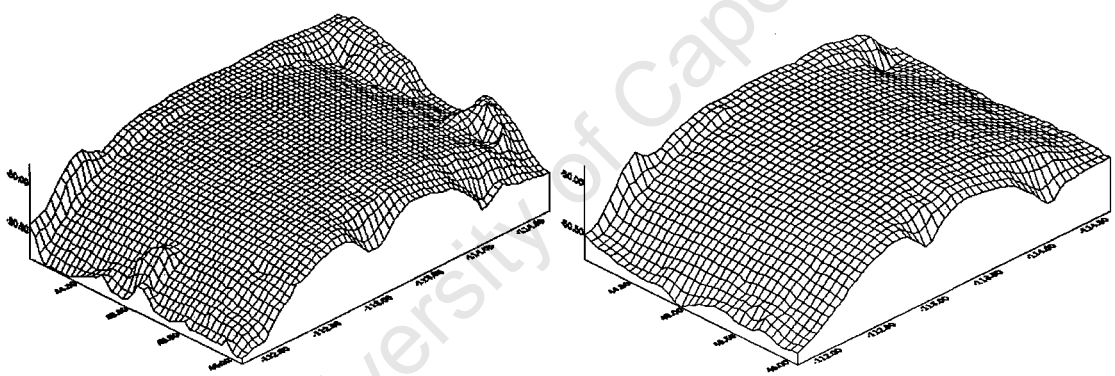

Figure 4.31 DSM 3a: original (left) and edited using 45 ° incidence angle (right)

The figures relate to a portion of the tower described in section 4.2.1.4. Figure 4.31 shows, on the left, the raw data containing mismatches and a total of 2850 points. The edited DSM, shown on the right, has 1777 points remaining after an incidence angle threshold of 45° was imposed. (Threshold values of 15° and 30° were first attempted, but these did not remove the errors sufficiently.) It is clear from the figures that those points which were in error have been successfully removed, greatly improving the accuracy of the DSM.

4.3. Compilation and Visualisation

It is always difficult to visualise 3D structures when limited to a 2D portrayal thereof. The obvious example is in making 2D maps of our oblately spheroidal earth. Different methods exist whereby angles, distances or areas are preserved in the map projection, but no complete projection of any 3D structure onto a 2D surface is without distortion or inaccuracy in some form. It is therefore desirable to visualise 3D objects in their full dimensionality. In this section, some different methods of 3D visualisation of structures will be addressed, where the accuracy and realism as well as the usefulness of the portrayal will come under scrutiny. Section 4.3.1, however, deals with a 2D projection of a 3D structure: the tower section of Horvat Minnim partially dealt with in section 4.2.1.4.

4.3.1. 'Unrolling' the Tower

Figure 4.32 shows line drawings of the facades of the south eastern tower of Horvat Minnim. Viewed in this way, the projection of the curved tower surface may be called orthographic: scale is constant vertically and decreases sinusoidally in the horizontal direction away from the nadir point (from left to right for 2a, right to left for 5a, and outwards from the centre for 3a and 4a).

This type of projection is undesirable, then, if accurate measurements of the surface are required. A far better projection, maintaining the coherence of the tower (i.e. which does not split the tower into individual sections as per Figure 4.32) and ensuring a constant scale both vertically and horizontally, is given by an equidistant, azimuthal projection. Distances from the centre of the tower are preserved.

Figure 4.33 illustrates the theory behind an equidistant, azimuthal projection. The mean radius of the tower, r_m, and the x co-ordinate of the projected point, x_p, are related through the arc distance given by Equation 4-3:

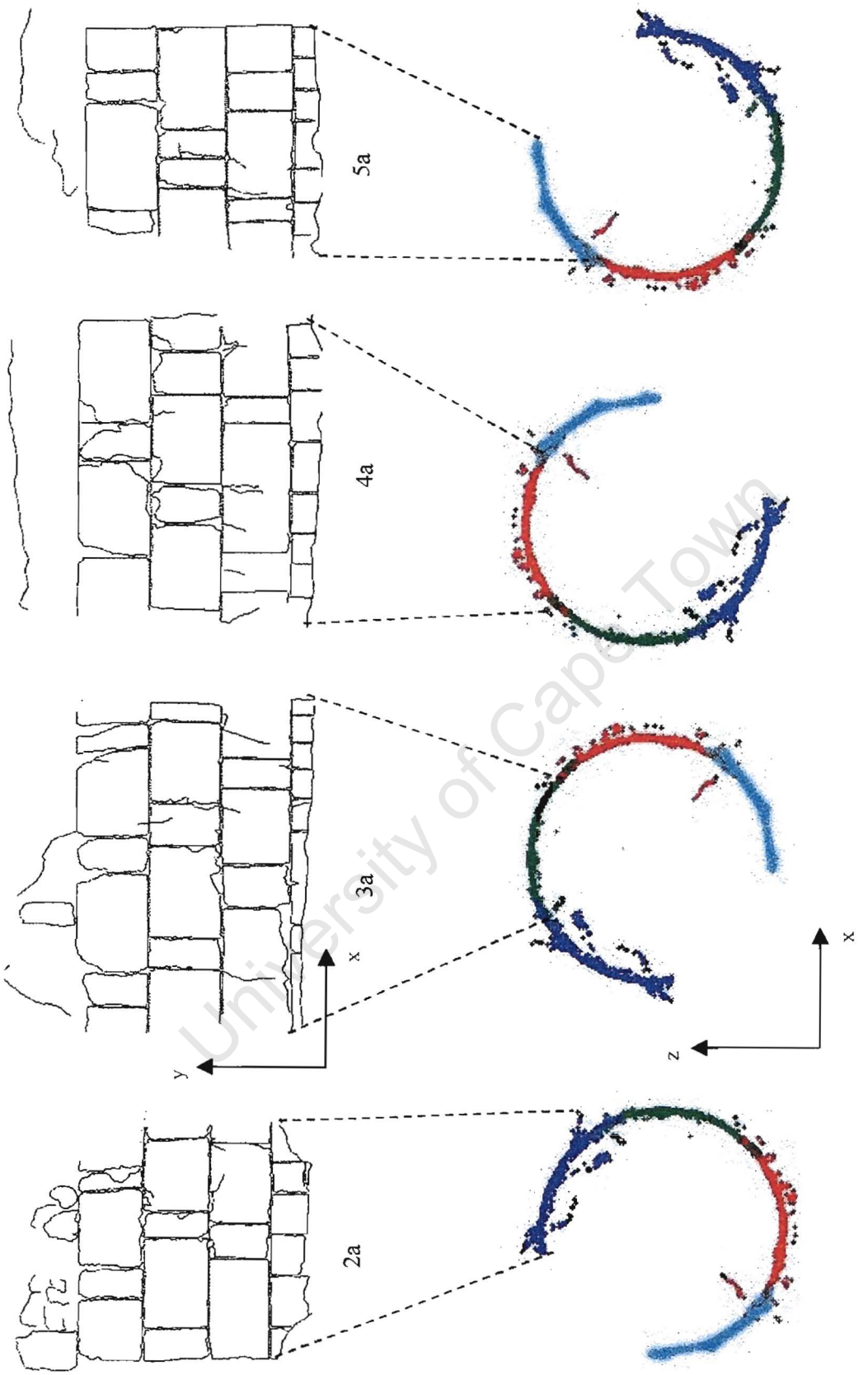

Figure 4.32 Facades of the south eastern tower, Horvat Minnim

$$r_p = \phi_{rad} r_m$$

Equation 4-3

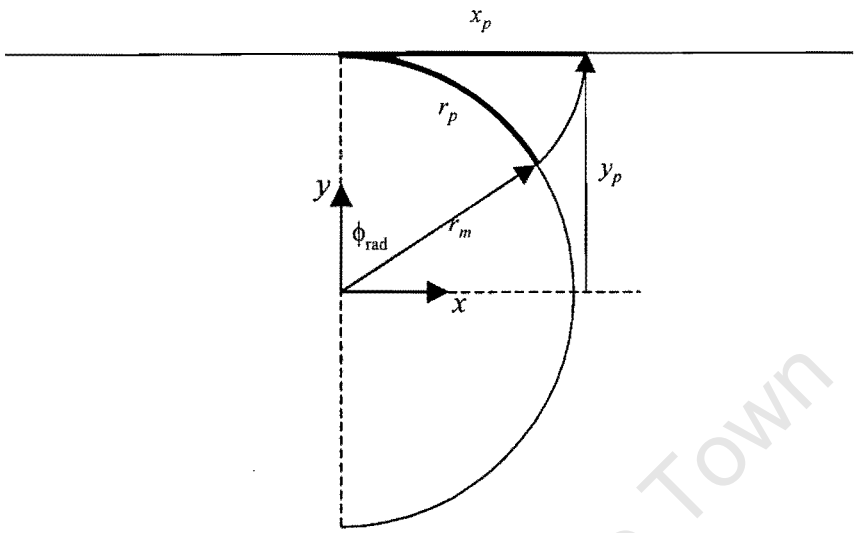

Figure 4.33 Equidistant azimuthal projection

where $x_p = r_p$. The y co-ordinate of the projected point, y_p, is equal in distance to r_i, the distance from the i^{th} point to be projected to the centre of the tower, and is given by:

$$y_p = \sqrt{x_i^2 + y_i^2}$$

Equation 4-4

for a co-ordinate system with origin on the tower centre point. The first step towards realising this projection, then, is finding the central point of the tower (defined, in this case, by the x, z co-ordinates; the y co-ordinate defines vertical height, as shown in Figure 4.32). This requires that the individual DSMs making up the tower surface be amalgamated into one continuous model.

Since the four DSMs making up the tower were each generated in a different co-ordinate system, each of which maintains $z = f(x, y)$ as shown in Figure 4.34, they first had to be rotated and translated into one system. Only then could the centre point of the tower be calculated using the quasi-parametric case of least squares adjustment.

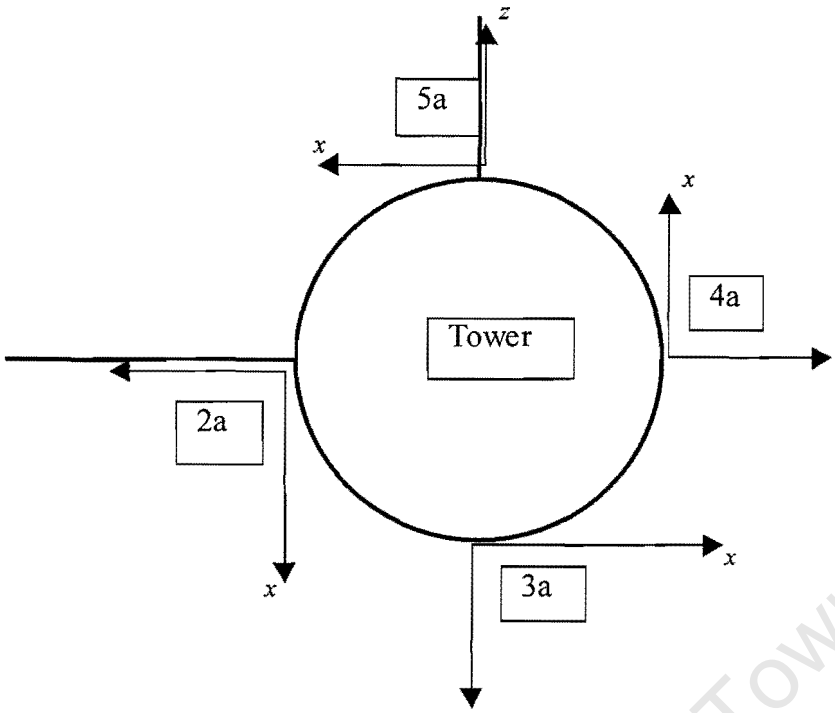

Figure 4.34 Co-ordinate systems used when creating DSMs of the tower

Provisional values for the centre point and radius were calculated as follows:

$$X_m = \frac{1}{n}\sum_{n}^{i=1} X_i$$

$$Z_m = \frac{1}{n}\sum_{n}^{i=1} Z_i$$

$$r_m = \frac{1}{n}\sum_{n}^{i=1} \sqrt{(X_i - X_m)^2 + (Z_i - Z_m)^2}$$

Equation 4-5

where X_m, Z_m are mean values for the point co-ordinates X_i, Z_i, and r_m is the mean value of the radii from the provisional centre point to the n individual DSM points. The condition equation was:

$$F(\overline{X}, \overline{Z}) = (X_i - X_m)^2 + (Z_i - Z_m)^2 - r_i^2$$

Equation 4-6

from which the co-efficient matrices were calculated as:

$$A = \begin{bmatrix} \frac{\partial F}{\partial Z_m} & \frac{\partial F}{\partial X_m} & \frac{\partial F}{\partial r_m} \end{bmatrix}$$

$$B = \begin{bmatrix} \frac{\partial F}{\partial Z_i} & \frac{\partial F}{\partial X_i} & 0 & 0 & \dots & 0 & 0 \\ 0 & 0 & \frac{\partial F}{\partial Z_i} & \frac{\partial F}{\partial X_i} & \dots & 0 & 0 \\ & & & & \dots & & \\ & & & & \dots & & \\ 0 & 0 & 0 & 0 & \dots & \frac{\partial F}{\partial Z_i} & \frac{\partial F}{\partial X_i} \end{bmatrix}$$

Equation 4-7

Shifts to the provisional values were then calculated using:

$$\hat{x} = -\left(A'\left(BB'\right)^{-1}A\right)^{-1}A'\left(BB'\right)^{-1}\overline{w}$$

Equation 4-8

where w is the vector of misclosures. These shifts were then added to the provisional values.

The differences between the adjusted values and the provisional values were calculated, and while these each exceeded a threshold value (0,0001 m), the whole procedure was iterated. After four iterations, the solution reached convergence. The standard errors of the parameters are given in Table 4.6 and the variance of the adjustment was 0,0042 m. The residuals had a standard deviation of 0,0459 m, which means that the difference between the variations in the tower's surface and a cylindrical approximation are approximately 4,6 cm. Maximum and minimum values of around 53 and –47 cm respectively occurred in the areas where DSMs overlapped.

Table 4.6 Standard errors of tower centre co-ordinates and radius

	Z_m	X_m	r_m
Standard errors	0,0015	0,0013	0,0010

Having obtained precise values for the x and z co-ordinates of the tower centre and the radius of the tower, it was possible to project the cylindrical tower onto a vertical, planar surface. The process is akin to 'unrolling' the tower along the ground. The new co-ordinates for every DSM point were given by Equation 4-3 and Equation 4-4, mirrored here as:

$$Z_p = \sqrt{Z_i^2 + X_i^2}$$
$$X_p = r\phi$$

Equation 4-9

where Z_i, X_i are the co-ordinates of the DSM points translated into a co-ordinate system centred on the centre point of the tower; r is the radius calculated from the least squares adjustment; and ϕ is given by:

$$\phi = \frac{\pi}{2} - \tan^{-1}\left(\frac{Z_i}{X_i}\right)$$

Equation 4-10

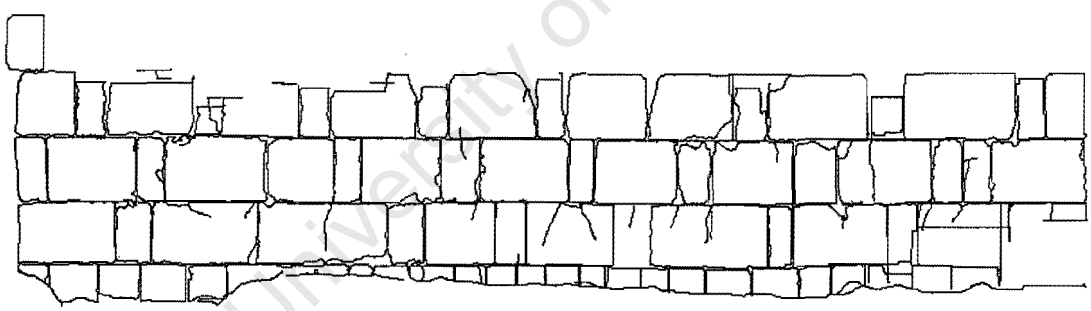

Figure 4.35 'Unrolled' tower line drawing

Figure 4.35 shows the 'unrolled', combined line drawing, using AutoCAD, while Figure 4.36 shows the DSM using 'Surfer'. It was initially hoped that, using the 'unrolled' DSM and corresponding camera centres, a continuous orthophoto of the flat DSM could be produced. This was not possible using the resources at hand as, to maintain the original geometry of the perspective projection, the raw images would need to be 'rolled up' an equivalent amount. This is illustrated in Figure 4.37. The distances AB and $A'B'$ (i.e. from image plane into object space) must be maintained

uniformly across the image. This can only be done by warping *AA'* to *aa'* an equivalent amount as *BB'* to *bb'*, as shown.

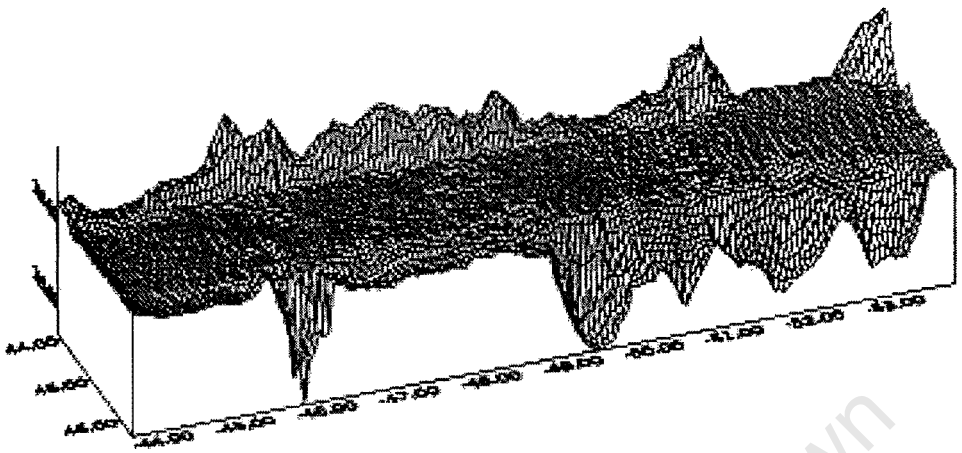

Figure 4.36 'Unrolled' tower DSM

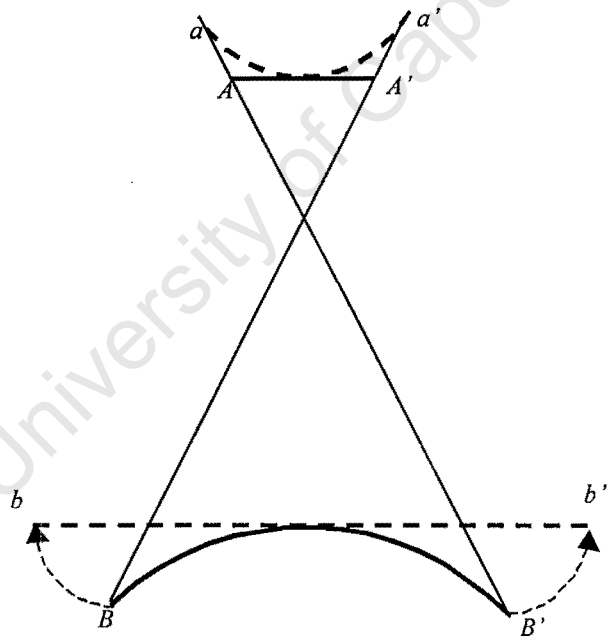

Figure 4.37 Relationship between original and 'unrolled' DSMs and original image

A more feasible alternative would be to associate a grey value to each DSM point, as a fourth 'co-ordinate'. By including this value in the unrolling process, a coarse

orthophoto of the unrolled tower surface could be obtained. Some interpolation of the grey values would be required to obtain a smooth image.

4.3.2. CAD Visualisation

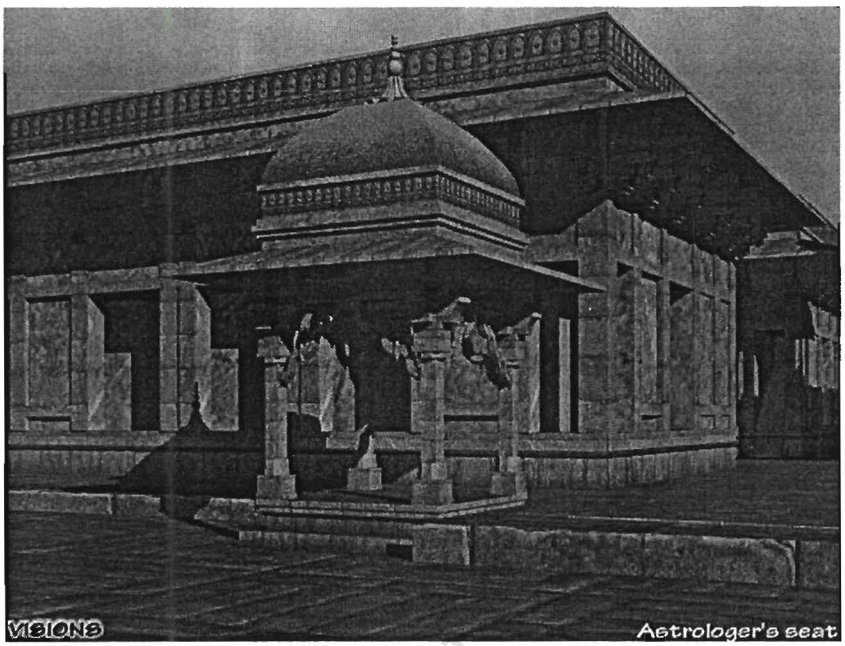

Figure 4.38 Effective use of lighting and texture on a CAD model (Haval, 1999)

Using standard CAD packages such as AutoCAD and MicroStation it is fairly simple to create realistic computer models of structures. Examples of the possibilities open to an experienced CAD user are given in Figure 2.13, Figure 2.14 and Figure 4.38. By applying lighting and texture to the surfaces of the building, a greater degree of realism is attained than through observing the base map alone. See, for example, Figure 4.38 , which uses artificial texture very effectively to give the impression of realism (from Haval, 1999). In the case of Horvat Minnim, it was possible to extend the base map (Figure 4.1) vertically by a user-defined number of metres, to try to roughly simulate its appearance at the time it was built (Figure 2.14 and Figure 4.39).

Although somewhat time-consuming, the process of creating a realistic, 3D portrayal of a structure from a 2D base map and measurements taken thereof is fairly simple mathematically. To create the structure, or wireframe model, requires only the correct geometrical model. To visualise this as it may have once stood, however, requires

both the perceptual and artistic abilities of the human user. These tools, combined with a numerical basis, help the designer to 'look into the past' and produce a convincing replication of the existing structure, as per Figure 4.38.

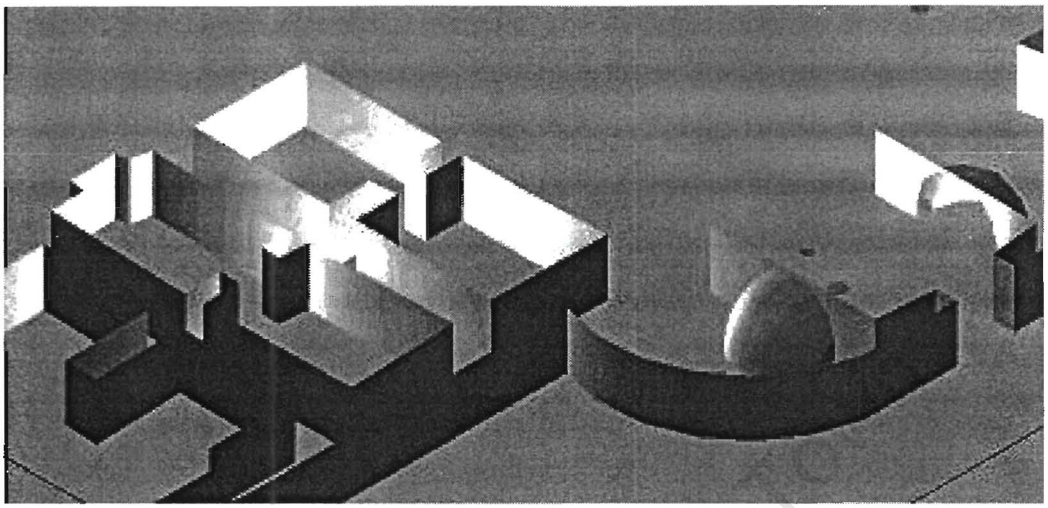

Figure 4.39 CAD model of section of Horvat Minnim with 2,0 m walls

Without denying the importance of the visual aspect of any accurate 3D reconstruction, this thesis focuses primarily on the geometrical integrity of models produced photogrammetrically. Hence CAD visualisation will not be further explored here.

4.3.3. VRML Visualisation

Using a MicroSoft Visual Basic 5.0 program developed at the Department of Geomatics, UCT (Taylor, 2000), it was possible to convert lists of DSM points output by SOCET SET, into a VRML format. This format consists of a few lines of definitions text, specifying viewpoints, background colours etc., followed by a declaration of the number of points in x and y and the grid spacing of the points. This, in turn, is followed by a list of z values.

For each DSM file converted into the VRML format, the origin of a local co-ordinate system is specified at the bottom left (south west) corner of the DSM. To represent the four DSMs used to create the tower, in one co-ordinate system, requires translations

and rotations of the DSMs. Once the required figures have been calculated, these are carried out simply through two commands in the definitions section of the file, e.g.

```
translation 1.418 -1.32 0.18
rotation 0 0 1 1.5708
```

The three figures following 'translation' indicate by how much the origin of the local co-ordinate system must be shifted within the viewer's co-ordinate system, in the x, z and y directions respectively. The first three figures following 'rotation' specify the direction of a unit vector from the origin of the DSM's local system about which the DSM should be rotated. The angle of rotation is given by the fourth figure, in radians.

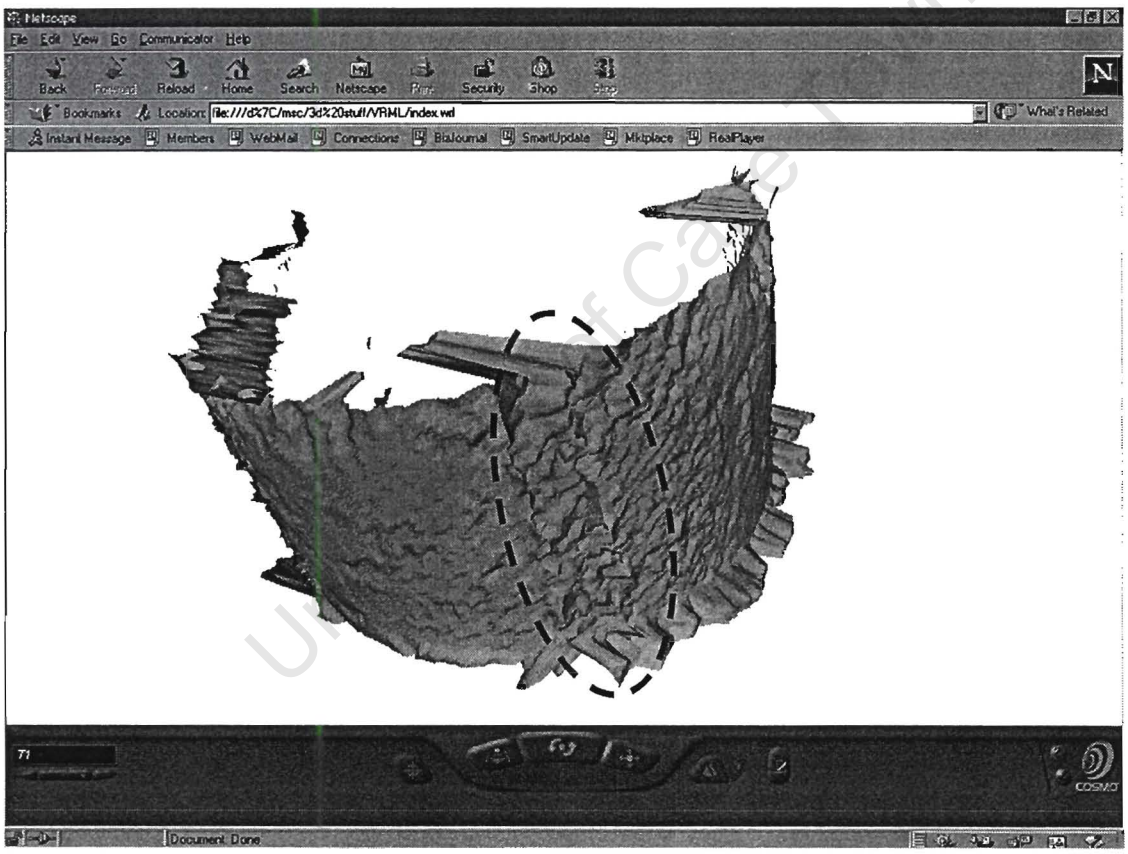

Figure 4.40 VRML tower model without ortho-images. Dashed ellipse shows overlap errors.

The representation of a series of different surfaces in one co-ordinate system using VRML follows easily. The tower surfaces so united are shown in Figure 4.40 as they would appear on a computer screen. The portions of the surface jutting back at the top of the tower and forward at the bottom, are not errors, as they appear. At the bottom,

they are points modelling the ground surface at the foot of the tower. At the top, they are points modelling the broken top surface of the tower.

The texture applied to the surfaces of Figure 4.40 is the default texture from VRML. A more realistic impression is gained using geo-referenced ortho-images (Figure 4.41). The ortho-images are created directly from the DSMs used to make the tower model and hence conform to each partial surface perfectly in terms of size. It is then simply a case of specifying which image goes where in the model, and the recreation of Figure 4.41 is achieved: a much more realistic impression.

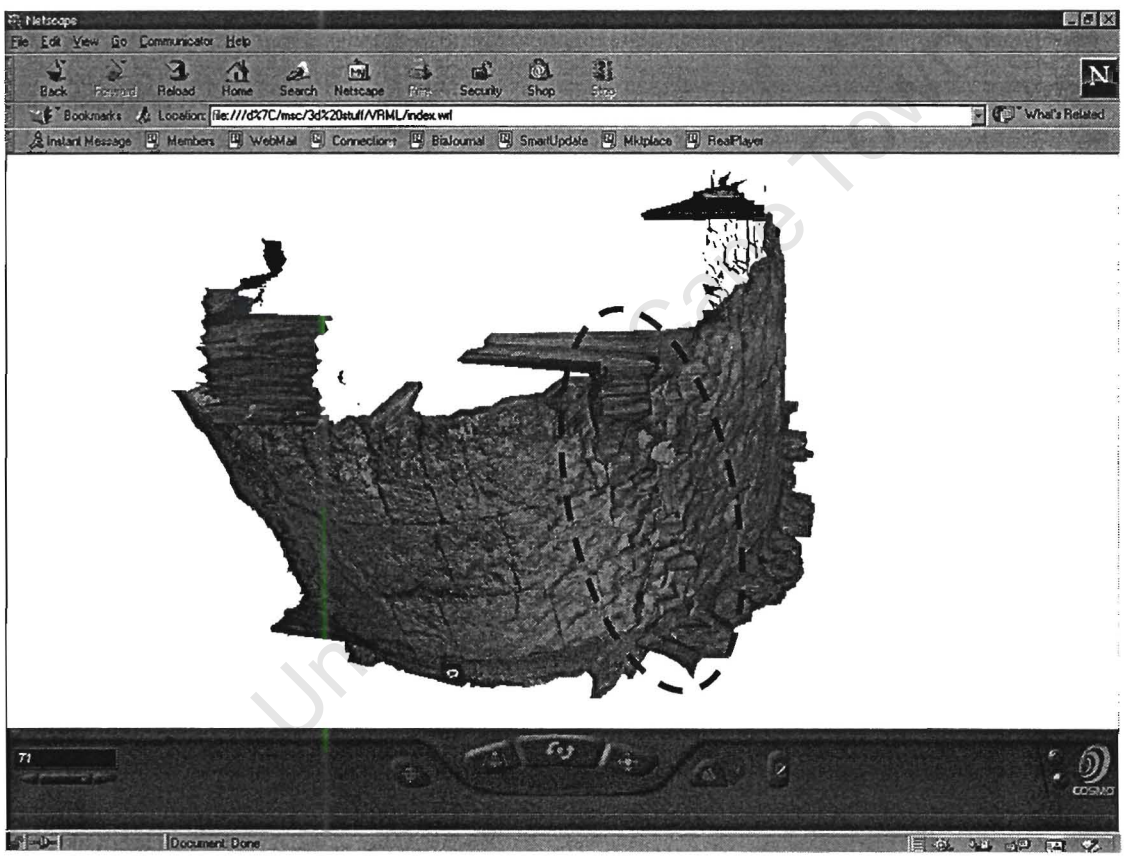

Figure 4.41 VRML tower model with ortho-images. Dashed ellipse shows overlap errors.

In Figure 4.40 and Figure 4.41 errors are apparent where two DSMs overlap, indicated by a dashed ellipse in the figures. This is because, as Baltsavias (1991) suggested and Davey (1999) confirmed, matching on curved surfaces is least accurate as the surface dips further away from the cameras. Davey's surface editing routine could not, however, be run on these surfaces as the conversion program requires

regular grids: after editing, some points would be missing, creating gaps in the grid structure. To overcome this difficulty, either the points in the overlapping regions should:

- be averaged,
- be treated as redundant and deleted, or
- be identified as erroneous by running Davey's program, and an interpolation algorithm applied to the surface to fill in the gaps.

The first option either improves 'bad' data or degrades 'good' data, and hence was not considered. By taking option two and only deleting those points which are most likely to be inaccurate, i.e. those closest to the edge of the respective DSMs, the 'good' data would be saved. The third option has the disadvantage of producing DSMs with, possibly, a substantial amount of interpolated data. We have already seen in section 2.3.4.4(b) that this is undesirable: by interpolating, a smooth mathematical surface is presumed, which is often not the case in architecture. Additionally, the first and third points above still allow overlapping of the orthophotos. To obtain a smooth, seamless representation of the tower, the orthophotos would need to be mosaicked. The second option, above, was deemed to be the best, even though it necessitates the reproduction of additional orthophotos.

An algorithm describing the process is given below, concentrating on the overlap between models 2a and 3a (blue and green DSMs in Figure 4.42, respectively).

1. The minimum and maximum x values of model 2a, and the minimum and maximum z values of model 3a, were found. These are given by 'min x2', 'max x2', 'min z3' and 'max z3' respectively, in Figure 4.42. The regular grid structure of the DSMs means that there is more than one point sharing the minimum or maximum value, as illustrated in Figure 4.42 (bottom).
2. The points found above were converted from Cartesian to polar co-ordinates. Whereas, in Cartesian co-ordinates, these points all have equal x or z values, depending on the model, in polar co-ordinates they have a range of values (shown by dotted, coloured lines in the figure). To find a single value for the maximum and minimum angles, the means of max x2 and max z3 (in polar co-ordinates)

were calculated. The maximum polar co-ordinate of min x2 was chosen as the reference angle. These are shown as 'a2a', 'a23a' and 'ref_angle' respectively in Figure 4.42.

3. The mean of angles a2a and a23a is the 'angle of overlap' for models 2a and 3a, shown as 'mean(a2a, a23a)' in Figure 4.42.
4. The co-ordinates of every point in model 2a are converted from Cartesian to polar, and the angles stored as an array called A2.

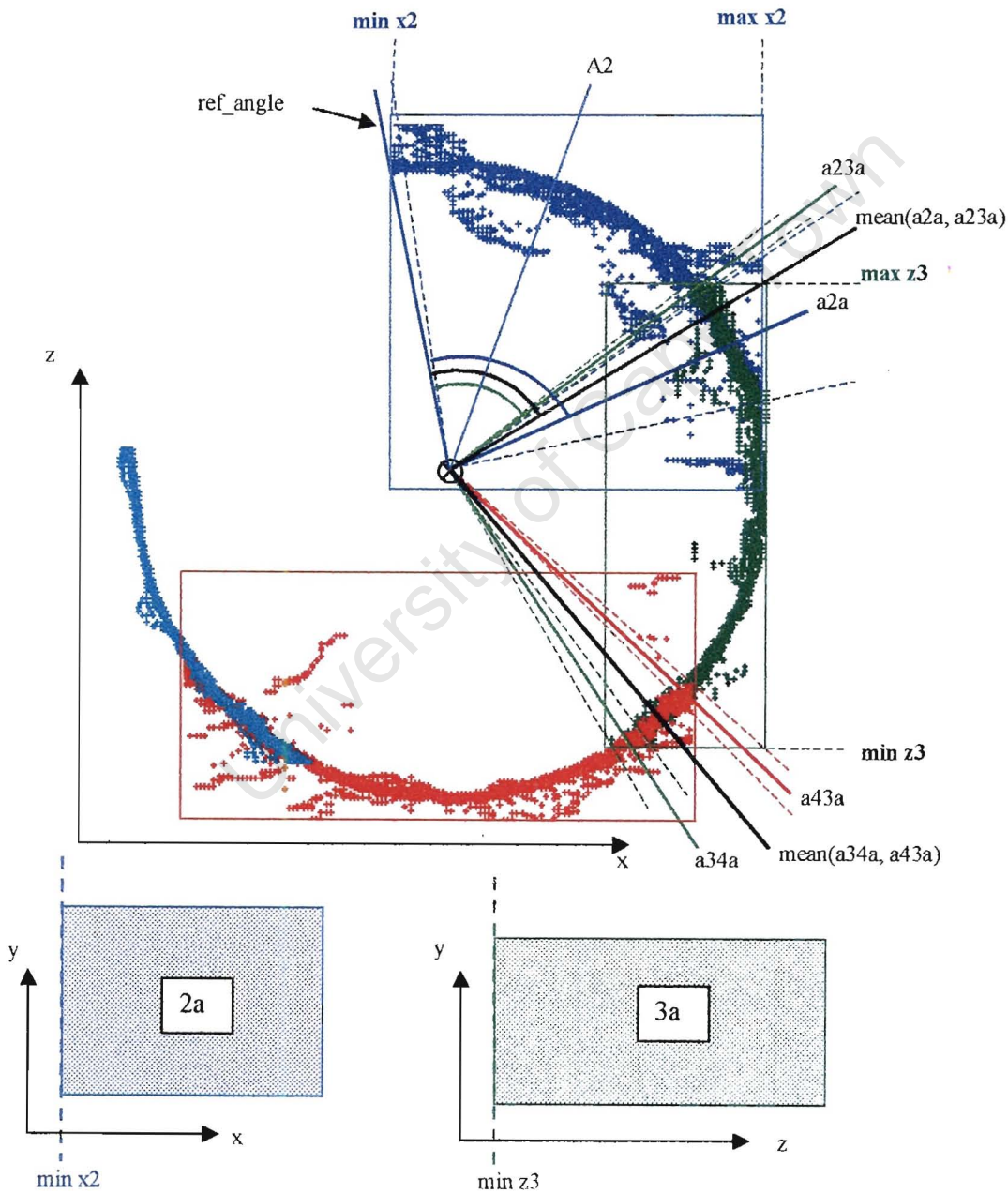

Figure 4.42 Eliminating overlaps. Top: view of tower DSMs from above. Bottom: view of models 2a and 3a showing grid structure of the DSMs.

By finding all of the points corresponding to the angles of A2 lying between ref_angle and the angle of overlap, the 'good' data should be identified. A problem, however, is that the regular grid structure of the input DSM is not maintained; i.e. referring to the bottom two figures of Figure 4.42, points are not removed sequentially from left to right. To maintain the regular grid, a different method had to be used, as follows:

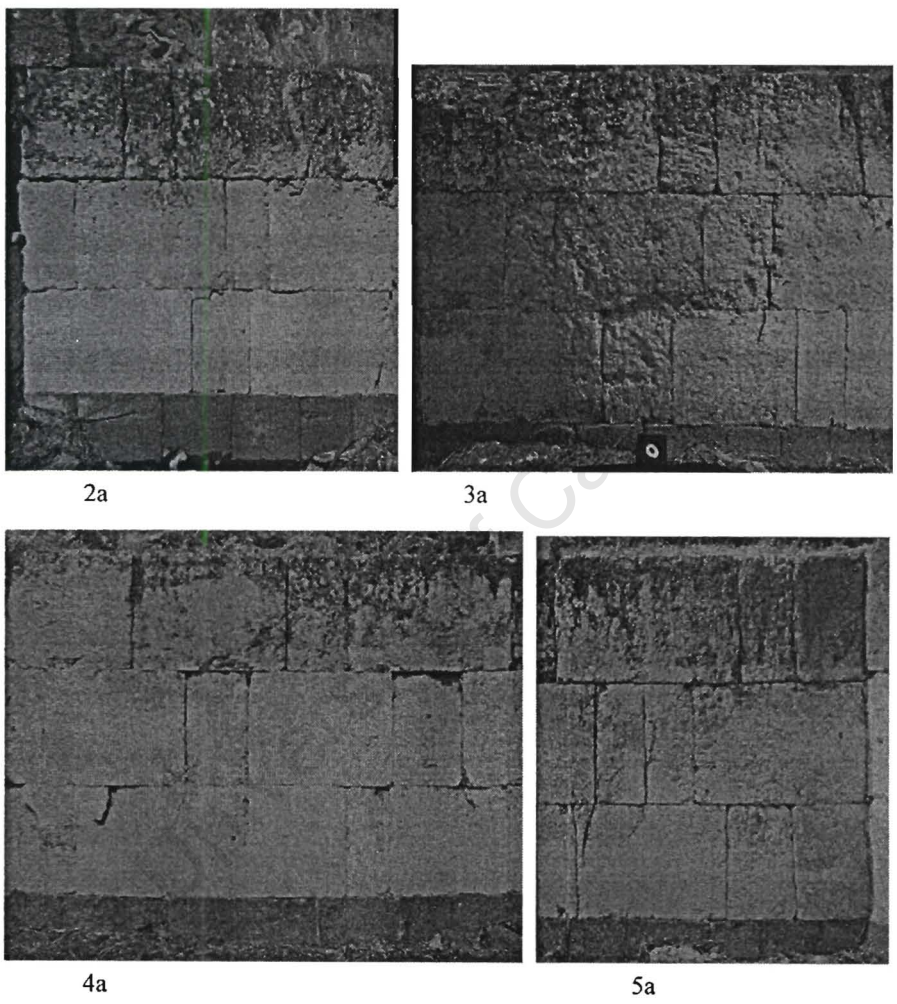

Figure 4.43 Orthophotos from reduced tower DSMs: clockwise from top left, stereo-models 2a, 3a, 5a and 4a are shown.

5. The Cartesian co-ordinates of the points corresponding to the angles of A2 lying between ref_angle and the angle of overlap, were found. Let us call these points A2o.
6. Similarly, the Cartesian co-ordinates for the points of model 3a between the angles of overlap 'mean(a2a, a23a)' and 'mean(a34a, a43a)', were also found. Let

us call them A3o. The angle 'mean(a34a, a43a)' between models 3a and 4a was calculated in a similar way as 'mean(a2a, a23a)' described above.

7. By finding the average x, z co-ordinates for the means of A2o and A3o, a point is defined in the DSMs that lies on or near the angle of overlap. Those points with x value less than the x value of this point belong to the new DSM 2a, and those with z value less than the z value of this point belong to the new DSM 3a. By defining the new DSMs in this way, a regular grid is maintained without any overlap between adjacent DSMs.
8. The process is repeated for the overlaps between 3a and 4a, and 4a and 5a.

The edited DSMs were then used to create new orthophotos, shown in Figure 4.43. Unfortunately, due to a problem with the conversion program, the DSMs could not be converted into VRML format for interactive display. Figure 4.44 is a point cloud Matlab plot of the reduced DSMs. It is not possible to texture map orthophotos onto such a plot in Matlab.

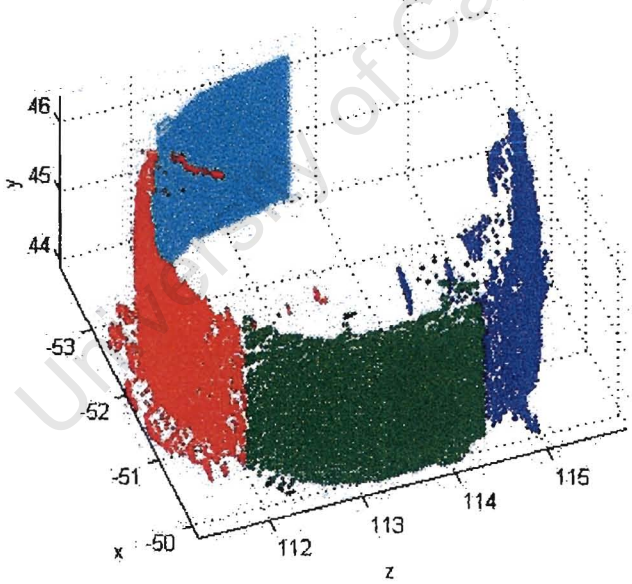

Figure 4.44 Matlab plot of reduced tower DSMs

4.3.4. Visualisation and GIS

The visualisation described in the preceding section serves to aid the user in terms of orientation and familiarisation with the subject. It would be even more beneficial if

the virtual model were to be presented in an interactive environment where analysis of the structure is also possible. This would then serve as both a research and an educational tool. Such a 3D GIS would allow the user to make measurements across the tower surfaces, compare models constructed from data captured at different times, and construct "what if" scenarios. The comparison of different types of data (line vs. point, raster vs. vector, for example) would also be useful.

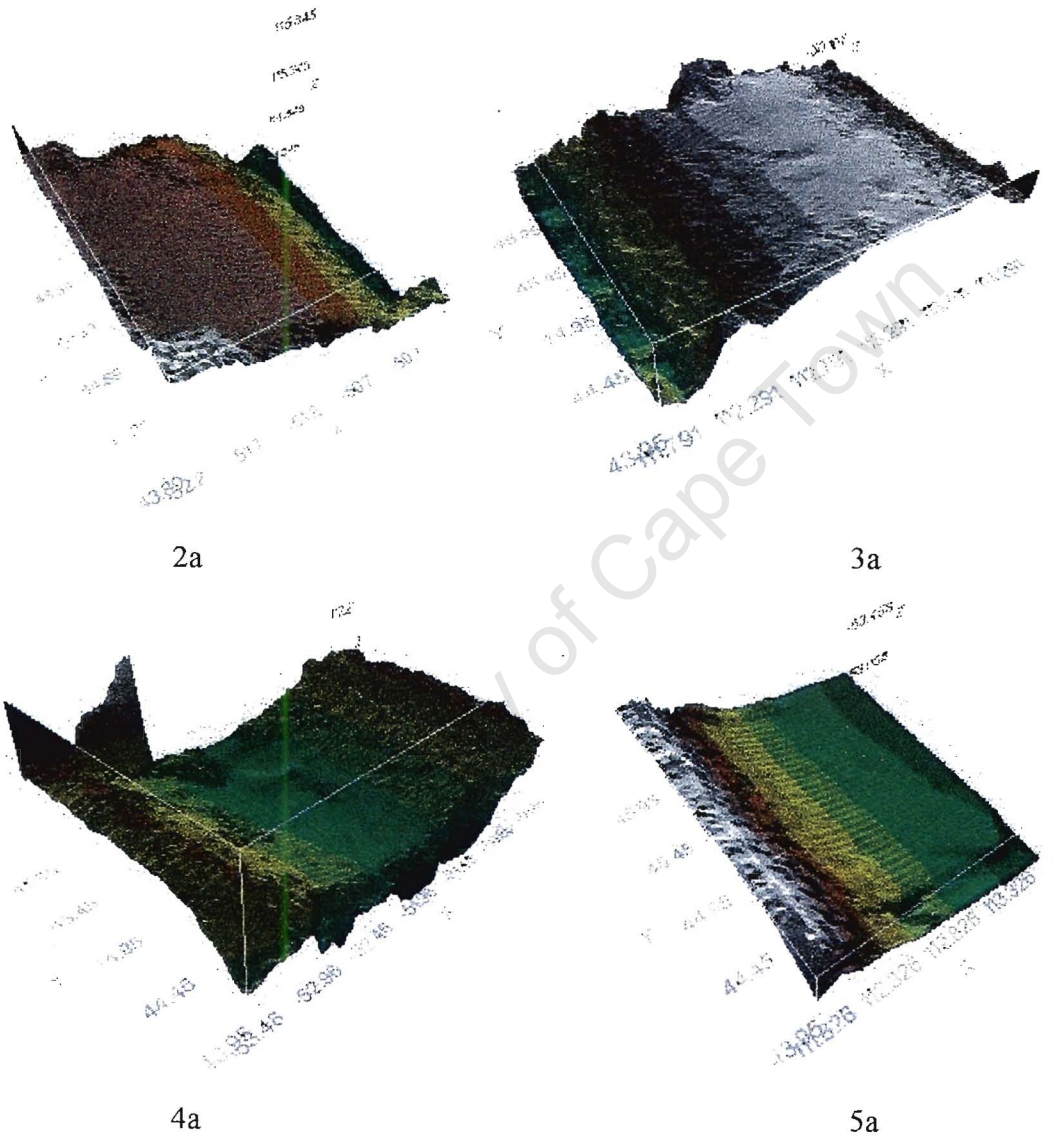

2a 3a

4a 5a

Figure 4.45 2.5D DSM visualisations: clockwise from top left, stereo-models 2a, 3a, 5a and 4a.

Since GIS packages deal with objects geographic, they have been developed to handle 2.5D data sets and not objects with full 3D extent. True 3D, and 4D, representation

and visualisation requires specialised software. Continuous volumes are represented instead by slices through a 3D image, for example (Burrough & McDonnell, 1998). It can be said that the development of a 3D GIS is far from trivial and it is, indeed, a matter of intense research at present (see e.g. Schlüter (1998) and Wei *et al* (1998)).

The individual DSMs making up the tower are 2.5D models, and hence it was a matter of course to visualise these using ArcView's 3D Analyst extension (Figure 4.45). Each DSM is viewed in a separate co-ordinate system with graduated colours showing the elevation of the surface above a datum. The surfaces may be rotated and viewed from any angle, contours can be added and orthophotos overlaid. They cannot, however, be viewed all together in one system. That is the situation of Figure 4.46. DSMs 2a and 4a are projected without any errors, as they maintain the $z = f(x, y)$ condition. For DSMs 3a and 5a, the local z co-ordinate is modelled by a global x co-ordinate (see, for example, Figure 2.11), causing serious errors. This is especially visible in model 3a (circled in the figure).

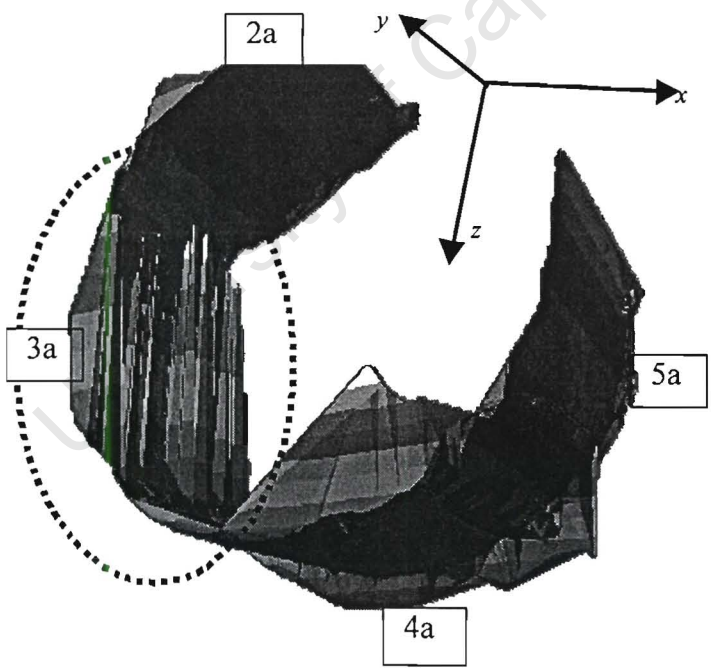

Figure 4.46 Adding the third dimension

The model created in section 4.3.3 does not contain these errors. This is because each surface is created in its own unique co-ordinate system (e.g. Figure 4.45), where the z

$= f(x, y)$ condition is true. The surfaces themselves are then rotated and translated into another system. In ArcView, surfaces can only be created and viewed in the same system. The surfaces of Figure 4.45 cannot, therefore, be imported into the co-ordinate system of Figure 4.46. That is why surfaces 2a and 4a are viewed correctly, but 3a and (to a less observable degree) 5a contain errors.

The prospect of true, 3D / volumetric GIS is an exciting one which will open up a range of new possibilities once it is realised. Until then, GIS will be limited to 2.5D in terms of visualisation and in terms of the calculations that can be carried out.

CHAPTER 5
Discussion and Conclusions

5.1. Conclusions

The objectives for this thesis, as stipulated in section 1.4, were:

1. Production of DSMs of the complete Horvat Minnim palace, modelling the structure as closely as possible.
2. Production of orthophotos of each stereo-model from the DSMs produced.
3. Comparison with other 3D models (CAD-based and line drawing).
4. Visualisation of the palace, or part thereof, using suitable software.

The site of Horvat Minnim was surveyed using photogrammetric measurement techniques. DSMs and orthophotos were produced for most of the stereo models of Horvat Minnim, as per objectives 1 and 2 above. The DSMs had a general grid spacing of 3 cm, requiring up to 35000 points per stereo model. The co-ordinates of these points were stored in ASCII files ranging from as little as 30 Kb to 4,5 Mb in file size. Compiling all of the DSMs into one model would therefore require large amounts of disk space and RAM, bearing in mind that just under 100 models of Horvat Minnim were surveyed. State of the art computers, with processing capabilities superior to those of the average PC's, would be required to visualise the entire site using, for example, VRML.

The performance and capabilities of two different visualisation tools, VRML and ArcView, were assessed, as per objective 4. It can be concluded from this assessment that the aims set out in CHAPTER 1 (complete, accurate documentation of archaeological structures) are too stringent if regular hardware is to be used (Pentium II 333 MHz processors with 64 Mb RAM). Either the hardware must be upgraded to something like a dual Pentium II, as per Haval (1999), or the post spacing must be decreased with an associated lack of accuracy.

In spite of the limitation of large file size and consequent slow processing speed, VRML proved to be a most useful tool for visualisation of a part of the Horvat Minnim palace. It was a matter of course to bring adjacent DSMs together in one co-ordinate system, with orthophotos texture-mapped onto the surfaces. VRML also allows easy navigation around the site and as such could be used as an educational tool to teach students, scholars etc. about the ancient architecture. Additional programming is required if measurement and analysis is to be done on the surface of the model, and so the capabilities of ArcView in this regard were also investigated.

It was found that ArcView, although capably visualising individual, 2.5D surfaces with its 3D Analyst extension and allowing interactive measurement and analysis to take place, cannot consider objects having full 3D extent. The development of such an interactive measurement information system is on-going (see, for example, Schlüter (1998), Boochs *et al* (1998), Wei *et al* (1998), and Heckes & Hornschuch (1997)).

3D models which use primitive entities rather than individually measured points to describe their surfaces (CAD-based models) will continue to be relevant at least until faster PCs with more memory become standard. In fulfilment of objective 3, a CAD model of Horvat Minnim was created using AutoCAD software. As has been shown in the literature review (section 3.2), these types of models are also useful educational tools.

5.2. Relevance of the Research

The different models created in this thesis all have a dual purpose, the first being scientific in nature, while the second involves education and transfer of knowledge to the general public:

1. Archaeologists benefit through a better understanding of past cultures. Cultural use, as indicated through intervisibility and spatial interaction within a particular building or monument, can only be assessed through reconstruction of the contemporary architecture and other relevant artefacts (Chalmers *et al*, 1996). As a research tool, a 3D model can be used to test reconstruction ideas,

archaeological interpretation of the site, and even the simulation of structural stress.

Accurate and precise computer models of heritage monuments can be a rich and valuable reference for conservationists, archaeologists, researchers, historians and students. Throughout history, historic monuments and structures have been documented using various media of communication (from cave paintings to paper and video). According to Haval (1999) this could be the advent of a new form of communication and accurate archiving of valuable data.

2. On the other hand, they also have publicity and marketing value, and can be used for presentation, education and communication. Computer reconstructions will undoubtedly help to stimulate a greater interest and appreciation, amongst the general public, of the monument and its structural history. The ability to "get inside and walk around" (Wood *et al*, 1992, 130) reconstructed buildings gives the lay person and scientist alike a stronger feeling of the enclosed space and volume, and possibly even a real sense of actually being there.

   It is difficult to assess what the result of public access to 3D reconstructions of monuments will be. From the viewpoint of tourism, computer models may help reduce the pressure on often fragile historical monuments (Chalmers *et al*, 1996). Having viewed the monument through electronic media, however, the public's interest may also be pricked with a resultant increase in the flow of tourists to the site. What is certain is that a wider audience will have 'access' to the monuments through the Internet or the distribution of CD-ROM, etc.

Depending on the purpose of the generated model, a simple surface or solid model, as described previously, may be adequate and a far better option than a model involving a high degree of surface accuracy. However, there are instances where attention to detail is not only desirable, but also necessary.

- There may (and most likely will) be better technologies developed in the future which will allow large databases to be loaded on a personal computer without affecting its performance to any great degree. Better technologies will also allow more interaction with the model by an operator. It makes sense, then, to extend

the boundaries of what is possible now to include what will be possible in the future.

- Where reconstruction and preservation of the structure is the purpose behind developing a 3D model, a high degree of accuracy is required if this is to be done sufficiently. An accurate reconstruction of an ancient building can only be achieved to the same, or lesser, degree of accuracy as the survey.

If we are to preserve our archaeological heritage for the benefit of ourselves and future generations, then on-going research in this field is imperative and the work done in this thesis is not purely academic.

References

Abouaf, J. (1999), The Florentine Pietà: can visualisation solve the 450-year-old mystery?, *IEEE Computer Graphics and Applications*, Potel, M. (ed.), January/February 1999, pp. 6-10.

Ackermann, F. (1996), Some considerations about feature matching for the automatic generation of digital elevation models, *Proceedings of the OEEPE workshop on Application of Digital Photogrammetric Workstations*, Kölbl, O. (ed.), Lausanne, pp. 231-240.

ADAM Technology (1994), *Using the ADAM System Software Version 3.0*, ADAM Technology, Australia.

Adolfsson, B. (1997), Documentation and reconstruction of architectural elements at the fortress of Freriksborg and at the Swedish National Art Museum, *International Archives of Photogrammetry and Remote Sensing*, Vol XXXII, Part 5C1B, pp. 161-167.

Bacher, U. (1998), Experimental studies into automated DTM generation on the DPW770, *IAPRS*, Vol. 32, Part 4, *GIS – Between Visions and Applications*, Stuttgart, pp. 35-41.

Bacigalupo, C., Cessari, L. & Fangi, G. (1997), Experiences of geometrical monitoring and survey of defects by using laser technologies and photogrammetry, *International Archives of Photogrammetry and Remote Sensing*, Vol XXXII, Part 5C1B, pp. 168-174.

Bacigalupo, C., Cessari, L. & Fangi, G. (1998), Geometric monitoring and integration of geodetic survey techniques to improve the knowledge of the historic building, *International Archives of Photogrammetry and Remote Sensing*, Vol. XXXII, Part 5, pp. 502-506.

Balletti, C. & Pilot, L. (1998), Plan, execution and representation of an architectonic survey: the Torrazzo of Cremona, Italy, *International Archives of Photogrammetry and Remote Sensing*, Vol. XXXII, Part 5, pp. 507-512.

Baltsavias, Emmanuel P. (1991), *Multiphoto Geometrically Constrained Matching*, unpublished PhD thesis, ETH-Zürich, Switzerland.

Baltsavias, E. & Käser, C. (1998), DTM and orthoimage generation – a thorough analysis and comparison of four digital photogrammetric systems, *IAPRS*, Vol. 32, Part 4, *GIS – Between Visions and Applications*, Stuttgart, pp.42-51.

Baum, J., Robinson, D., Carrington, P., Mason, D. & Strickland, T. (1998), *The Chester Project: Reconstructing Roman Chester*, Online, Available: http://dialspace.dial.pipex.com/julianbaum/tcp.shtml 8 February, 2000.

Biddle, M. (1991), Jerusalem: the tomb of Christ, *Current Archaeology*, Vol 11 (3), pp. 107-112.

Bill, R., & Fritsch, D. (1991), *Grundlagen der Geo-Informations-systeme: Hardware, Software und Daten*, Volume 1, Wichmann, Karlsruhe.

Biran, A. (1996), *Biblical Dan*, Israel Exploration Society, Jerusalem.

Biran, A., Ilan, D. & Greenberg, R. (1996), *Dan I: A Chronicle of the Excavations, the Pottery Neolithic, the Early Bronze Age and the Middle Bronze Age Tombs*, Nelson Glueck School of Biblical Archaeology, Hebrew Union College – Jewish Institute of Religion, Jerusalem.

Boochs, F., Garnica, C. & Wolter, F. (1998), Determination and interactive visualisation of 3D-objects, *International Archives of Photogrammetry and Remote Sensing*, Vol. XXXII, Part 5, pp. 316-322.

Burrough, P. & McDonnell, R. (1998), *Principles of Geographical Information Systems*, Oxford University Press, Oxford.

Campbell, D. & Wells, M. (1994), *A Critique of Virtual Reality in the Architectural Design Process*, Seattle: University of Washington, Human Interface Technology Laboratory.

Chalmers, A, Stoddart, S, Belcher, M & Day, M (1996), *An Interactive Photo-Realistic Visualisation System for Archaeological Sites*, Online, Department of Archaeology, University of Bristol, Available: http://www.bris.ac.uk/Depts/Archaeology/html/research/comvis/insite2.htm 8 February, 2000.

Christensen, D. (1999), Sculpting Virtual Reality: 3-D models offer new ways of seeing art, *Science News*, Vol. 156, No. 12, p. 184, Online, http://www.sciencenews.org/sn_arc99/9_18_99/bob1.htm Available 8 February, 2000.

Collins, P. (1998), PhotoModeler – low-cost photogrammetry comes of age!, *Engineering Surveying Showcase '98*, Autumn 1998, GITC.

Colombo, L. (1998), Photogrammetric imaging for virtual reality: an example of settlement documentation, *International Co-operation and Technology Transfer*, Vol. XXXII (6w4), pp. 111-116.

Daniels, R (1997), The need for the solid modeling of structures in the archaeology of buildings, *Internet Archaeology 2* (http://intarch.ac.uk/journal/issue2/daniels_index.html)

Davey, J. (1999), *Object Reconstruction Using Close-Range All-Round Digital Photogrammetry for Applications in Industry*, unpublished MSc thesis, UCT, Cape Town.

Demas and Rosen-Ayalon (1999), Horvat Minnim, GCI unpublished report.

Drollinger & Miller (1995), Strategy Information for ATE, General Dynamics Corporation unpublished report.

Dupéret, A. (1996), Automatic derivation of a DTM to produce contour lines, *Proceedings of the OEEPE workshop on Application of Digital Photogrammetric Workstations*, Kölbl, O. (ed.), Lausanne, pp. 193-221.

Eckstein, G. (1997), Photogrammetric measurement to interpret the damage evolution of the stone sculpture in the Holy Cross Minster in Schwäbisch Gmünd, Germany, *International Archives of Photogrammetry and Remote Sensing*, Vol XXXII, Part 5C1B, pp. 154-160.

El-Hakim, S., Brenner, C. & Roth, G. (1998), An approach to creating virtual environments using range and texture, *International Archives of Photogrammetry and Remote Sensing*, Vol. XXXII, Part 5, pp. 331-338.

Förstner, W. (1986), A feature based correspondence algorithm for image matching, *International Archives of Photogrammetry and Remote Sensing*, Vol XXVI, No. 3/3, pp. 176-189.

Fryer, J. (1996), Introduction, *Close Range Photogrammetry and Machine Vision*, K. B. Atkinson (ed.), Whittles Publishing, Scotland, pp 1-7

Gasior, D. (1996), Automatic derivation of a DTM with the Helava system, *Proceedings of the OEEPE workshop on Application of Digital Photogrammetric Workstations*, Kölbl, O. (ed.), Lausanne, pp. 241-250.

Greenfeld, J., & Schenk, A. (1989), Experiments with edge-based stereo matching, *Photogrammetric Engineering and Remote Sensing*, Vol. 55, No. 12, pp. 1771-1777.

Guerra, F. (1997), Survey and representation of domes, *International Archives of Photogrammetry and Remote Sensing*, Vol XXXII, Part 5C1B, pp. 175-178.

Gülch, E. (1996), Fundamentals of softcopy photogrammetric workstations, *Digital Photogrammetry: an Addendum to the Manual of Photogrammetry*, American Society for Photogrammetry and Remote Sensing, Maryland, pp. 213-226.

Hanke, K, & Ebrahim, M. (1997a), Monument presentation using digital architectural photogrammetry, *International Archives of Photogrammetry and Remote Sensing*, Vol XXXII, Part 5C1B, pp. 147-153.

Hanke, K. & Ebrahim, M. (1997b), A low cost 3D-measurement tool for architectural and archaeological applications, *International Archives of Photogrammetry and Remote Sensing*, Vol XXXII, Part 5C1B, pp. 113-120.

Haval, N. (1999), *The Challenge: Resurrection of Fatehpur Sikri, a World Heritage Society Site in India*, Online, Available http://westwood.fortunecity.com/karan/133/chall.htm 8 February, 2000.

Heckes, J. & Hornschuch, A. (1997), Digital photogrammetry and image processing for the documentation of monuments and sites, *International Archives of Photogrammetry and Remote Sensing*, Vol XXXII, Part 5C1B, pp 108-112.

Heine, E. (1999), *Interdisciplinary Association for Maya Studies*, Erwin Heine (ed.), Online, Available http://www.cis.tu-graz.ac.at/IAM 8 February, 2000.

Heipke, C. (1996), Overview of image matching techniques, *Proceedings of the OEEPE workshop on Application of Digital Photogrammetric Workstations*, Kölbl, O. (ed.), Lausanne, pp. 173 – 189.

Helava Associates Inc. (1997), *SOCET SET® Windows NT User's Manual*, GDE Systems, Inc.

Henrickson, O., Streilein, A., and Gruen, A. (1996), Automated 3-D reconstruction of buildings and visualisation of city models, Presented paper at the 3D-City Models Workshop, University Bonn, October 9-11, 1996

Hoffman, P (1996), *VRML House Project*, Online, EOS Systems Inc., Available http://www.photomodeler.com/PROJS/HOUSE/HOUSE.HTM 8 February, 2000.

Ioannidis, C, Potsiou, C & Badekas, J (1997), The use of contemporary photogrammetric procedures for the recording and documentation of large monuments and their graphic representation, *International Archives of Photogrammetry and Remote Sensing*, Vol XXXII, Part 5C1B, pp 131-140.

Karara, H. (1989), An introduction to non-topographic photogrammetry, *Non-Topographic Photogrammetry*, 2nd edition, American Society for Photogrammetry and Remote Sensing, Falls Church, Virginia, pp. 1-6.

Karras, G., Patias, P., Petsa, E., & Ketipis, K. (1997), Raster projection and development of curved surfaces, *International Archives of Photogrammetry and Remote Sensing*, Vol XXXII, Part 5C1B, pp. 179-185.

Kempa, M. & Schlüter, M. (1993), DEM evaluation by an operator and facets stereo vision: a comparison based on close range imagery, *Optical 3D Measurement Techniques II: Applications in Inspection, Quality Control and Robotics*, Gruen / Kahmen (eds.), Wichmann, Karlsruhe, pp. 502-507.

Kersten, T. & O'Sullivan, W. (1996), Digital aerial triangulation with the Helava Automated Triangulation System, *Proceedings of the OEEPE workshop on Application of Digital Photogrammetric Workstations*, Kölbl, O. (ed.), Lausanne, pp. 139-148.

Kleiner, T. & Wehr, A. (1993), Fast digital survey of historical sites and monuments by using the 4D-LaserScanner system, *Optical 3D Measurement Techniques II: Applications in Inspection, Quality Control and Robotics*, Gruen / Kahmen (eds.), Wichmann, Karlsruhe, pp. 301-307.

Kölbl, O. (1996a), An outlook on the use of digital work stations in practice, *Proceedings of the OEEPE workshop on Application of Digital Photogrammetric Workstations*, Kölbl, O. (ed.), Lausanne, pp. 35-39.

Kölbl, O. (1996b), An overview on commercial software products for digital arerial triangulation, *Proceedings of the OEEPE workshop on Application of Digital Photogrammetric Workstations*, Kölbl, O. (ed.), Lausanne, pp. 125-137.

Kraus, K. (1993), *Photogrammetry – Fundamentals and Standard Processes*, Vol. 1, 4th edition, Institute for Photogrammetry, Vienna University of Technology, Dümmler / Bonn.

Kraus, K. (1997), *Photogrammetry – Advanced Methods and Applications*, Vol. 2, 4th edition, Institute for Photogrammetry and Remote Sensing, Vienna University of Technology, Dümmler / Bonn.

Koch, R (1994), Model-based 3-D scene analysis from stereoscopic image sequences, *ISPRS Journal of Photogrammetry and Remote Sensing*, Vol 49 (5), pp. 23-50.

Kölbl, O. (1996), Scanning and state-of-the-art scanners, *Digital Photogrammetry: an Addendum to the Manual of Photogrammetry*, American Society for Photogrammetry and Remote Sensing, Maryland, pp. 3-5.

LaPrade, G., Briggs, S., Farrell, R., & Leonardo, E. (1980), Stereoscopy, *Manual of Photogrammetry*, 4th edition, American Society of Photogrammetry, Falls Church, Virginia, pp. 519-544.

Li, M. (1989), *Hierarchical Multi-point Matching with Simultaneous Detection and Location of Breaklines*, unpublished PhD thesis, Royal Institute of Technology, Department of Photogrammetry, Stockholm.

Li, M. (1991), Hierarchical multipoint matching, *Photogrammetric Engineering and Remote Sensing*, Vol. 57, No. 8, pp. 1039-1047.

Lillesand, T.M. & R.W. Kiefer (1994), *Remote Sensing and Image Interpretation 3rd edition*", John Wiley & Sons, New York.

Luhmann, T. (1998), CAD-based photogrammetry for 3-D reconstruction of large objects, , *International Archives of Photogrammetry and Remote Sensing*, Vol. XXXII, Part 5, pp. 236-241.

Marten, W, Mauelshagen, L & Pallaske, R (1994), Digital orthoimage-system for architecture representation, *ISPRS Journal of Photogrammetry and Remote Sensing*, Vol 49 (5), pp. 16-22.

Mason, S. & Streilein, A. (1996), Photogrammetric reconstruction of buildings for 3D city models, *South African Journal of Surveying and Mapping*, Vol 23, Part 5, pp. 249-262.

Mathur, S. (1997), *Three-Dimensional Representation of Archaeological Data in American Archaeology*, Online, University of Iowa, Available http://www.uiowa.edu/~anthro/plains/Termppr.htm 8 February, 2000.

Maune, D. (1996), Introduction to digital elevation models (DEM), *Digital Photogrammetry: an Addendum to the Manual of Photogrammetry*, American Society for Photogrammetry and Remote Sensing, Maryland, pp. 131-134.

McGlone, J. (1989), Analytic data-reduction schemes in non-topographic photogrammetry, *Non-Topographic Photogrammetry*, 2nd edition, Karara (ed.), American Society for Photogrammetry and Remote Sensing, Falls Church, Virginia, pp. 37-57.

Mikhail, E. (1989), Introduction to metrology concepts, *Non-Topographic Photogrammetry*, 2nd edition, Karara (ed.), American Society for Photogrammetry and Remote Sensing, Falls Church, Virginia, pp. 7-14.

Miliano, V. (1999), *Unrealty: Application of a 3D Game Engine to Enhance the Design, Visualization and Presentation of Commercial Real Estate*, Online, Perilith Industrielle, Available, http://www.unrealty.net/vsmm99 8 February, 2000.

Miller & Drollinger (1995), *Strategy Information for ATE*, unpublished notice, General Dynamics Corporation.

Patias, P., Stylianidis, E. & Terzitanos, C. (1998), Comparison of simple off-the-shelf and of wide-use 3D modeling software to strict photogrammetric procedures for close-range applications, *International Archives of Photogrammetry and Remote Sensing*, Vol. XXXII, Part 5, pp. 628-632.

Reilly, P. (1992), Three-dimensional modelling and primary archaeological data, *Archaeology and the Information Age: a Global Perpsective*, Routledge, London, pp 147-173.

Reilly, P. & Rahtz, S. (1992), Introduction: archaeology and the information age, *Archaeology and the Information Age: a Global Perpsective*, Routledge, London, pp 1-28.

Rosenholm, D. (1989), Multi-point matching using the least-squares technique for evaluation of three-dimensional models, *Photogrammetric Engineering and Remote Sensing*, Vol. 53, No. 6, pp. 621-626.

Rüther, H. (1989), An overview of software in non-topographic photogrammetry, *Non-Topographic Photogrammetry*, 2nd Edition, Karara (ed.), American Society for Photogrammetry and Remote Sensing, Falls Church, pp. 129-145.

Schenk, T. (1994), Concepts and algorithms in digital photogrammetry, *ISPRS Journal of Photogrammetry and Remote Sensing*, Vol 49 (6), pp. 2-8.

Schlüter, M. (1998), Multi-image matching in object space on the basis of a general 3-D surface model instead of common 2.5-D surface models and its application for urban scenes, *International Archives of Photogrammetry and Remote Sensing*, Vol. 32, Part 4, pp. 545-552.

Scott, M. (*n.d.*),*The Extension Of Cartographic Modeling For Volumetric Geographic Analysis*, Online, Department of Geography, University of South Carolina, Available http://www.spatial.maine.edu/ucgis/testproc/scott_m/scottm.html 8 February, 2000.

Sims, D. (1997), Archaeological models: pretty pictures or research tools?, *IEEE Computer Graphics and Applications*, Potel, M. (ed.), January/February 1997, pp. 13-15.

Streilein, A. (1994), Towards automation in architectural photogrammetry: CAD-based 3D-feature extraction, *ISPRS Journal of Photogrammetry and Remote Sensing*, Vol. 49, No. 5, pp. 4-15.

Streilein, A. (1995), *Digital Architectural Photogrammetry and CAAD*, Online, ETH Zurich, Available http://www.p.igp.ethz.ch/p02/projects/dapcad/dapcad.html 8 February, 2000.

Streilein, A. & Niederöst, M. (1998), Reconstruction of the Disentis monastery from high resolution still video imagery with object oriented measurement routines, *International Archives of Photogrammetry and Remote Sensing*, Vol. XXXII, Part 5, Hakodate, pp. 271-277.

Taylor, S. (2000), *Interactive 3D Visualisation over the Internet* (preliminary title), unpublished MSc thesis, UCT, Cape Town.

Thompson, E. H. (1962), Photogrammetry, *The Royal Engineers Journal*, Vol 64 (4), pp 432-444.

Thompson, M. & Gruner, H. (1980), Foundations of Photogrammetry, *Manual of Photogrammetry*, 4th edition, American Society of Photogrammetry, Falls Church, Virginia, pp. 1-36.

Torre, M. & Ruiz, A. (1996), Experiences with MATCH-T for orthophoto production, *Proceedings of the OEEPE workshop on Application of Digital Photogrammetric Workstations*, Kölbl, O. (ed.), Lausanne, pp. 223-228.

Toth, C. (1996), Image compression in photogrammetric practice: an overview, *Digital Photogrammetry: an Addendum to the Manual of Photogrammetry*, American Society for Photogrammetry and Remote Sensing, Maryland, pp. 75-82.

Van der Merwe, N. (1995), *Development of an Image Matching Scheme Using Feature- and Area Based Matching Techniques*, unpublished PhD thesis, Department of Geomatics, UCT, Cape Town.

Vuoskoski, J. (1996), *Exchange of Product Data between CAD systems and a Physics Simulation Program*, Online PhD thesis, Tampere University of Technology, Available http://cadd.cern.ch/cad_geant_int/thesis/vaitos_main.html 8 February, 2000.

Wei, G., Ping, Z. & Jun, C. (1998), Topological data modelling for 3D GIS, *International Archives of Photogrammetry and Remote Sensing*, Vol. 32, Part 4, pp. 657-661.

Wood, J. & Chapman, G. (with contributions by Delooze, K. & Trueman, M.) (1992), Three-dimensional computer visualization of historic buildings – with particular reference to reconstruction modelling, *Archaeology and the Information Age: a Global Perpsective*, Routledge, London, pp 123-146.

Woodwark, J. (1991), Reconstructing history with computer graphics, *IEEE Computer Graphics & Applications*, January 1991, pp. 18-20.

Wong, K. (1980), Basic mathematics of photogrammetry, *Manual of Photogrammetry*, 4th edition, American Society of Photogrammetry, Falls Church, Virginia, pp. 37-101.

Woytowicz, D. (1993), PHAUST – a photogrammetric evaluation system for digital images, *Optical 3D Measurement Techniques II: Applications in Inspection, Quality Control and Robotics*, Gruen / Kahmen (eds.), Wichmann, Karlsruhe, pp. 81-87.

Wrobel, B. (1987), Digital image matching by facets using object space models, *4th International Symposium on Optical and Optoelectronic Applications for Science and Engineering*, The Hague, Netherlands, pp. 325-333.

Xu, M. and Zhu, Y. (1998), Computer-based simulation and quality control for building of the large-scale timber structures, *International Archives of Photogrammetry and Remote Sensing*, Vol. XXXII, Part 5, Hakodate, pp. 660-664.

APPENDIX A

Definitions

The following definitions relate to the parameters of SOCET SET's matching strategy files. "Signal Power" in the definitions below refers to the sum of the squares of the grey levels divided by the number of grey levels within the correlation area.

MIN_ELEV_CHANGE: Elevation change threshold. After each pass of elevation calculation, the largest single change in elevation for that pass is compared to this value. If the largest change falls below the MIN_ELEV_CHANGE value, terrain extraction will stop without performing any remaining iterations. The default is 0, which allows ATE to perform all passes in the strategy, regardless of actual elevation change.

NUM_PASSES: Number of measurement passes.

ATE_MODE: A flag which sets the mode of terrain extraction:

1 = Hierarchical Relaxation Correlation (HRC) processing

2 = Iterative Orthophoto Refinement (IOR) processing

CORR_AREA_2D: Dimension of the square window used for 2D correlation, in pixels. The size may be automatically expanded if the computed signal power is too low. CORR_AREA_2D is expanded until signal power in the master patch is greater than LOW_SP_LIM, up to a maximum of MAX_CORR_AREA_2D.

CORR_CURV_LIM: Minimum curvature of the correlation function at the peak. Curvature is the absolute value of the second derivative of the correlation function. A high curvature indicates a sharp peak, which implies a precise measurement.

CORR_CUTOFF: Minimum correlation value at a post. Correlation is normalised to the range -1.0 to 1.0.

DELZ_LIM: Not used when MAX_ITER = 0. When MAX_ITER > 0, iterations will stop if the maximum change in *x*-parallax (i.e. u_shift at the given pass's RRDS level) is less than the DELZ_LIM. If the MAX_ITER is reached and the u_shift (x_parallax) is greater than DELZ_LIM, the point is flagged as LARGE ELEV CHANGE FOM.

DIFF_SP_LIM: Limit for the difference in the signal power between the two images, computed as a percentage. If the signal power difference is below the DIFF_SP_LIM then the point is flagged as LARGE_DIFF_SIGNAL_POWER fom.

HW_ERR: Not used. It is assigned a default value of 0.5.

LOW_SP_LIM: Low signal power limit. If the signal power squared is below this value, the CORR_AREA is expanded until the signal power squared is above this limit or MAX_CORR_AREA is reached.

MAX_CORR_AREA_2D: Maximum square area dimension used for 2D correlation, in pixels. If the initial size specified by CORR_AREA_2D results in an area too low in signal power, the area is iteratively increased until MAX_CORR_AREA is reached.

MAX_ITER: Maximum number of iterations to perform during correlation.

MMDL_ERR: Constant error associated with the math model computations, in pixels. Used to compute the precision of a post.

RETRIES: Indicates whether the correlation automatically retries to remeasure a failed post with adjusted strategy (0 = no, 1 = yes).

SEC_PEAK_LIM: Percentage of the primary correlation peak that a potential secondary peak must be in order to be considered a secondary peak. The FOM for posts with secondary peak is set to SECONDARY_PEAK. (See also VLLY_LIM)

SP_CUTOFF: Minimum signal power of correlation area. If below this limit, the FOM is set to LOW SIGNAL POWER.

AUTO_U_SRCH: A 1 or a 0. If 1 and not the first pass, then U_SRCH_DIST is computed instead of using the given U_SRCH_DIST value.

U_SRCH_DIST: Search distance in epipolar *u* direction, from the center of the search patch, in pixels. Indicates how many correlation "trial centers" there are, i.e., how many cross-correlations will be performed (7 means a total of 15 trial centers, 7 to the left and right and 1 at the center).

V_SRCH_DIST: Search distance in epipolar *v* direction for 2D correlation.

U_SRCH_MAX: Maximum search distance in epipolar *u* direction. The search area is iteratively expanded to this maximum if the correlation peak occurs at the edge of the search area.

V_SRCH_MAX: Maximum search distance in epipolar *v* direction for 2D correlation.

VLLY_LIM: Percentage of the primary peak that a valley between the primary and a potential secondary peak must be in order for the correlation to be considered to have a secondary peak. (See also SEC_PEAK_LIM)

WINDOW: Indicates which image is the fixed image during correlation (0 = left, 1 = right). Currently not used.

YP_LIM: Maximum y-parallax for 2D correlation, in pixels. If the y-parallax is greater than the limit, the FOM is set to EXCESSIVE_Y_PARALLAX. Not used when V_SRCH_DIST = 0.

RRDS: Minification level of imagery to use for current measurement pass.

X_SPACING: Used to skip measuring points in the grid in the x direction. A value of 1 will measure all points in the grid, a value of 2 will measure every other point in the grid etc.

Y_SPACING: See X_SPACING

FOM_LIMIT: Not used for ATE. Used in Exterior Orientation and Mosaic strategies.

SLOPE_LIMIT: Used to check for excessive slope between elevations grid points. The units are degrees.

SPIKE_LIMIT: Used to check for spikes or wells in the DTM. The units are degrees.

INTERPOLATE: When set to "yes", the elevation values for posts with suspect correlation results will be interpolated from elevations of surrounding posts with good FOM values.

APPLY_THIN_FILTER: When set to "yes", a filter is applied to smooth the DTM in the non critical areas; i.e. it will not smooth in the ridges and drains, only in the planar areas. This filter uses the filter threshold below.

THIN_FILTER_THRESH: This threshold is a percentage of the post spacing; e.g. if the post spacing is 10 meters and the threshold is input as 30.0, this would be 30% of 10 meters or 3 meters. The 3 meter value is then used to examine the DTM for roughness of 3 meters RMS. Only areas with less than this "roughness" are smoothed.

APPLY_OBSTRUCTION_FILTER: This filter will remove objects protruding from the general DTM surface. It is limited by the OBSTRUCTION_SIZE and OBSTRUCTION_SLOPE parameters below.

OBSTRUCTION_SIZE: This is the size in numbers of points of an obstruction; e.g. if the post spacing is 10 meters and the size is 30 then objects which are less than 10x30 = 300 meters will be searched for only.

OBSTRUCTION_SLOPE: This is the slope used to determine if an object in the DTM is an obstruction. A Slope of 55 degrees would find only objects which are causing a steep slope. The lower the slope, the more objects which will be smoothed out. It is used in conjunction with OBSTRUCTION_SIZE.

OVER_COLLECT: This will cause ATE to run faster for dense data because benign or flat areas of the DTM will be skipped and critical areas will still be measured.

APPENDIX B

Matching Strategies

B.1. Adapt.strat

num_passes 8								
CORR_AREA_1D	21	15	15	15	15	15	15	15
corr_area_2d	15	15	15	15	15	7	7	7
corr_curv_lim	0.01	0.02	0.02	0.02	0.02	0.02	0.02	0.02
corr_cutoff	0.5	0.5	0.5	0.45	0.45	0.4	0.4	0.45
delz_lim	3.0	3.0	3.0	3.0	3.0	2.0	2.0	2.0
diff_sp_lim	9.24	9.24	9.24	9.24	9.24	9.24	9.24	9.24
gsd	0.0	0.0	0.0	0.0	0.0	0.0	0.0	0.0
hw_err	0.5	0.5	0.5	0.5	0.5	0.5	0.5	0.5
lines	3	3	3	3	3	3	3	3
low_sp_lim	400.0	400.0	400.0	400.0	200.0	200.0	200.0	200.0
MAX_CORR_AREA_1D	61	61	61	61	121	121	121	121
MAX_CORR_AREA_2D	21	21	21	21	21	15	15	15
MAX_ITER	0	0	0	0	0	1	1	1
MAX_LINES	5	3	3	3	5	5	5	5
MODE_CORR	2	2	2	2	2	2	2	2
MMDL_ERR	0.5	0.5	0.5	0.5	0.5	0.5	0.5	0.5
RETRIES	0	0	0	0	0	0	0	0
SEC_PEAK_LIM	0.99	0.99	0.99	0.99	0.99	0.99	0.99	0.99
SP_CUTOFF	6.0	6.0	6.0	6.0	6.0	2.0	2.0	1.0
SRCH_U_PATCH_SIZE	37	25	25	25	37	37	37	37
SRCH_V_PATCH_SIZE	17	31	37	32	45	45	45	45
AUTO_U_SRCH	1	0	0	0	0	0	0	0
U_SRCH_DIST	27	15	15	15	15	15	15	15
V_SRCH_DIST	00	00	00	0	0	0	0	0
U_SRCH_MAX	27	15	15	15	15	15	15	15
V_SRCH_MAX	00	00	00	00	0	0	0	0
VARXP_LIM	16.0	16.0	16.0	16.0	16.0	16.0	16.0	16.0

VLLY_LIM	0.09	0.09	0.09	0.09	0.09	0.09	0.09	0.09
WINDOW	0	0	0	0	0	0	0	0
WNDW_U_PATCH_SIZE	32	32	32	32	32	32	32	32
WNDW_V_PATCH_SIZE	32	32	32	32	45	45	45	45
YP_LIM	4.0	4.0	4.0	4.0	4.0	4.0	4.0	4.0
RRDS	32	16	16	8	8	4	2	1
X_SPACING	4	4	4	2	2	2	2	1
Y_SPACING	4	4	4	2	2	2	2	1
FOM_LIMIT	60	60	60	55	50	50	50	50
SLOPE_LIMIT	60.0	60.0	60.0	60.0	60.0	60.0	55.0	55.0
SPIKE_LIMIT	20.0	20.0	20.0	15.0	15.0	15.0	15.0	3.0
APPLY_THIN_FILTER								yes
THIN_FILTER_THRESH								30.0
APPLY_OBSTRUCTION_FILTER								no
OBSTRUCTION_SIZE								20.0
OBSTRUCTION_SLOPE								10.0
OVER_COLLECT								no

B.2. Flat.strat

num_passes	6					
ATE_MODE	1	1	1	1	1	1
corr_area_2d	15	15	15	15	15	15
corr_curv_lim	0.01	0.02	0.02	0.02	0.02	0.02
corr_cutoff	0.6	0.55	0.5	0.45	0.4	0.5
delz_lim	3	3	3	3	2	2
diff_sp_lim	9.24	9.24	9.24	9.24	9.24	9.24
hw_err	0.5	0.5	0.5	0.5	0.5	0.5
low_sp_lim	400	400	400	200	200	200
MAX_CORR_AREA_2D	15	15	15	15	15	15
MAX_ITER	0	0	0	3	3	3
MMDL_ERR	0.5	0.5	0.5	0.5	0.5	0.5
RETRIES	0	0	0	0	0	0
SEC_PEAK_LIM	0.99	0.99	0.99	0.99	0.99	0.99
SP_CUTOFF	6	6	4	3	2	1
SRCH_U_PATCH_SIZE	25	25	25	37	37	37
SRCH_V_PATCH_SIZE	17	37	32	45	45	45

AUTO_U_SRCH	0	0	0	0	0	0
U_SRCH_DIST	7	7	7	7	7	7
V_SRCH_DIST	0	0	0	0	0	0
U_SRCH_MAX	15	15	15	15	15	15
V_SRCH_MAX	0	0	0	0	0	0
VLLY_LIM	0.09	0.09	0.09	0.09	0.09	0.09
WINDOW	0	0	0	0	0	0
YP_LIM	4	4	4	4	4	4
RRDS	8	8	8	4	4	2
X_SPACING	8	4	4	4	2	1
Y_SPACING	8	4	4	4	2	1
FOM_LIMIT	60	60	55	50	50	50
SLOPE_LIMIT	40	30	30	30	30	20
SPIKE_LIMIT	20	15	15	10	3	0.5

B.3. Rolling.strat

num_passes	8							
ATE_MODE	1	1	1	1	1	1	1	1
corr_area_2d	15	15	15	15	15	15	15	15
corr_curv_lim	0.01	0.02	0.02	0.02	0.02	0.02	0.02	0.02
corr_cutoff	0.5	0.5	0.5	0.45	0.45	0.4	0.4	0.5
delz_lim	3	3	3	3	3	2	2	2
diff_sp_lim	9.24	9.24	9.24	9.24	9.24	9.24	9.24	9.24
gsd	0	0	0	0	0	0	0	0
hw_err	0.5	0.5	0.5	0.5	0.5	0.5	0.5	0.5
low_sp_lim	400	400	400	400	200	200	200	200
MAX_CORR_AREA_2D	15	15	15	15	15	15	15	31
MAX_ITER	0	0	0	0	3	3	3	3
MMDL_ERR	0.5	0.5	0.5	0.5	0.5	0.5	0.5	0.5
RETRIES	0	0	0	0	0	0	0	0
SEC_PEAK_LIM	0.99	0.99	0.99	0.99	0.99	0.99	0.99	0.99
SP_CUTOFF	6	6	6	6	6	4	2	1
SRCH_U_PATCH_SIZE	25	25	25	25	37	37	37	63
SRCH_V_PATCH_SIZE	17	31	37	32	45	45	45	45
AUTO_U_SRCH	0	0	0	0	0	0	0	0
U_SRCH_DIST	15	15	15	15	15	15	15	15

V_SRCH_DIST	0	0	0	0	0	0	0	0
U_SRCH_MAX	15	15	15	15	15	15	15	15
V_SRCH_MAX	0	0	0	0	0	0	0	0
VARXP_LIM	16	16	16	16	16	16	16	16
VLLY_LIM	0.09	0.09	0.09	0.09	0.09	0.09	0.09	0.09
WINDOW	0	0	0	0	0	0	0	0
WNDW_U_PATCH_SIZE	32	32	32	32	32	32	32	32
WNDW_V_PATCH_SIZE	32	32	32	32	45	45	45	45
YP_LIM	4	4	4	4	4	4	4	4
RRDS	16	16	16	8	8	4	4	2
X_SPACING	8	8	4	4	4	2	2	1
Y_SPACING	8	8	4	4	4	2	2	1
FOM_LIMIT	60	60	60	55	50	50	50	50
SLOPE_LIMIT	40	40	40	40	40	40	35	30
SPIKE_LIMIT	20	20	20	15	15	10	10	1

B.4. Steep.strat

num_passes	8							
ATE_MODE	1	1	1	1	1	1	1	1
corr_area_2d	15	15	15	15	15	15	15	15
corr_curv_lim	0.01	0.02	0.02	0.02	0.02	0.02	0.02	0.02
corr_cutoff	0.5	0.5	0.5	0.45	0.45	0.4	0.4	0.45
delz_lim	3	3	3	3	3	2	2	2
diff_sp_lim	9.24	9.24	9.24	9.24	9.24	9.24	9.24	9.24
hw_err	0.5	0.5	0.5	0.5	0.5	0.5	0.5	0.5
low_sp_lim	400	400	400	400	200	200	200	200
MAX_CORR_AREA_2D	15	15	15	15	15	15	15	15
MAX_ITER	0	0	0	0	3	3	3	3
MMDL_ERR	0.5	0.5	0.5	0.5	0.5	0.5	0.5	0.5
RETRIES	0	0	0	0	0	0	0	0
SEC_PEAK_LIM	0.99	0.99	0.99	0.99	0.99	0.99	0.99	0.99
SP_CUTOFF	6	6	6	6	6	2	2	1
SRCH_U_PATCH_SIZE	25	25	25	25	37	37	37	37
SRCH_V_PATCH_SIZE	17	31	37	32	45	45	45	45
AUTO_U_SRCH	0	0	0	0	0	0	0	0
U_SRCH_DIST	15	15	15	15	15	15	15	15

V_SRCH_DIST	0	0	0	0	0	0	0	0
U_SRCH_MAX	15	15	15	15	15	15	15	15
V_SRCH_MAX	0	0	0	0	0	0	0	0
VLLY_LIM	0.09	0.09	0.09	0.09	0.09	0.09	0.09	0.09
WINDOW	0	0	0	0	0	0	0	0
YP_LIM	4	4	4	4	4	4	4	4
RRDS	32	16	16	8	8	4	4	2
X_SPACING	4	4	4	2	2	2	2	1
Y_SPACING	4	4	4	2	2	2	2	1
FOM_LIMIT	60	60	60	55	50	50	50	50
SLOPE_LIMIT	60	60	60	60	60	60	55	55
SPIKE_LIMIT	20	20	20	15	15	15	15	3

APPENDIX C

Survey Control Point Standard Deviations

Station	Y(mm)	X(mm)
A	n/a	n/a
B	2.0545	2.2867
C	2.9618	n/a
1A	1.9643	3.0920
1B	2.1177	5.1912
2A	1.0527	2.7882
2B	0.9534	1.0083
3A	2.3452	1.8634
3B	5.1098	3.0689
4A	1.4740	1.7874
4B	2.1244	3.4198
5A	1.6095	2.6843
6A	2.9764	2.7132
6B	5.7983	4.2528
7A	4.4747	1.6410
8A	4.1468	2.2925
8B	4.6840	2.7651
9A	4.3703	3.5683
9B	4.3118	3.7104
10A	2.9988	2.2167
10B	2.8492	2.1347
11A	2.3488	1.7900
11B	2.8808	2.5549
12A	1.6859	1.5652
12B	2.0661	2.1862
13	2.4739	3.0423
14	1.7533	3.2779